2008

Electrochemical fabrication of AuCo nanostructures

Maoshi Guan
Louisiana State University and Agricultural and Mechanical College

Recommended Citation

Guan, Maoshi, "Electrochemical fabrication of AuCo nanostructures" (2008). *LSU Doctoral Dissertations*. 1048.
https://digitalcommons.lsu.edu/gradschool_dissertations/1048

ELECTROCHEMICAL FABRICATION OF AuCo NANOSTRUCTURES

A Dissertation

Submitted to the Graduate Faculty of the
Louisiana State University and
Agricultural and Mechanical College
in partial fulfillment of the
requirements for the degree of
Doctor of Philosophy

in

The Interdepartmental Program in Engineering Science

By
Maoshi Guan
B.S., University of Petroleum, China, 1999
M.S., Louisiana State University, 2005
May, 2008

To my dear family…

ACKNOWLEDGEMENTS

I would like to thank Dr. E. J. Podlaha for her insightful guidance, continued inspiration and support, and great patience throughout the duration of this project, which make this study possible.

I would like to thank Dr. W. D. Constant to be my co-advisor, and thank Dr. R. W. Pike, Dr. J. E. Henry, Dr. M. C. Murphy and Dr. M. Cherry to serve on my graduate committee.

Many thanks to Dr. D. Cao in Mechanical Engineering Department and Dr. X. Xie in Geology Department for SEM analysis, Dr. D. P. Young and Dr. Moldovan in Physics Department for GMR analysis, and Ms. C. Henk in Department of Biological Science for TEM analysis.

This work was financially supported by LSU Center for BioModular Multi-Scale Systerms and NSF-NIRT (#CTS-0210832).

TABLE OF CONTENTS

LIST OF TABLES

LIST OF FIGURES

ABSTRACT

Electrodeposited Au/CoAu multilayered nanowires are materials with alternating layers of Au and CoAu in a wire where the layer thickness and wire diameter are nanometer size. They can be used for different applications. For example, the wires may exhibit giant magnetoresistance (GMR), a change in the materials resistance with a magnetic field, having applications as a sensor material for microdevices. If Co is etched from CoAu nanowires, rough, porous gold nanostructures will be left behind, which could be used as novel catalysts.

In this study, the electrodeposition of Au/CoAu multilayered nanowires and nanotubes in nanoporous templates was explored from a non-cyanide electrolyte. The multilayers were deposited with a pulse current control and the template pore size played an important role in determining whether nanowires or nanotubes were formed. The magnetic and magnetoresistive properties of Au/CoAu multilayered nanostructures were examined. Au/CoAu multilayered thin films exhibited both normal and inverse CIP GMR.

After electrodeposition, the solid nanowires were released from the template and one component was electrochemically etched from the nanowires. The electrochemical etching conditions were predetermined by the investigation of electrochemical etching behavior of CoAu alloy and pure Co thin films. By precisely controlling the electrochemical etching potential and time, the surface area of the nanowires was enhanced. Nano-bamboo structures were created after partial etching and Au nanodisk structures were created after complete etching. Compared to conventional chemical etching, the anodization etching process presented here can be controlled to produce partially etched structures. The anodization process was monitored by two techniques.

The current was recorded during etching and the total charge was proportional to the layer size. In addition, cyclic voltammetry (CV) was used as a way to observe the partial etching of the nanowires. In addition, the annealing post-treatment was tested to enhance the magnetoresistive properties of Au/CoAu multilayered nanostructures and to improve the quality of the multilayer interface by promoting phase segregation. Furthermore, hollow nano-bamboo structure and ordered nanorings with various aspect ratios were developed through the electrochemical etching of Au/CoAu nanotubes in a similar way. To the best of the author's knowledge, this has not been done before.

CHAPTER 1   INTRODUCTION

In this study, nanowires containing Au and Co are to be examined. First, due to their unique properties, various applications have been explored for the Au/Co system. For example, if a nonferromagnetic layer of Au and a ferromagnetic layer of Co are in a multilayer form, they can be used as giant magnetoresistance (GMR) materials. GMR refers to the change in electrical resistance in response to an applied magnetic field. In multilayered systems, GMR is caused by the applied magnetic field changing the relative electron scattering of the magnetic layers, which has extensive industrial applications for hard disk read heads, bio-sensors and vehicle detection for traffic, among others.[1] Second, due to the large difference in degree of nobility between Au and Co, Co can be easily etched away chemically or electrochemically from a CoAu alloy, resulting in a porous surface. In this way, rough, porous nanostructures can be fabricated, including nanowires, nanodisks, and nanorings. All of them have potential applications in biosensing, optics, nanoelectronics, and catalysis.

There are few reports concerning the electrodeposition of Au/CoAu nanowires, but most of them are from cyanide-containing electrolytes. For example, Valizadeh *et al.*[2, 3] studied the electrodeposition of AuCo alloy and Au/CoAu multilayered nanowires from a single bath with citric acid, cobalt sulphate and gold cyanide electrolyte. Since his prior MS work,[4] Guan has been expanding on the electrodeposition of the AuCo system via a more environmentally friendly approach by using cyanide free electrolytes.

1.1 GMR

GMR multilayers are comprised of alternating nanometric layers of ferromagnetic materials (such as Co, Ni, and Fe) and nonmagnetic materials (such as Au, Cu, and Cr). To

exhibit GMR properties, the thickness of non-magnetic spacer layers has to be smaller than a critical length. In multilayer thin films, the spacer layer thickness has to be comparable to the electron mean free path (a few nanometers) to exhibit current-in-plane (CIP) GMR. To date, several conventional techniques have been used to produce magnetic multilayers, including molecular beam epitaxy, electron-beam evaporation, ion-beam sputtering, and magnetron sputtering. In multilayer nanowires, the electron diffusion length (a few tens of nanometers) is the critical length for the exhibition of current-perpendicular-to-plane (CPP) GMR.[5] Compared with the current-in-plane GMR, current-perpendicular-to-plane GMR has been proven to show a larger magnetoresistance change in some systems.[6, 7] Velu *et al*.[8] measured a CPP GMR of 3 % at 4.2 K for Co/Au sandwiches, which were fabricated by ultrahigh vacuum evaporation. Hutten *et al.*[9] reported Au/Co granular structures with GMR of 2.4 % at 10 K, fabricated by a melt-spinning technique.

However, when depositing on irregular shape substrates or deep recesses, these conventional physical methods have intrinsic limitations. In contrast, electrodeposition can fulfill this task cost effectively. Because of the feasibility of electrodeposition in irregular or deep recessed areas, template electroplating has been widely investigated for the fabrication of nanowires, which refers to a three-dimensional, wire type structure having a diameter of nanometer scale and enormous surface area. A variety of multilayer nanowires, including Co/Cu, Fe/Cu, and NiFe, have been fabricated by electrodeposition techniques with CPP GMR reported.[10-12] However, to the best of our knowledge there has been no electrodeposited Au/Co multilayer GMR reported, since most of the research effort has focused on the Cu/Co system[10, 13-15] because of the low cost of Cu. The closest study related to our goal is the one presented by Valizadeh *et al.*[2] They electrodeposited Au/Co multilayered nanowires onto polycarbonate membranes from a cyanide-containing electrolyte, but no GMR was reported. Vapor deposited

Au/Co multilayers have been prepared[8, 9] that do exhibit GMR; thus our study explores the analogous structure by electrodeposition.

1.2 Porous Nanowires

Recently, nanoporous nanowires with enhanced surface area and well-defined pore morphology have attracted attention due to their anisotropic properties. Those nanowires have potential applications in surface reactions, immobilizing molecules, BioMEMS and nanoelectronics. The conventional technique to fabricate nanoporous structures is chemical dissolution of a single phase binary alloy containing a noble metal with a strong acid[16, 17] (e.g. HNO_3) or alkaline[18] solution (e.g. ammonium hydroxide), usually in the presence of oxidizing agents. A variety of binary alloy systems, e.g. Cu-Zn, Cu-Al, Au-Ag and Au-Cu,[19-21] have been studied.

Ji and Searson[16, 17] studied the fabrication of Au-Ag nanoporous nanowires with high surface area and a well-defined pore morphology. Two processing steps are involved in the fabrication of nanoporous nanowires. First a single-phase, binary Au-Ag alloy is electrochemically deposited into a nanoporous template from a single electrolyte. Second, the solid nanowires are then removed from the template and one component is chemically etched from the alloy with concentrated nitric acid. The porosity and morphology of the nanoporous nanowires can be controlled by varying the composition of the Au-Ag alloy. Qin *et al.*[18] later reported a novel, high-yielding lithographic process that allows one to generate designed gap structures on nanowires templates. This procedure combines advances in template-directed synthesis of nanowires with electrochemical deposition and wet-chemical etching and allows routine fabrication of face-to-face disk arrays and gap structures in the range of five to several hundred nanometers. First, Au-Ag or Au-Ni nanowires were electrochemically deposited in

porous alumina templates. After the nanowires were released, the Ni segments were removed from Au-Ni wires by selective wet-chemical etching in concentrated HNO_3, and the Ag segments were removed with an etching solution consisting of methanol, ammonium hydroxide, and hydrogen peroxide. Compared to those binary alloy systems discussed previously, AuCo is a better choice for preferential etching. Au, as a noble metal, has a very positive standard reversible potential and from a thermodynamic perspective, it is stable at room temperature in pure water. In contrast, Co is less noble and much easier to be etched away from a AuCo alloy, resulting in a porous Au structure. Therefore, due to the large difference in their degree of nobility, the AuCo system lends itself well to preferential etching.

To date, there are some challenges existing in the study of the AuCo system. For example, compared to the widely studied Cu/Co system, most reported GMR values from the Au/Co system are small, less than 5 %, even measured at low temperatures. One of the possible reasons for the low values is that there are multi magnetic domains formed inside a single magnetic layer, which will ruin the antiferromagnetic coupling for the GMR. Another more plausible reason is attributed to the non-distinct interface between Au and Co layers. Au/Co multilayered thin films showed rather diffuse interfaces at which there appeared significant intermixing of Co and Au species. As for the fabrication of porous nanowires, since preferential wet-chemical etching is the method most widely used, there are some intrinsic disadvantages which cannot be avoided. For example, *i.* there is little control over the etching and *ii.* there can be an evolution of harmful gases and byproducts due to the strong acids, bases and oxidizing agents in the solutions.

1.3 Goal of the Study

In this dissertation, we are going to develop conditions to electrodeposit Au/CoAu multilayered nanowires and nanotubes in various porous templates from non-cyanide electrolytes,

as shown schematically in **Figure 1-1 (a)**. The magnetic properties of Au/CoAu multilayered nanowires will be examined. Second, the solid nanowires are then removed from the template and one component is electrochemically etched from the nanowires. By precisely controlling the electrochemical etching potential and time, the surface area of the nanowires can be enhanced, as shown in **Figure 1-2 (b)**. Nano-bamboo structures were created after partial etching and Au nanodisk structures were created after complete etching. To prove the electrochemical etching effectiveness, nanostructures before and after etching will be examined by scanning electron microscopy (SEM), controlled potential coulometry (CPC), cyclic voltammetry (CV) and other techniques. Compared to the conventional chemical etching, by using anodization, etching of the layers can be controlled much better to form these intermediate bamboo structures. To the best of the author's knowledge, this has not been done before.

Next, two areas are going to be explored: (*i*) the magnetic and magnetoresistive properties in Au/CoAu multilayered nanowires and thin films, and (*ii*) the development of controlled porosity/shape of multilayered Au/CoAu nanowires and nanotubes. First, post-deposition annealing will be employed to improve the magnetic and magnetoresistive properties of Au/Co system. As an extensively studied technique, annealing is believed to be able to segregate the layer interface and sharpen the composition profile, which is necessary for the appearance of GMR. Second, a sharper layer interface from annealing treatment may be helpful to realize a more precisely controlled electrochemical etching of Au/CoAu multilayered nanowires to produce nano-bamboo structures and nanodisks. Furthermore, hollow nano-bamboo structures and ordered nanorings with various aspect ratios will be developed through the electrochemical etching of Au/CoAu nanotubes in a similar way.

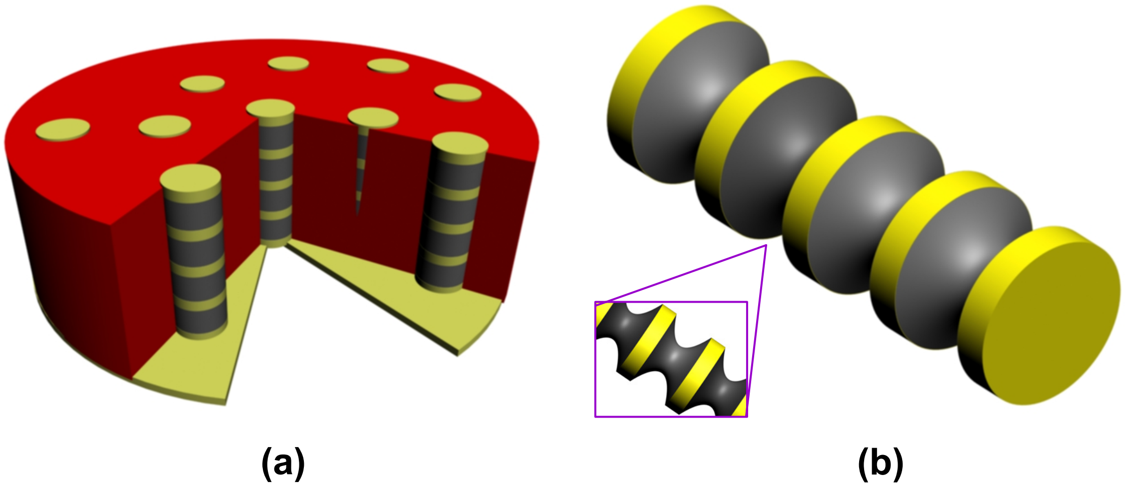

Figure 1-1 Schematic illustrations of (a) porous template electrodeposition of Au/CoAu multilayered nanowires, and (b) electrochemical etching of Au/CoAu nanowires in a controllable manner

CHAPTER 2 LITERATURE REVIEW

2.1 Concepts of Electrochemical Deposition and Etching

An electrochemical reaction is a heterogeneous chemical process involving the transfer of charge to or from an electrode, generally a metal, carbon or a semiconductor. The charge transfer may be a cathodic process in which an otherwise stable species is reduced by the transfer of electrons from an electrode. In the Au/Co electrodeposition system, the reduction of Au(I) and Co(II) ions on the cathode surface are the main electrochemical reactions. There are also several possible side reactions that can occur simultaneously. The anodic reactions are dependent on the anode materials chosen. Those reactions are listed as following:

Main reactions:

$$\mathrm{Au\ (I)} + e^- \rightarrow \mathrm{Au\ (s)}$$

$$\mathrm{Co\ (II)} + 2e^- \rightarrow \mathrm{Co\ (s)}$$

Side reactions:

$$2H_2O + 2e^- \rightarrow 2OH^- + H_2$$

$$O_2 + 2H_2O + 4e^- \rightarrow 4OH^-$$

Conversely, the charge transfer may be an anodic process where otherwise stable species are oxidized by the removal of electrons from the electrode. In the process of selectively electrochemical etching of Co from AuCo process, the oxidization of Co on the anode is the main reaction. Meanwhile, the possible side reactions include the oxidization of Au and the electrolyzing of water. Those reactions are listed as following:

Main reaction:

$$Co \rightarrow Co\ (II) + 2e^-$$

Side reactions:

$$Au \rightarrow Au\ (I) + e^-$$

$$2H_2O \rightarrow O_2 + 4H^+ + 4e^-$$

All electrochemical reactions take place in an electrochemical cell, which is a device converting electrical energy into chemical energy. An electrochemical cell is schematically depicted in **Figure 2-1**. It consists of at least two electrodes (cathode and anode) where the electrochemical reactions occur, an electrolyte for conduction of ions, and an external conductor to provide for continuity of the circuit. The third possible electrode is a reference electrode which has a stable electrochemical potential.

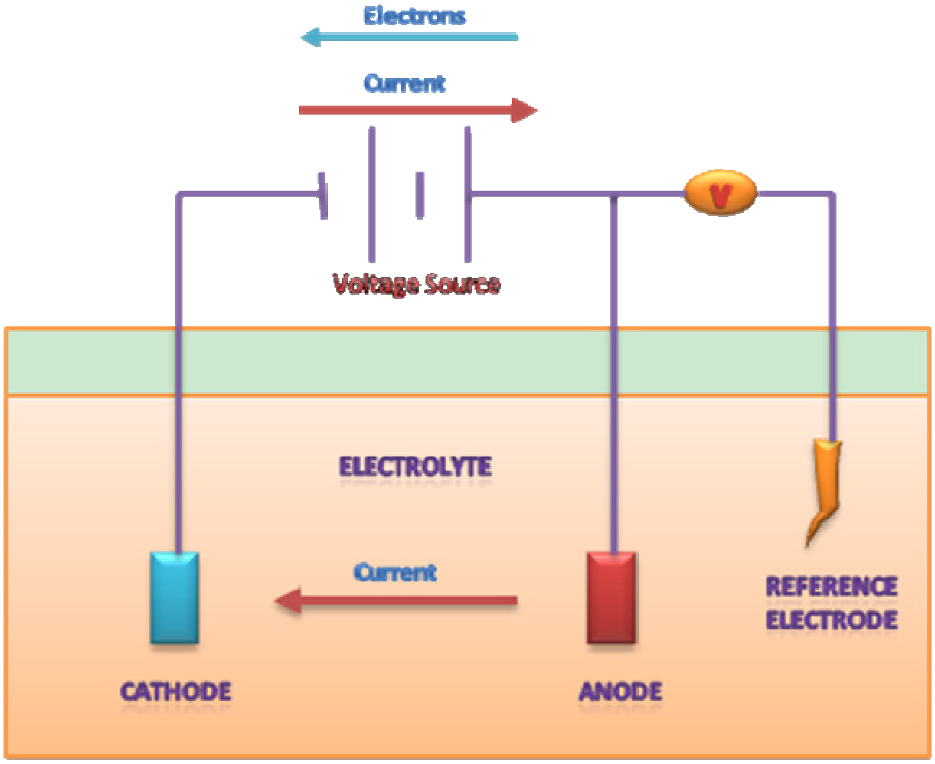

Figure 2-1 Schematic of an electrochemical cell

Faraday's law relates the amount of charge passed to the amount of substance oxidized or reduced, which can be used to calculate the thickness of deposited metal films in electrodeposition.

$$It\eta = nF\left[\frac{m}{sM}\right]$$

where I is the applied current, t is the charging time, η is the current efficiency, n is the number of electrons transferred, F is the Faraday's constant (96485 C/equiv), m is the mass reacted, s is the stoichiometric coefficient and M is the molecular weight.

The current efficiency (η) is the ratio of current density used to electrodeposit the metals compared to the total applied current density, which is usually expressed on a percent basis

$$\eta = \frac{\sum i_{metal}}{i_{total}} * 100\% = \frac{\sum i_{metal}}{\sum i_{metal} + i_{side}} * 100\%$$

Each partial current density is calculated from Faraday's Law, which is described as:

$$i_j = \frac{n_j F m_j}{s_j M_j t A}$$

where i is the current density for each metal, n is the number of electrons transferred, F is the Faraday's constant, m is the mass actually plated, s is the stoichiometric coefficient, M is the molecular weight, t is the plating time, and A is the effect area of the working electrode. The mass actually plated (m) is the product of the deposit thickness, plated surface area and mass density.

All the possible electrochemical reactions involved in the investigation of AuCo system are listed in **Table 2-1**, including their standard equilibrium potentials (E^0).

Table 2-1 Standard equilibrium potentials (V vs. NHE)[22]

	Electrochemical reactions	*E^0 (V vs. NHE)*
More Noble →	$Au^+ + e^- = Au$	1.692
	$O_2 + 4H^+ + 4e^- = 2H_2O$	1.229
	$2H^+ + 2e^- = H_2$	0.000
	$Co^{2+} + 2e^- = Co$	-0.277
	$2H_2O + 2e^- = H_2 + 2OH^-$	-0.828

At large applied current or potentials the mass transport mechanism dominates and causes the current to reach a limiting value. **Figure 2-2** shows the current response to an applied potential at steady state for a single reactant. At a low applied potential, the reduction reaction is under kinetic control. The surface concentration is approximately equal to the bulk concentration, and the reduction rate is dependent on the applied potential in an exponential way. The system is under a mixed control of kinetic and mass transport when the overpotential becomes larger. The surface concentration becomes less than the bulk concentration, and a concentration gradient of metal ions appears on the electrode surface. Finally when the surface concentration drops to zero, the mass transport control becomes completely dominant and the concentration gradient reaches a maximum value. At this moment, a maximum current, referred to as the limiting current, is reached and the reaction rate reaches a maximum.

As for an electrochemical system containing several reactants, the current response as a function of potential sweep will be a combination of each partial reaction, shown in **Figure 2-3**. In the Au/Co system, as the working potential is swept from open circuit potential (OCP) to a more negative value, the electrodeposition reaction of Au (green **••••••** curve in **Figure 2-3**) starts first due to its distinguished nobility. Because of the extreme low concentration of Au ion

in the solution, the limiting current of Au deposition will be reached. When the potential gets close to the equilibrium potential of Co/Co^{2+}, Co ions start to be reduced too and finally approach a limiting current (purple solid curve in **Figure 2-3**). If the working potential is swept to an even more negative value, the side reaction of water reduction will occur and the reaction rate increases dramatically (red – • – curve in **Figure 2-3**). The start of the side reaction will decrease the current efficiency dramatically. By combining those three partial current densities together, the total current response is achieved, which is plotted as the blue dotted line in **Figure 2-3**.

The situation described in both **Figure 2-2** and **Figure 2-3** is steady state when the potential sweep rate is very small, for example 2 mV/s. Under that circumstance, the limiting current exhibits a plateau. However if the potential is swept in a much larger step (e.g. 100 mV/s), the limiting current will be manifested as a peak. A commonly used electrochemical technique involving non-steady state potential sweep is referred to as cyclic voltammetry (CV).

A typical cyclic potential sweep, as shown in **Figure 2-4 (a)**, contains two linear potential sweeps, one is called the first (forward) scan, and the other is called the second (reverse) scan. From time zero, the potential is swept from an initial value at a fixed scan rate up to a pre-defined limiting value, which is usually called the switching potential (E_λ). Right after that point, the direction of the potential scan is reversed and the voltage is swept back to the initial value, in a cycle, hence the name cyclic voltammetry. During the whole potential sweep, the potential is measured between the reference electrode and the working electrode and the current is measured between the working electrode and the counter electrode. The data is typically represented in a plot of current (I) vs. potential (E), as shown in **Figure 2-4 (b)**.

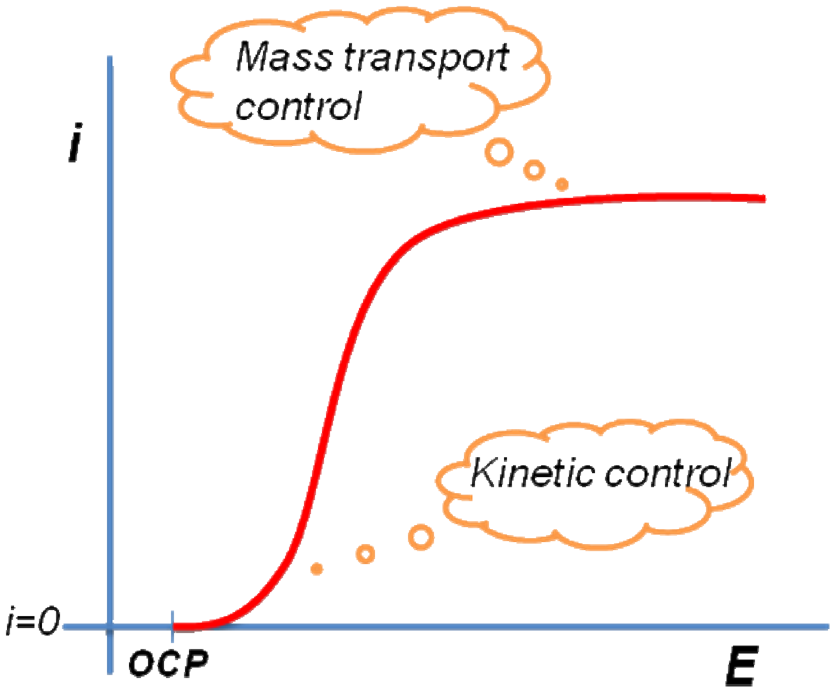

Figure 2-2 Schematic of kinetic and mass transport control for a single reactant

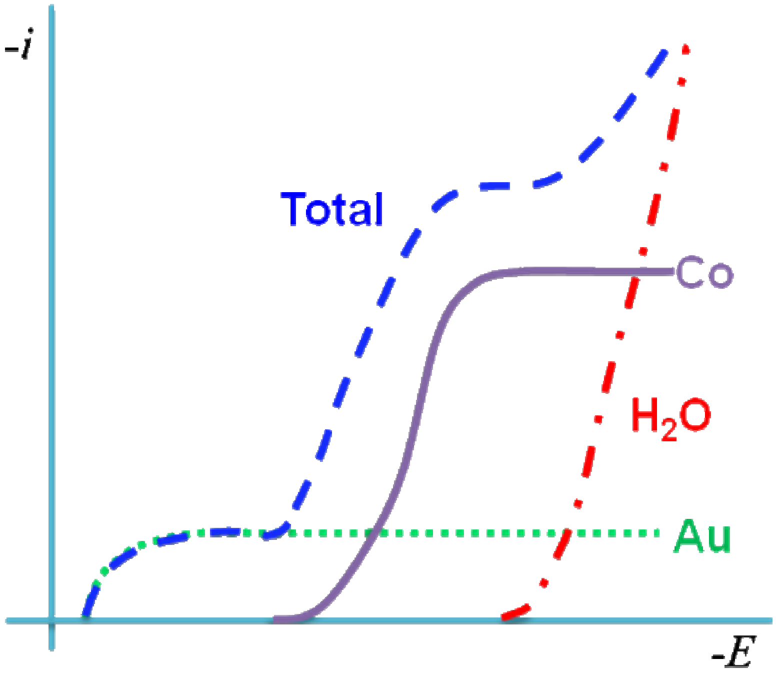

Figure 2-3 Schematic of the partial current densities in Au/Co system

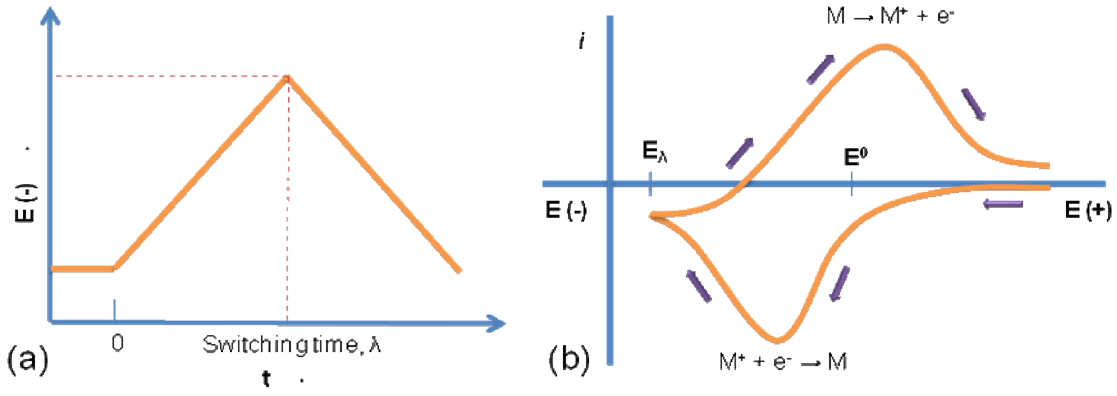

Figure 2-4 (a) Cyclic potential sweep, (b) resulting cyclic voltammogram

In the forward scan, the potential is started well positive of equilibrium potential ($E^{0'}$) for the reduction, at zero current. Only nonfaradaic currents (or capacitive current due to the double layer charging effects) flow for a while. When the electrode potential reaches the value where reduction occurs in the vicinity of $E^{0'}$ the reduction begins and faradaic current starts to flow (a faradaic current is the current due to a redox reaction). As the potential continues to grow more negative, the surface concentration of the reacting ion, M^+, must drop, hence the flux to the surface (and the current) increases. As the potential moves past $E^{0'}$, the surface concentration drops nears to zero, mass transfer of M^+ to the surface reaches a maximum rate, and then it declines as the depletion effect sets in. The observation is therefore a peaked current-potential curve like that depicted in **Figure 2-4 (b)**.

At time λ when the applied potential is reversed, suddenly the potential is sweeping in a positive direction, and in the electrode's vicinity there is a large concentration of the reduced species left from previous forward scan. Soon, the working potential will be approach then pass the equilibrium potential ($E^{0'}$) and reoxidize the product formed in the first reduction reaction, and produce a current of reverse polarity from the forward scan. This oxidation peak will usually have a similar shape to the reduction peak. As a result, information about the redox potential and

electrochemical reaction rates of the compounds are obtained. The current is affected by different experimental variables, such as scan rate, concentration, electrode surface, and etc.

2.2 Electrodeposition of Au/Co Multilayers and Nanowires

To date, there are few reports concerning the electrodeposition of Au/Co multilayers, and none from a non-cyanide-containing electrolyte. Valizadeh *et al.*[3] studied the electrodeposition of compositionally modulated AuCo/CoAu alloy layers of a thin film from a single bath with citric acid, cobalt sulphate and gold cyanide. The Au content in the Co layers and Co content in the Au layers was found to be 3 and 0.1 wt %, respectively. The interfacial roughness was about 1.5 nm for a coating with a bilayer thickness of about 10 nm. The Co layers showed a grain size of 2 nm. Later they[2] investigated the electrodeposition of Au/Co multilayered nanowires into 20 μm-thick ion track etched polycarbonate membranes with pore diameters of 110 – 150 nm from a single electrolyte. The Co-rich metallic nanowires were deposited at -1100 mV and the Au nanowires at -49 mV vs. Ag/AgCl. The magnetic measurements of 12 nm Co/4 nm Au nanowires for fields applied parallel and perpendicular to the film plane indicated a low remnant magnetization.

In a previous study by Guan,[4, 23, 24] the electrodeposition of AuCo and Au/CoAu multilayered thin films from a non-cyanide electrolyte were explored. Two variables were considered: the concentration of citric acid and pH. The changes in composition were described by the difference in the partial current densities. Results showed that a lower citric acid concentration and/or a lower pH were favored for multilayered Au/CoAu deposits with disparate composition in each layer. The current efficiency dropped with increasing citric acid concentration and pH. The citric acid concentration of 0.67 M, pH of 6.15 and the Au concentration of 0.00042 M were chosen as the final electrolyte composition for multilayer

plating. The Au content reached 99.5 (wt %) when the current density was lower than -1 mA/cm^2, and the Co content was higher than 98.7 (wt %) when the current density was higher than -100 mA/cm^2.

Valizadeh *et al.*[25] also studied the electrodeposition of Ag/Co multilayered nanowires in polycarbonate membranes (20 μm thickness and 120 nm pore diameter) using a single bath containing cobalt sulphate, silver cyanide and potassium pyrophosphate. Hydrogen evolution or initial layer re-dissolution of Co during Ag deposition occurred and a current efficiency of 58 % was determined for pulsed plating of Co. Multilayered nanowires with 8 nm Ag/ 15 nm Co layers were well defined as observed by TEM. The Ag/Co multilayered nanowire electrodeposition conditions were based on another study of Co-Ag composition-modulated alloys electrodeposition by Valizadeh *et al.*,[26] in which study, pure Ag was deposited at current densities below 1 mA/cm^2, and 97 % pure Co was obtained at a current densities of 40 mA/cm^2.

Cagnon *et al.*[27] investigated the anion effects on the structure and magnetic behavior of electrodeposited Co/Au (111) layers from different $CoSO_4$ solutions with anions of Cl^- and SCN^- added in amount traces. Results revealed that the anion had a strong influence and the growth was 2-D in the Cl^- solution and 3-D in the SCN^- solution. Perpendicular magnetization anisotropy (PMA) was observed in both solutions. In another study, Cagnon *et al.*[28] found that Cu/Co/Au (111) layers, electrodeposited from a sulfate plus chloride solution, exhibit enhanced PMA due to the magnetoelastic effects at the Co/Au interface.

Gundel *et al.*[29] characterized in-situ the magnetic state of electrodeposited ultrathin Co, Ni and Fe/Au (111) layers. The magnetization is out-of-plane at the Co/Au (111) and Fe/Au (111) interfaces below a critical thickness of few monolayers (MLs). For Co/Au (111) interfaces, the magnetization (M) is strictly out-of-plane for a cobalt thickness smaller than 1-2 MLs. The

magnetization is then completely in the plane of the cobalt when the cobalt thickness is above 2 ML.

2.3 Physical Mechanism of GMR

Giant magnetoresistance (GMR) was first discovered in 1988 by Baibich *et al.*[30] in Paris. Like other magnetoresistive effects, GMR is the change in electrical resistance in response to an applied magnetic field. It was found that the application of a magnetic field to a single crystalline (100)-oriented FeCrFe multilayer resulted in a significant reduction of the electrical resistance of the multilayer. This effect was found to be much larger than either ordinary or anisotropic magnetoresistance and was, therefore, called “giant magnetoresistance” or GMR. These films were prepared by molecular beam epitaxy (MBE), which is a sophisticated and expensive ultra-high vacuum deposition technique ($\Delta R/R$=50 % at 4.2 K under a magnetic field of 5 Tesla).

Within a decade of GMR being discovered, GMR has generated a lot of interest among academic and industrial laboratories, commercial devices based on this phenomenon, such as hard-disk read-heads, magnetic field sensors and magnetic memory chips had become available in the market. To date, various structures which display GMR have been found, such as superlattice multilayers,[12] granular materials, [31, 32] spin valve structures with asymmetric magnetic layers, spin valves with an exchanged-biased layer, and current perpendicular to plane pillars. Values of GMR vary in a great range, depending on the material and temperature.[33] But, GMR is most usually seen in magnetic multilayered structures, where two ferromagnetic layers are closely separated by a thin nonmagnetic spacer layer a few nm thick.

GMR is distinguished from both ordinary magnetoresistance and anisotropic magnetoresistance (AMR), which are also present in layered and granular magnetic systems. Ordinary magnetoresistance arises from the effect of the Lorentz force on the electron

trajectories due to the applied magnetic field. In contrast to GMR, it does not saturate at the saturation magnetic field and is usually small in metals[34] (less than 1 % in fields of the order of 1 Tesla). AMR originates from the spin-orbit interaction and causes the resistance to depend on the relative orientations of the magnetization and the electric current. The magnetic field range in which the AMR effect occurs is governed by the field needed to change the direction of the magnetic moment.

Figure 2-5 shows a Cu/Co multilayer system schematically, including: (a) change in the resistance of the magnetic multilayer as a function of applied magnetic field, (b) the magnetization configurations of the multilayer at various magnetic fields and, (c) the magnetization curve for the multilayer.

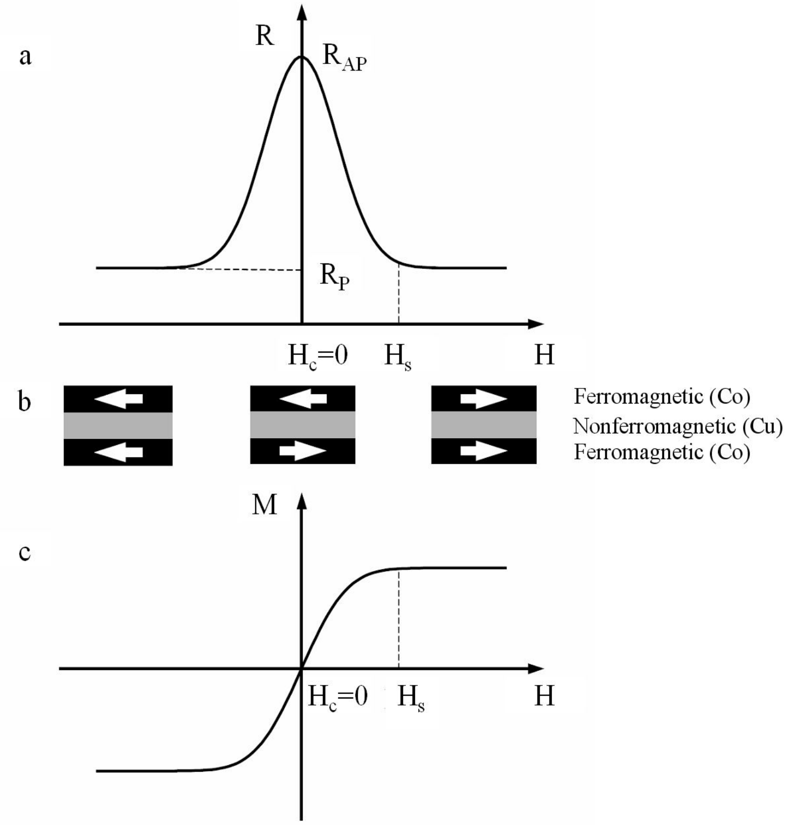

Figure 2-5 Schematic representation of the GMR effect: (a) resistance as a function of applied magnetic field, (b) the magnetization configurations of the multilayer at various magnetic fields and, and (c) the magnetization curve[35]

In the absence of the magnetic field, the internal magnetic (M) vectors of the neighboring ferromagnetic layers are aligned in an anti-parallel manner through the nonmagnetic interlayer by a quantum effect, which is the exchange coupling effect. When applying an external magnetic field, it aligns the magnetic moments in a parallel way, saturates the magnetization of the multilayer and then leads to a drop in the electrical resistance of the multilayer. **Figure 2-5** (a) and (c) are given for the case when the coercivity, H_c is zero, in an ideal case. In the electrodeposited films and vapor deposited ones the coercivity is not always zero, which creates a small hysteresis in the magnetoresistance curve and the M vs. H curve.

Mott's model[36] of the electrical conduction in ferromagnetic metals can be used to describe the governing features of GMR. First the electrical current in ferromagnetic metals is carried independently in two conduction channels that correspond predominately to the spin-up and spin-down s-p electrons. The up-spin and down-spin electrons do not mix over long distances and, consequently, the electrical conduction occurs in parallel for the two spin channels. Secondly, whatever the nature of the scattering centers, the scattering rates of the up-spin and down-spin electrons are quite different due to the fact that the scattering rates are spin-dependent. Therefore, the conductivity can be significantly different in the two channels.

The behavior is depicted by a two-current series resistor model. It is assumed that the scattering is strong for electrons with spin antiparallel to the magnetization direction, and is weak for electrons with spin parallel to the magnetization direction. Also the mean free path is much longer than the layer thicknesses and the net electric current flows in the plane of the layers. In the absence of an external magnetic field, neighboring ferromagnetic layers are aligned in an antiparallel manner (**Figure 2-6-a)**, both the up-spin and down-spin electrons are scattered strongly within one of the ferromagnetic layers, because within one of the layers the spin is

antiparallel to the magnetization direction. Since conduction occurs in parallel for the two spin channels, in this case the total resistivity of the multilayer is high.

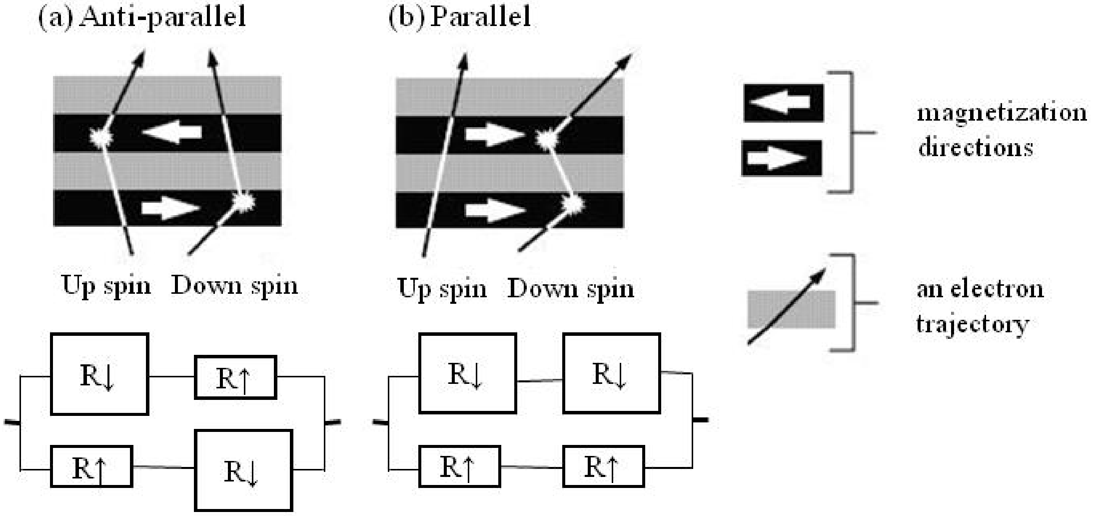

Figure 2-6 Schematic illustration of electron transport in a multilayer for antiparallel (a) and parallel (b) magnetizations of the successive ferromagnetic layers[35]

When applying an external magnetic field, the neighboring ferromagnetic layers are aligned in a parallel manner (**Figure 2-6-b)**. The up-spin electrons pass through the structure almost without scattering, because their spin is parallel to the magnetization of the layers. In contrast, the down-spin electrons are scattered strongly within both ferromagnetic layers. Therefore, the total resistivity of the multilayer is determined mainly by the highly-conductive up-spin electrons and appears to be low.[35]

According to different geometries in measurement, GMR can be listed into two categories: current-in-the-plane (CIP) geometry and current-perpendicular-to-the-plane (CPP) geometry. The current-in-the-plane CIP geometry is currently widely used in thin film structures in industrial application. While, measuring the current perpendicular to the multilayer plane is very difficult due to the very small thickness of the multilayer and consequently the very low resistance, which is difficult to detect. However, CPP is very attractive because its magnitude is

higher than the corresponding magnitude of CIP GMR. One way to engineer the CPP mode is to use nanowires. As an example, electrodeposited multilayered nanowires grown within a polycarbonate membrane constitute a new medium in which GMR perpendicular to the plane of the multilayers can be measured. A CPP GMR of at least 22 % at ambient temperature has been reported in CoNiCu/Cu multilayered nanowires.[37]

2.4 MR of Au/Co System

For the last few years, a large number of studies have been devoted to ferromagnetic metallic layers which have been widely used as components of thin films, sandwiches and multilayer structures. Many new magnetic properties have emerged from these materials: large perpendicular anisotropy, giant magnetoresistance effect due to the spin-valve effect,[38] oscillation in the coupling between two ferromagnetic layers through a non-magnetic spacer layer. In the scope of these features, Au/Co multilayers, fabricated by different methods on different substrates,[39] have already attracted much interest.

Based on reported literature findings, the magnetoresistance (MR) change of Co/Au system is lower than that of Co/Cu system. For example, Velu *et al.*[8] reported the MR effects of perpendicular magnetic Co/Au sandwiches, which was fabricated by ultrahigh vacuum evaporation on a glass substrate with very small surface roughness; the maximum resistivity appeared at the coercive field H_c of a few 10^2 G and the MR ratio was about 3 % at 4.2 K. Later, Velu *et al.*[40] extended the measurement of the MR to even lower temperature. At 1.4 K, the MR ratios for Au/Co (0.66 nm)/Au (5 nm)/Co (0.34 nm)/Au and Au/Co (0.2 nm)/Au (4.7 nm)/Co (0.6 nm)/Au were 5.3 % and 5.7 % respectively. Different mechanisms were proposed by Takahata *et al.*[41] and Vavra *et al.*[42] for perpendicular magnetic Co/Au multilayers.

Grolier *et al.*[43] studied the thickness of the gold spacer layer in the bilayer Au/Co/Au/Co/Au and found that at 1.2 nm antiferromagnetic coupling occurred between the two cobalt layers. The MR ratio ΔR/R was equal to 2.5 % at 300 K. Araki *et al.*[44] reported a maximum change of MR of 4 % at 77 K. Honda *et al.*[45] reported that Co/Au multilayers exhibited GMR consisting of hysteretic and nonhysteretic components. The former arose from antiparallel spin alignment between the adjacent Co layers due to the random wall position layer by layer, and the latter is related to the granular-type GMR. The MR ratio of the hysteretic component increased up to 20 % at 4.2K from the negligibly small value at room temperature. This temperature dependence is similar to that for the perpendicular giant magnetoresistance of multilayer Co/Cu nanowires.[46]

Barnas *et al.*[47] carried out theoretical and experimental studies on novel magnetoresistance effects in Fe/Cr and Au/Co multilayers. They fabricated Co/Au/Co double layers on GaAs, with the Au interlayers were thick enough to avoid exchange coupling between the Co films. Only at sufficiently high magnetic fields, the magnetic alignments of both ferromagnetic films change from antiparallel to parallel. In the same study, they concluded, that for magnetoresistivity in Co/Au/Co structures, the antiparallel alignment was achieved by different coercive fields of the Co films and not by an antiferromagnetic exchange coupling between the ferromagnetic films, as in the case of the Fe/Cr layered structures.

Oscillation of magnetoresistance as the thickness of the nonferromagnetic spacer layers, between the ferromagnetic layers, increases is a signature of GMR. The oscillatory coupling between ferromagnetic layers through a nonmagnetic (NM) metallic spacer layer, was first observed on rare-earth[48] and transition metal[49] multilayers, has been shown to be a fairly general behavior.[50] The oscillating GMR depends on the nature of the magnetic metal and on

the growth direction of the multilayer. Based on experimentally determined Fermi surfaces of the bulk metals, quantitative prediction can be made for noble metal spacer layers. The oscillation period was typically about 1 nm. The magnetic coupling was shown to oscillate between antiferromagnetic and ferromagnetic so that the magnetic moment of successive ferromagnetic layers were either parallel (ferromagnetic) or antiparallel (antiferromagnetic) in small magnetic fields.

Bartenlian *et al.*[51] first reported the unambiguous evidence of oscillatory coupling in Co/Au (111)/Co trilayers. The maximum MR ratio was 2 %. Both the oscillation period and the dependence of the coupling strength on the spacer layer thickness are in good agreement with theoretical predictions based on a (Ruderman-Kittel-Kasuya-Yosida) RKKY model.[52] Parkin *et al.*[53] studied the oscillations of interlayer exchange coupling and GMR in (111) oriented permalloy/Au multilayers. They found the oscillation period is around 10 Å, which is significantly shorter than the period of 11.5 Å predicted in RKKY based models. Roussigne *et al.*[54] also observed the oscillatory behavior of the interlayer exchange interactions in Co/Au/Co sandwiches and a pseudo-period of 9.6 Å was reported.

GMR effects not only occur due to a multilayer structure, but also could occur in the metal/metal granular systems. As Baibich *et al.*[30] reported, the granular alloy with GMR should consist of ferromagnetic single domain particles embedded in a nonmagnetic well-conducting matrix in order to substitute for the role of the ferromagnetic layers in multilayered systems. As long as the particle size as well as the interparticle distance of these ferromagnetic particles is less than or comparable to the electron mean free path, a large magnetoresistance was anticipated due to the same spin-dependent scattering mechanism, which was already established for multilayers. Hutten *et al.*[9] investigated the melt-spun $Au_{71.6}Co_{28.4}$ granular structures and the highest GMR amplitude ΔR/R was reported to be 2.4 % at 10 K and decreased to about 1 % at

room temperature. At relatively low fields, the MR rapidly decreased with increasing external field starting from zero field up to about 0.5 T. This high field dependence of metal/metal granular systems was originated from small ferromagnetic clusters (Co) distributed within the nonmagnetic well-conducting matrix phase (Au). Kolb *et al.*[55] also fabricated granular multilayers by MBE for both magnetization and MR measurements. At 300 K, the MR is only less than 2 % at high fields up to 10 T.

2.5 Etching of Alloy Nanostructures

For the last few years, solid metallic nanoparticles have been exploited for a wide range of applications that take advantage of their high surface-to-volume ratio. Recently there has been increasing interest in the anisotropic properties of nanorods and nanowires. In contrast to nanoparticles, nanoporous nanowires have a high surface area and well-defined pore morphology. Furthermore, nanoporous segments can be incorporated into multi-segment nanowires. Those nanowires with enhanced surface area and modified surface morphology are of interest due to potential applications in surface reactions, immobilizing molecules, BioMEMS and nanoelectronics.

2.5.1 Wet-chemical Etching

Nanoporous structures are formed when a single phase binary alloy containing a noble metal is etched in a suitable solution. To date, etching of nanowires has been carried out via chemical dissolution with a strong acid[16, 17] (e.g. HNO_3) or alkaline[18] solutions (e.g. ammonium hydroxide), usually in the presence of oxidizing agents. Usually there are two modes of formation of porous structures by anodic dissolution: (a) simultaneous dissolution of the two constituent metals of the alloy, or (b) preferential dissolution of the less noble metal of the alloy with the more noble metal accumulating on the alloy surface.[56] For the latter mode, it is

necessary that the difference between the single electrode potentials of the constituent metals in the electrolyte, involving complexing agents, is sufficiently large, i.e., several times greater than RT/F (where R, T, and F are the gas constant, temperature and Faraday constant, respectively), and that the potential of the dissolving alloy is higher than that of the less noble metal A, and significantly lower than that of the more noble metal B. Dealloying processes are of interest because a high surface area, and the porous layer of the remaining more noble metal can be produced in a variety of systems, e.g. Cu-Zn, Cu-Al, Au-Ag and Au-Cu.[19-21]

Ji and Searson[16, 17] reported a method for the fabrication of Au-Ag nanoporous nanowires with high surface area and well-defined pore morphology. The Au-Ag system is of interest because Au and Ag both have face-centered-cubic structures with similar lattice parameters and exhibit solid solubility across the entire composition range. Two processing steps are involved in the fabrication of nanoporous nanowires. First a single-phase, binary Au-Ag alloy is electrochemically deposited into a nanoporous template from a solution containing 100 mM $KAg(CN)_2$, 20 mM $KAu(CN)_2$, and 0.25 M Na_2CO_3 (Ph 13) or from a solution containing 50 mM $KAg(CN)_2$, 20 mM $KAu(CN)_2$, and 0.25 Na_2CO_3 (Ph 13) at -1.2 V (vs. Ag/AgCl). Second, the solid nanowires are then removed from the template and one component is chemically etched from the alloy. The Au-Ag alloy nanowires were etched with concentrated nitric acid. The porosity and morphology of the nanoporous nanowires can be controlled by varying the composition of the Au-Ag alloy.

This approach can be applied to other systems as long as two requirements are met. First, a procedure for electrodeposition of a suitable single-phase binary alloy in the relevant composition range must be developed. Second, the element that forms the nanoporous structure must be stable in a solution that will etch the other component.

Qin *et. al.*[18] later reported a novel, controllable and high-yielding lithographic process that allows one to generate designed gap structures on nanowires templates. This procedure, termed on-wire lithography, combines advances in template-directed synthesis of nanowires with electrochemical deposition and wet-chemical etching and allows routine fabrication of face-to-face disk arrays and gap structures in the range of five to several hundred nanometers. In their research, Au-Ag and Au-Ni systems were tested. First, Au-Ag and Au-Ni nanowires were electrochemically deposited in porous alumina templates in a controlled fashion from suitable plating solutions. Then the nanowires were released from the template by dissolution of the template. Finally the Ni segments were removed from Au-Ni wires by selective wet-chemical etching in concentrated HNO_3 for 1 hour, and the Ag segments were removed by treating the Au-Ag wires with an etching solution consisting of methanol, 30 % ammonium hydroxide, and 30 % hydrogen peroxide (4:1:1 v/v/v) for 1 hour. Using this procedure, they fabricated nanowires with designed gaps of 5, 25, 40, 50, 70, 100, 140, 200 nm. The transport properties of 13-nanometer gaps with and without nanoscopic amounts of conducting polymer deposited within by dip-pen nanolithography were also studied.

The disadvantages of the chemical etching processes are *i*. there is little control over the etching and *ii.* there can be an evolution of harmful gases and byproducts due to the strong acids, bases and oxidizing agents in the solutions. Comparatively, the electrochemical anodization etching process can help circumvent these problems. In electrolytic or anodic etching, an electrical potential is applied to the specimen by means of an external circuit. Typical setup consists of the specimen (anode) and its counter electrode (cathode) immersed in an electrolyte. The dissolution can be controlled more precisely by control of the applied charge and it can be carried out in more benign solutions.

2.5.2 Electrochemical Etching

As a classic surface processing technique, electrochemical etching has been recently used to etch at the nanoscale. For example, Wang *et al.*[57] developed a new synthetic approach to fabricate Ni/Cu nanocable arrays by co-depositing nickel around a copper core and then selectively etching the copper. The formation of the Ni-shelled Ni/Cu nanocables was achieved by adsorbing Ni ions on the pore walls of anodic alumina oxide membrane (AAO) templates by chemical complexation. Ni/Cu nanocables consisting of Ni nanotubes filled with copper cores were electrodeposited into the AAO template from solution containing 0.4 M $Ni(H_2NSO_3)_2 \cdot 4H_20$, 0.05 M $CuSO_4 \cdot 5H_2O$, and 0.1 M H_3BO_3. Then the copper cores in the nanocables were selectively etched at +1.5 V vs. Ag/AgCl for 3 h in the same electrolyte to form Ni nanotubes. With this technique, the length of nanocables and nanotubes, the wall thickness, and the wall surface morphology of nanotubes can be easily controlled by varying the electrodeposition parameters.

Lim *et al.*[58] demonstrated that micropatterns of copper films can be fabricated by selective electrochemical etching of copper using microcontact printing of self-assembled monolayers (SAMS). In other words, the self-assembled alkanethiolate monolayer films can be a resist material for the electrochemical etching of copper. The composition of the electrochemical etchant for copper is copper sulfate pentahydrate 250 g/L, sulfuric acid 70 g/L, and sodium chloride 0.05~0.10 g/L in water and the electrochemical etching was done at room temperature.

Yi *et al.*[59] reported a new method which combines micro-electro-discharge machining (micro-EDM) and electrochemical etching (ECE) to fabricate high aspect-ratio and a high resolution stainless steel shadow for organic thin-film transistors (OTFTs). First, square holes are serially machined using micro-EDM. Then, the ECE process was used to reduce the spacing of

holes, which can be reduced down to 3.6 micron. Electrochemical etching (ECE) is basically an isotropic machining process. This characteristic of ECE prevents the production of a straight wall and high aspect ratios, whereas it can be effectively used to uniformly decrease the dimension of the structure already perforated. That is why ECE was used to decrease the width of the wall after micro-EDM. At the applied voltage of 1.2 V (vs. SCE) and with 0.1 M H_2SO_4 solution, the etching rate was 19 nm/min.

Another example of etching at the nanoscale is the preparation of STM tips. Ren *et al.*[60] reported a method of preparing gold scanning tunneling microscopy (STM) tips by direct current electrochemical etching in concentrated HCl and ethanol solution. Gold can be etched with a CN^- or Cl^- containing solution. However the former requires a high voltage and CN^- is very toxic although it produces a smooth surface. The advantage of the HCl etching method is its low etching voltage, e.g., 3.0 V. According to their previous study, in order to etch the gold in HCl solution, the voltage should be higher than 1.4 V. A higher voltage leads to a faster reaction rate but also to side reactions including the evolution of Cl_2 and O_2. The latter effect causes severe bubbling resulting in a rough surface structure. Considering the role of ethanol in the silicon industry, where ethanol is used to reduce the bubbling and, hence to produce a smooth surface during the etching process, in this study, they also added a certain amount of ethanol to an HCl solution to reduce the bubbling effect with the aim to obtain a smooth gold surface. Finally, tips with radii around or smaller than 30 nm and smooth surfaces can be reproducibly produced by etching in a solution mixed by fuming HCl and ethanol (1:1) using dc electrochemical method at 2.2 to 2.4 V.

Albonetti *et al.*[61] described a straightforward electrochemical method for fabricating sharp cobalt tips. The interest in Co lies in the fact that it is a ferromagnetic metal at room temperature (Curie temperature: 1388 K) with a polarization degree P > 10 % at the Fermi level

making it very attractive for spin polarized scanning tunneling microscopy (SPSTM). The formation of a homogeneous thin oxide layer in air at room temperature prevents Co from further oxidation assuring very low degradation of the tips. Co tips were prepared from 0.25 mm diameter Co wire by electrochemical etching. A KCl (2 M in water) solution was used as the electrolyte at 2.5-3 V dc voltage. During the etching process, the electrolyte film shows a variety of color ranging from blue to pink. This indicates that the oxidation of Co in the presence of Cl^- ions leads to the formation of a variety of Co coordinated complexes, from nonhydrated chemical species, like tetrahedral $CoCl_4^{2-}$ (blue), to fully hydrated species, like octahedral $Co(H_2O)_6^{2+}$ (pink). After electrochemical etching the tips have to be washed first in distilled water in order to eliminate salts and then rinsed by isopropanol and petroleum ether (distilled) to eliminate organic contaminants. The opening angle of the Co tips obtained with this method is usually less then 20^o, while the mean value for the apex radius is about 30 nm, which is comparable to that of etched W tips. Those tips were successfully used in STM experiments with many samples in air.

Albonetti *et al.*[62] further developed a procedure to obtain high quality tips from wires of different materials such as Co and Ni. The procedure described here is a modification of an etching technique that allows us to prepare high-quality tips of a variety of materials. A Co or Ni wire is placed in the center of a Pt ring and fixed by a clamp at the upper end. The length of the wire under the ring is about 30 mm. At lower end of the wire, a small sphere of clay is attached (10 mm radius and mass about 2 g). The wire-Pt ring system is immersed in a beaker filled with 1 M KCl solution. The wire is the anode and Pt ring is the cathode. The bias voltage is 1 V for Ni, 3 V for Co. The mass of the sphere is crucial for the sharpness of both tips. When the etching process is complete, the lower part of the wire is stripped from the top one due to gravity. In this way, two tips are obtained. In the 1 M KCl solution, Co or Ni oxidation is thermodynamically

favored compared to water oxidation. The shapes of Co and Ni tips are analyzed in two ways: by optical microscopy at micrometer resolution and by scanning electron microscopy (SEM) at higher resolution.

Cavallini and Biscarini[63] reported a fast and simple method for the electrochemical preparation of sharp Ni tips for spin polarized scanning tunneling microscopy (STM). Ni tips combine the advantage of both Pt/Ir tips, since they are oxide free, and of W tips because of the greater reproducibility and control of the tip apex by means of the etching protocol, as compared with freshly cut tips. Ni tips were prepared from 0.25 mm diameter Ni wire by electrochemical etching. A 2 M KCl solution was used as the electrolyte at 2-2.5 V dc voltage. In the 2 M KCl solution, Ni oxidation is thermodynamically favored with respect to water oxidation. The performance of Ni tips in achieving atomic resolution is comparable to that of cut Pt/Ir or freshly etched W tips.

Nam *et al.*[64] established, in a systematic manner, some relatively benign electrolyte solutions, concentrations, and voltages suitable for making sharp tips of Pt, Ir, Au, Rh, and Pd. They mainly used aqueous solutions of $CaCl_2$, NaCl, KCl, NaBr, and occasionally tried HCl or another electrolyte. Only ac voltages were used.

Iwami *et al.*[65] reported a reliable preparation method of silver tips for scanning tunneling microscopy imaging with atomic resolution. The procedure was based on two-step electrochemical processing: ac electropolishing and subsequent dc electroetching. The first step was electropolishing of the wire to form the main taper of the tip and an ac voltage of 19 V was applied to the cell. The second step was electroetching of the tip to remove surface contamination and a dc voltage of 5 V was applied for a few seconds to the cell with the tip positive. A typical tip apex curvature obtained by this procedure was roughly 1 micron.

Muller *et al.*[66] investigated the shape and composition of electrochemically etched tungsten tips for use in scanning tunneling microscopy (STM) by transmission electron microscope (TEM) with a Gathan imaging filter (GIP). The tips were prepared by a lamella drop-off technique. The tip preparation was done in a 2 M NaOH solution at a dc voltage of 2-3 V. the highly resolved TEM image showed that the W tips consisted of polycrystalline material and the tip diameters were between 4 and 15 nm.

In this work, electrochemical etching of multilayers is examined, similar to tip preparation. The potential of the working electrode is controlled versus a reference electrode, and not the cell potential. Guided by previous electrochemical etching of Ni and Co wires in a KCl solution, our work will utilize a KCl electrolyte.

CHAPTER 3 EXPERIMENTAL

3.1 Nanowire and Nanotubes Electrodeposition

3.1.1 Electrolyte

In the electrodeposition of AuCo alloys and Au/CoAu multilayered nanowires and/or nanotubes, single, sulfite Au/Co electrolytes were developed. As previously described, unlike conventional Au plating, this electrolyte has no cyanide complexes. Based on the electrolyte we previously used for thin films deposition with a rotating disk electrode (RDE)[4, 23], this new Au/Co electrolyte for nanowire deposition had more concentrated Au ions in order to compensate for the longer diffusion distance in AAO/polycarbonate membrane templates and thus improve the deposition rate, and current efficiency. In order to obtain alloys rich in cobalt, and to make it possible to fabricate multilayers, the cobalt concentration was kept in great excess to the gold concentration. The pH value was 6.15. Analytical grade reagents and deionized water of 18 mega ohms-cm were used in the solution preparation. Details are listed in **Table 3-1**.

Table 3-1 Composition of AuCo bath for nanowire electroplating

Constituent	***Concentration, mol/L***
$CoSO_4 \cdot 7H_2O$	0.29
KOH	1.78
Au (Techni ® Gold 25E)	0.00125
$C_6H_8O_4 \cdot H_2O$	0.47
pH = 6.15	

3.1.2 Cell Design

The schematic of the electroplating cell used for nanowire and nanotube electrodeposition is shown in **Figure 3-1**. A 4 × 4 cm platinum mesh is used as the anode, affixed to a plastic support. A saturated calomel electrode (SCE) is employed as a reference electrode. To minimize the ohmic drop, the reference electrode is placed close to the working electrode, but not too close to shield the cathode. The solution was agitated by a PTFE blade-type agitator controlled by PINE AFMSRX Rotator at 900 rpm.

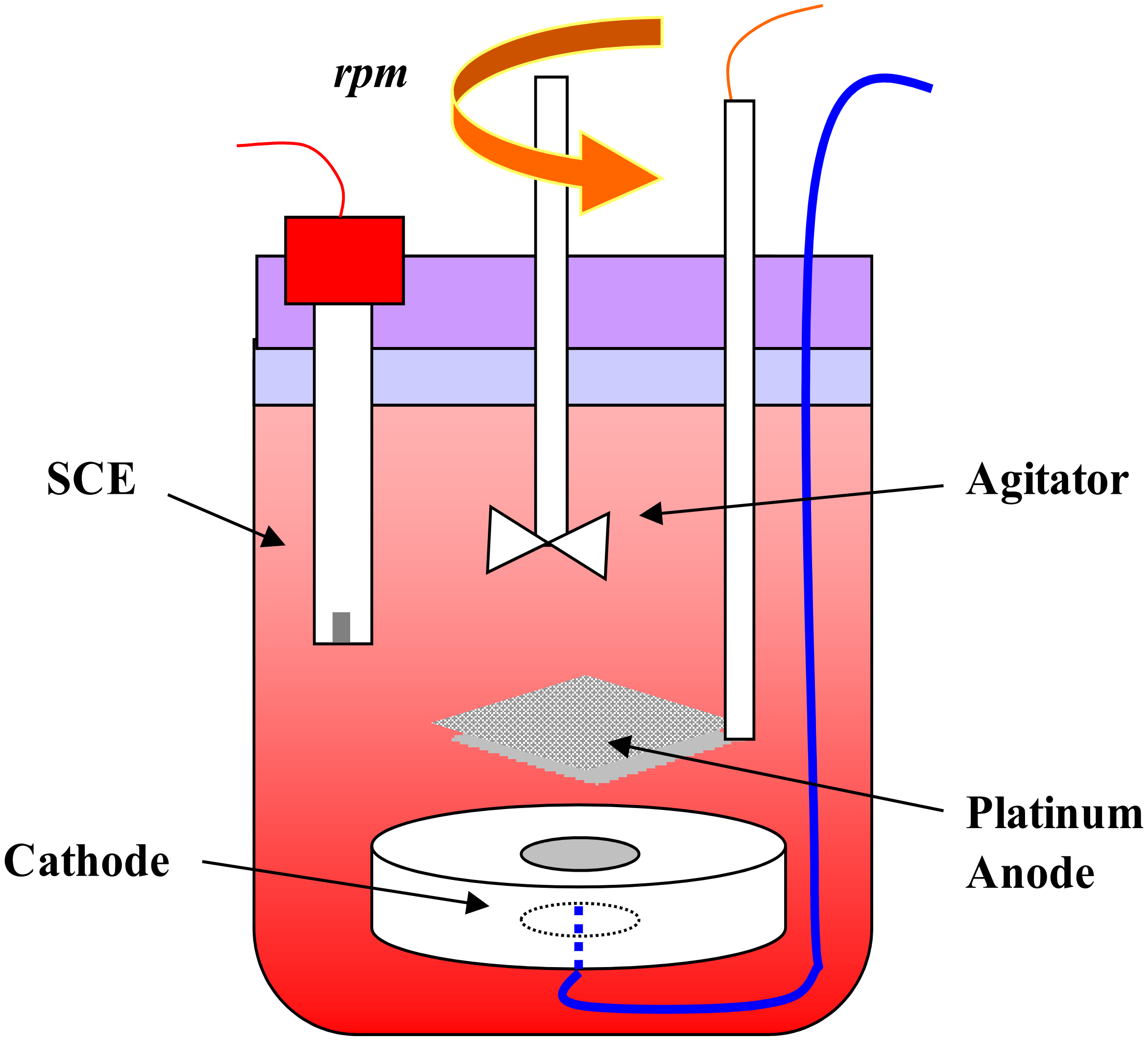

Figure 3-1 Schematic cell for nanowires electrodeposition

3.1.3 Working Electrode Holder Design

Figure 3-2 is a schematic of the electrode holder used for nanowire electroplating. This electrode holder is composed of two circular PEEK discs of radius 5.5 cm and thickness of 1.0 cm. The upper disc center is a round opening of diameter 1.5 cm, which provides a plating area of 1.767 cm^2. Through this circular hole, the substrate contacts with the electrolyte. On the back of the upper disc, two different O-rings were embedded in grooves to prevent the electrolyte from contacting the backside of the membrane.

A square stainless steel plate of 2.5 x 2.5 cm was embedded into a recess on the bottom plastic disc so that the entire surface was planar and conductive. Electrical contact was provided by means of an insulated copper wire to the back of the stainless steel plate, fixed and sealed with resin to insulate the bottom of the electrode from the electrolyte. The top and bottom pieces were fastened by six screws on the outer edge of the discs.

Anodic Alumina Oxide (AAO, Whatman® Anodisc®) and polycarbonate (Whatman® Nuclepore® and Osmonics Poretics®) membranes were used as templates for nanowire plating. Membranes having different pore sizes were tested, ranging from 0.01 μm to 2.0 μm. The deposition procedure is shown in **Figure 3-3**. Before plating, a layer of Au was sputtered onto one side of the membrane to serve as conductive substrate, **Figure 3-3(b)**, and to seal the nanometric pores. Then the membranes were fixed on the electrode holder, with the sputtered Au layer side contacted with the stainless steel electrode. As the plating proceeded, nanowires grew in the pores and filled up the pores, **Figure 3-3(c)**. After the nanowire plating, a solution of 1 M NaOH and another of dichloromethane were used to dissolve the AAO and polycarbonate membranes respectively, to release the nanowires for further analysis, **Figure 3-3(d)**.

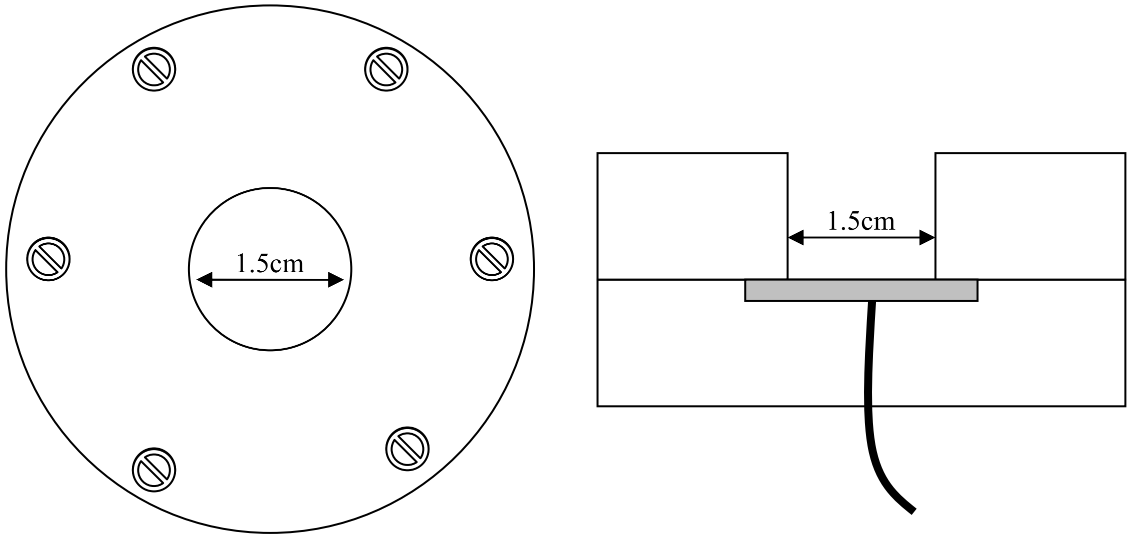

a. Top-view

b. Cross-section view

Figure 3-2 The stationary holder for nanowires electrodeposition

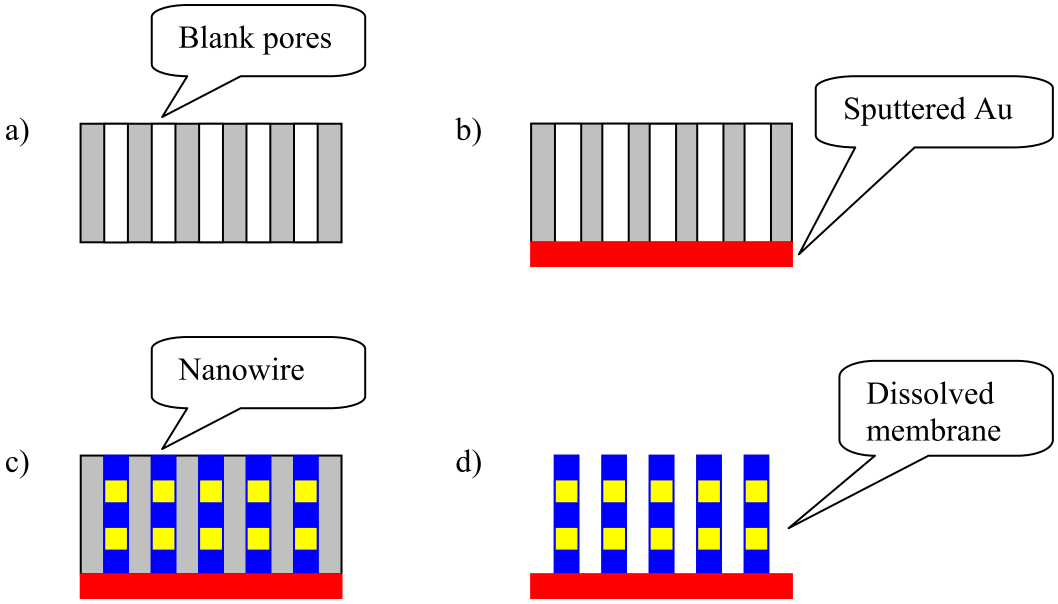

Figure 3-3 Nanowire growth procedure in AAO/polycarbonate membrane templates

3.2 Investigation of Electrochemical Etching Electrolyte

3.2.1 Rotating Disk Electrode (RDE)

A rotating disk electrode (RDE) is used in the Au/Co system experimental studies of the electrochemical deposition and etching due to (1) stable, laminar flow over a wide range of operating conditions, (2) uniform mass transport boundary layer thickness and (3) uniform limiting current density. As the disk rotated, fluid containing reactants is uniformly drawn towards its surface so that the reaction rate (current distribution) is uniform at the limiting current on the electrode. The Levich equation describes the relation between the boundary layer thickness and the rotation rate,

$$\delta_N = 1.61 \cdot D^{1/3} \cdot \omega^{-1/2} \cdot \nu^{1/6}$$

where δ_N is the boundary layer thickness, D is the diffusion coefficient, ω is the angular velocity and ν is the kinematic viscosity of the solution. In terms of the limiting current density the above equation can be recast, $i_{\lim} = nFDC^b / \delta$,

$$i_{\lim} = 0.62nFC^b D^{2/3} \nu^{-1/6} \omega^{1/2}$$

where $i_{\lim}$ is the limiting current density, n is the electrons transferred, F is the Faraday constant, and C^b is the bulk concentration.

The non-uniform current density distribution below the limiting current is one of the least desirable features of the RDE, which leads to edge effects, preferential plating on the edges of the disk. This effect is pronounced when the reaction rate is fast and mass transport is not dominating. Under these conditions, referred to as primary current distribution, the current

distribution is mostly determined by the electrolyte conductivity, geometry of the cell and the placement of the electrodes.

The RDE is placed in a PINE AFMSRX Rotator with precisely controlled rotation rate adjustable to within 1 % of the control setting over a range from 50 to 10,000 rpm.

3.2.2 Cell Design

The schematic of the electrochemical cell used for thin film deposition and/or etching is shown in **Figure 3-4**. The reaction kettle is a glass jar of 500 mL capacity. A copper rotating disk electrode (RDE) sputtered with a layer of pure Au with a diameter of 0.6 cm is used as the working electrode, where Co-rich CoAu alloy thin films are first plated and then electrochemically etched. A 4 x 4 cm platinum mesh is used as the counter electrode, affixed to a plastic support. A saturated calomel electrode (SCE) is employed as a reference electrode. To minimize the ohmic drop, the reference electrode is placed close to the working electrode, but not too close to shield the cathode. Potassium chloride (KCl) solutions with different concentrations will be tested for best etching results.

3.3 Nanowire and Thin Film Electrochemical Etching

3.3.1 Cell Set-up and Electrolyte

The electrochemical anodization process were performed in a three-electrode cell with a saturated calomel electrode (SCE) as reference electrode positioned close to the working electrode holder, and a platinum mesh (4 × 4 cm) as counter electrode, as shown in **Figure 3-5**. A 2 M KCl solution with pH 6.82 was used as the electrochemical etching electrolyte. All the experiments were carried out at room temperature.

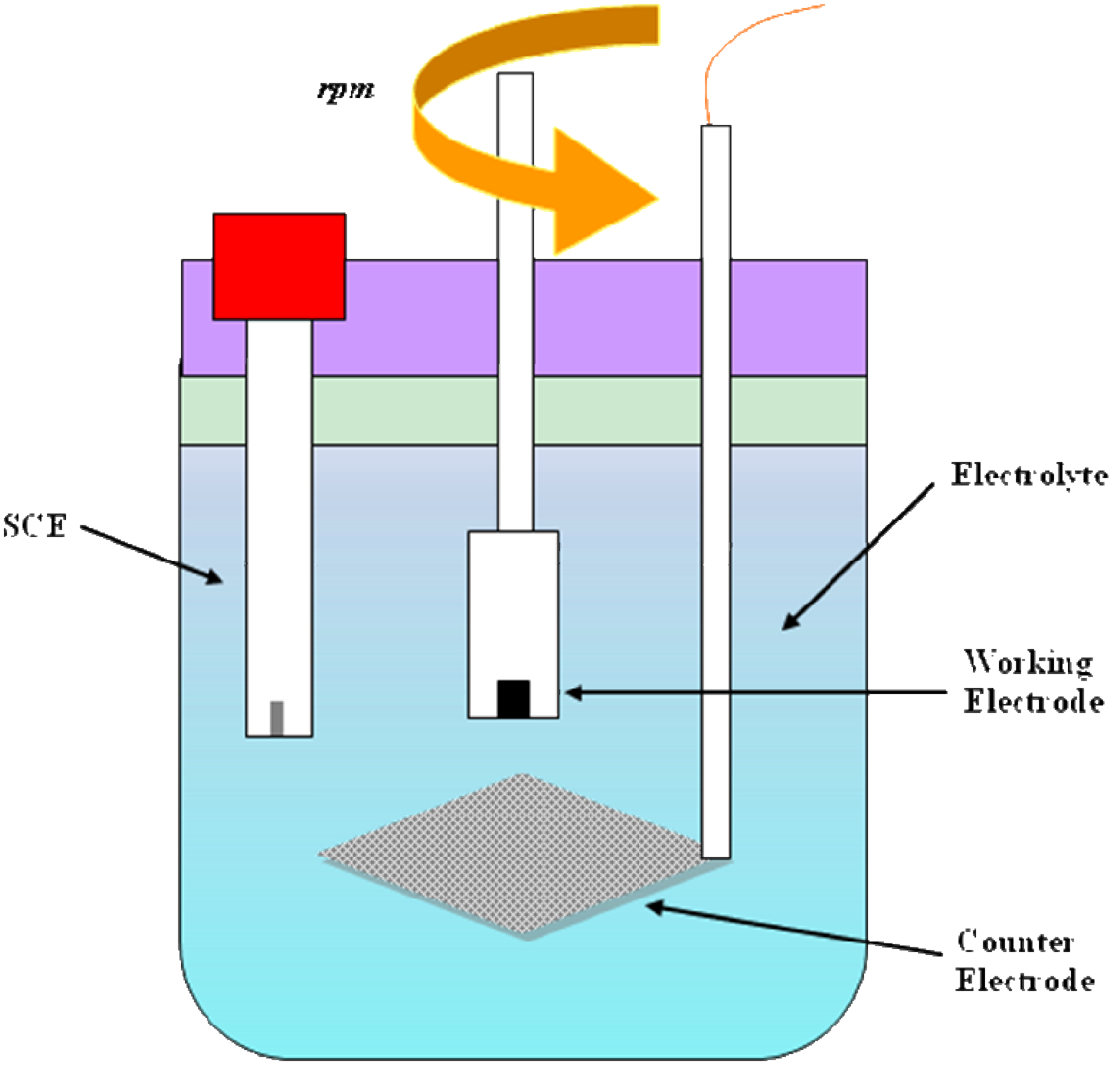

Figure 3-4 Schematic of the cell for the investigation of electrolyte for electrochemical etching on rotating disk electrode (RDE)

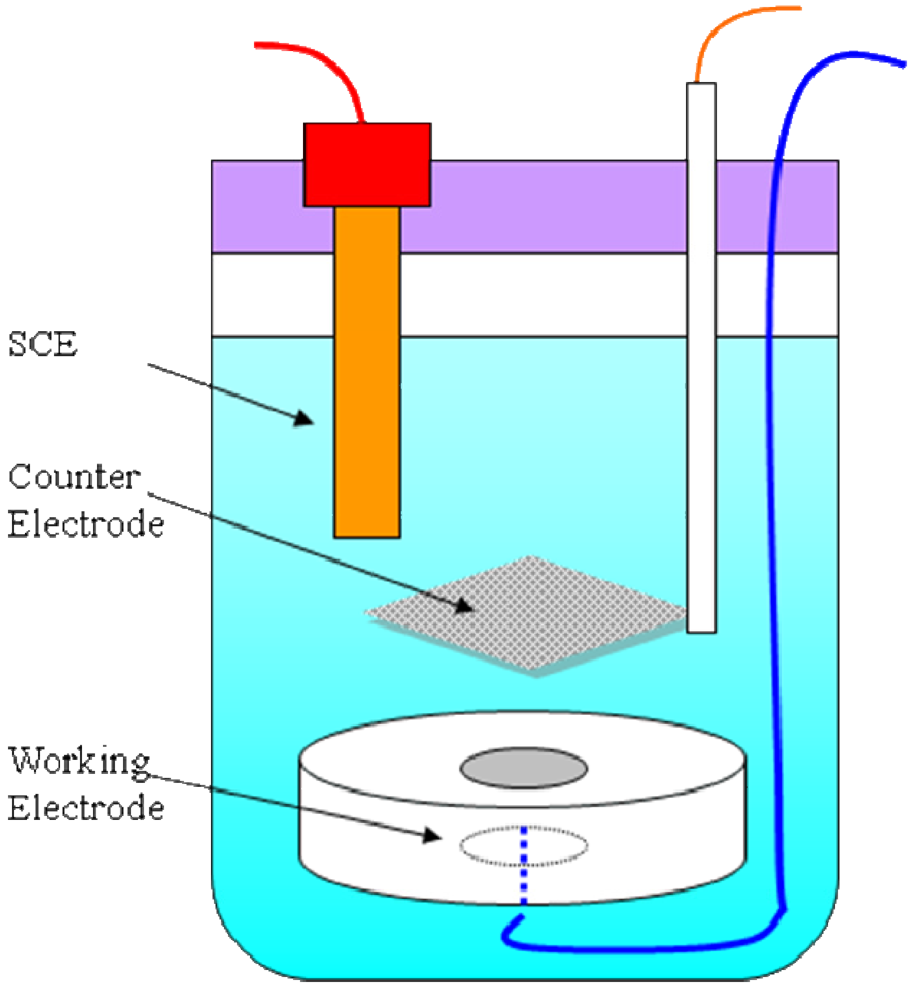

Figure 3-5 Schematic cell for nanowires, nanotubes, and thin film electrochemical etching

3.3.2 Working Electrode Design

After the Au/CoAu nanowires were electrodeposited and released from AAO/PC membrane, to electrochemically etch those nanowires, we were faced with two experimental challenges. The first one was to design a working electrode, on which surface those released single Au/CoAu nanowires/nanotubes could be fixed. And then, when passing positive current, only the Au/CoAu nanowires or nanotube were electrochemically etched, but the working electrode surface was unattacked.

3.3.2.1 Nanowires Fixed by Magnetic Force

The Au/CoAu nanowires can be regarded as tiny magnets; they are very sensitive to magnetic fields. When a small amount of Au/CoAu nanowires was suspended in ethanol, they dispersed randomly in the solvent as shown in **Figure 3-6 (A)**. Nevertheless, when a weak magnetic field was applied (by placing a small magnet on the left of the container), the Au/CoAu started to gather and assemble into an ordered pattern (the long axis of the Au/CoAu nanowires aligned toward the magnet), as shown **Figure 3-6 (B**). By increasing the magnetic field (moving the magnet close to the container), the nanowires get closer to each other and also aligned with their long axis toward the magnet (**Figure 3-6 (C)**). These phenomena suggested that the spin orientation of these Au/CoAu nanowires is along the long axis.

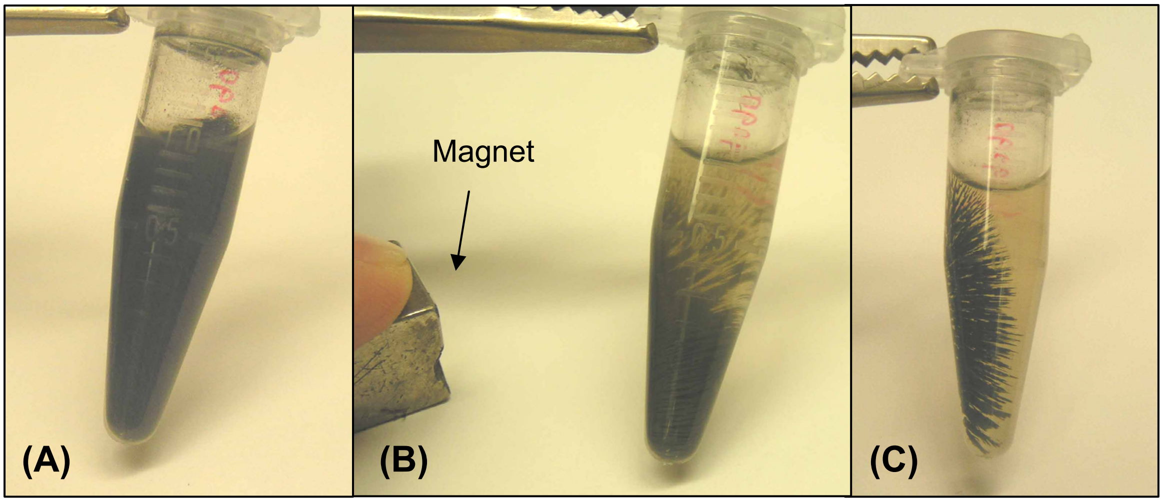

Figure 3-6 The photographs of Au/CoAu nanowires in ethanol solution: (a) without magnetic field, (b) under weak magnetic field, and (c) under strong magnetic field

Based on the tiny magnetic property, a working electrode shown in **Figure 3-7** was designed. It is composed of four parts. A stainless steel plate of 2.5 × 2.5 cm was placed on the bottom, and a small hole of diameter 5 mm was drilled through the center of the stainless steel plate. A disc magnet with a diameter of 4 mm was then put in the hole to provide magnetic field. On top of the stainless steel plate with a magnet in its center, a piece of Au foil (2.5 × 2.5 cm) or

Au-sputtered copper foil was attached, which behaves as a substrate on which a drop of nanowires/nanotubes suspension in ethanol was placed. Because of the disc magnet underneath, the released Au/CoAu nanowires/nanotubes would be attached to the substrate. After the ethanol solution dried completely, the working electrode was put into the stationary holder, shown in **Figure 3-2**, and the multilayered nanowires/nanotubes were ready for further selective electrochemical etching.

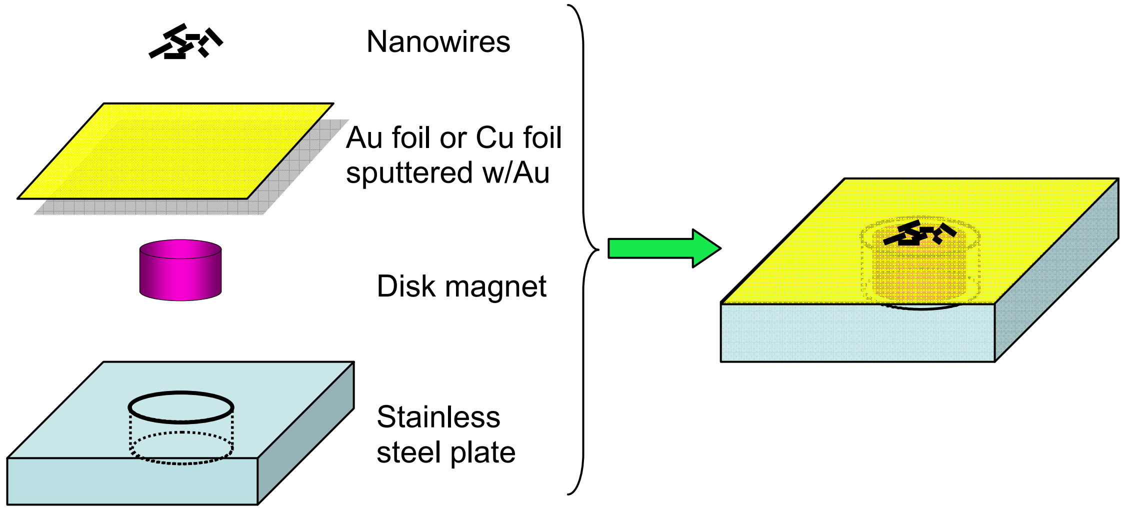

Figure 3-7 Schematic illustration of the working electrode of Au-sputtered copper foil, where nanowires/nanotubes were fixed by magnetic force

3.3.2.2 Nanowires Fixed by Carbon Conductive Tab

Another working electrode design had a more general application, shown in **Figure 3-8**, which could be used for both magnetic and nonmagnetic nanowires/nanotubes. Here, a double sided adhesive carbon conductive tab (from Electron Microscopy Science, diameter 9 mm) was employed to attach those released nanowires/nanotubes. As for this working electrode, a piece of Au foil (2.5 × 2.5 cm) or Au-sputtered copper foil was first put on top of the stainless steel plate of 2.5 × 2.5 cm. Then, the adhesive carbon conductive tab was stuck to Au foil. Then a drop of nanowires/nanotubes suspension in ethanol was put on the carbon tab substrate. After all the

ethanol evaporated, this carbon working electrode, on which nanowires and/or nanotubes attached, would be put into the stationary holder (**Figure 3-2**) for further selective etching.

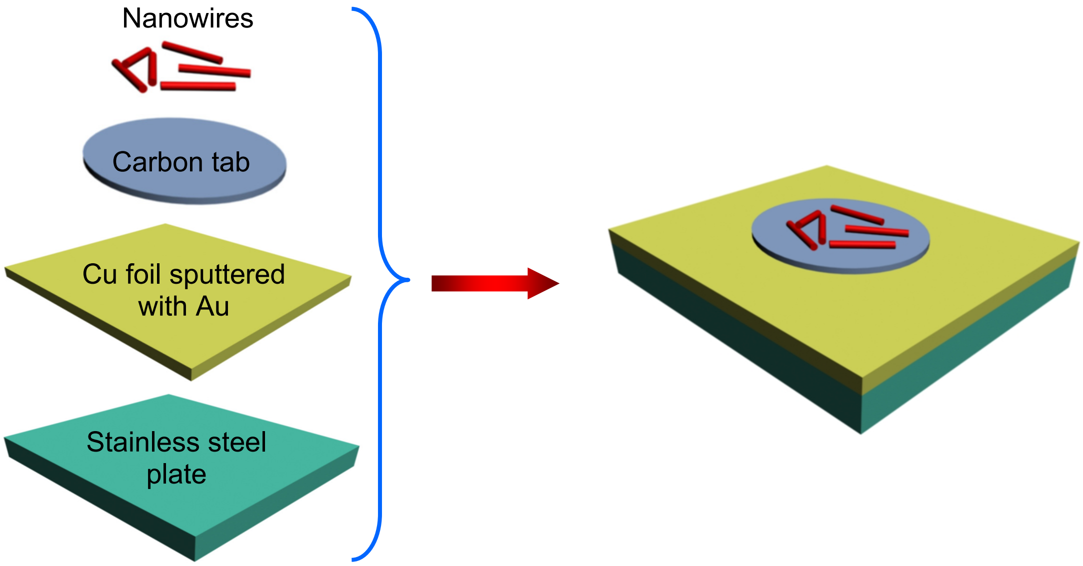

Figure 3-8 Schematic illustration of the working electrode of adhesive carbon conductive tab, where nanowires/nanotubes were stuck to

When comparing the merits of the above two working electrode configurations, the one using the carbon conductive tab seems to have wider applications in cases where there were no magnetic elements in the nanowire components, such as pure gold nanowires or semiconductor nanowires. Of course, when the electrochemical processing ended, nanowire samples fixed by the magnetic force are easy to release and transfer from the working electrode surface to other substrate for further analysis, such as a TEM grid. However, when etching was complete and only Au particles remained, the magnetic fixation method did not hold the particles in place.

3.3.2.3 Thin Film Electrochemical Etching

A stainless steel plate of 2.5 × 2.5 cm was used as the working electrode in the study of thin film electrochemical etching. The stainless steel electrodes were plated with Au to ensure matrix adhesion and to prevent substrate dissolution during anodic activity. The electrodes were

sanded smooth with sandpaper and rinsed in a 10 % v/v H_2SO_4 solution to clean the surface and to remove any oxide films. The Au solution (Techni ® Gold 25E by Technic Inc.), which is the same as the Au solution used in the electrodeposition of Au/CoAu nanowires, were heated to and maintained at 65°C using a temperature bath for the experiment. A strike solution (Acid Gold Strike by Technic Inc.) was need to pretreat the electrode surface and was kept at room temperature. The electrodes were plated at an agitation rate of 600 rpm. A Pt mesh counter electrode was used during the procedure.

The electrodes were DC plated in the Strike solution with an applied current density of -3.7 mA/cm^2 (-16.32 mA for 4.41 cm^2 electrode) for 3 minutes. The electrodes were then thoroughly rinsed with deionized water. Next, the electrodes were DC plated in the 65 °C Au solution with an applied current density of -1.06 mA/cm^2 (-4.67 mA for a 4.41 cm^2 electrode) for 40 minutes. This produced a Au layer approximately 1.33 μm thick.

3.4 Methods and Characterization

3.4.1 Polarization Curves

The polarization curve, the steady state relationship between current density and the applied potential, was determined on a Bas-Zahner IM6 Zahner® unit with a sweep rate of 2 mV/s and 100 mV/s for non-steady cyclic voltammetry. The potential sweep started at open circuit potential (OCP) and ended at 2 V vs. SCE. A copper rotating disk electrode (RDE) sputtered with a thick layer of Au was employed.

3.4.2 XRF

A Kevex Omicron X-ray fluorescence (XRF) unit, as shown in **Figure 3-9**, is used to measure the composition and thickness of the deposited alloy films. The XRF uses the energy-dispersive X-ray spectrometry (EDS) analytical method to analyze the elements. The x-ray

radiation, produced by an X-ray source consisting of an electron gun and a target sealed inside a vacuum envelop, is directed at the deposit and the energy emitted from the deposit is measured, which is proportional to the deposit thickness. The detected x-rays are presented as a spectrum. After calibrating with known standards, the composition of the alloy film can be determined. In this Kevex Omicron XRF, the collimator size is 100 μm, and the x-ray conditions were adjusted in an air environment to achieve a detector dead time around 50 %. The composition is integrated and averaged from 6 points scanned along the diameter of each rotating disk electrode and nanowire membrane.

Figure 3-9 Kevex Omicron X-ray fluorescence (XRF)[67]

3.4.3 XRD

A Bruker/Siemens D5000 dual goniometer X-ray diffractometer in Department of Geology and Geophysics, LSU, as shown in **Figure 3-10**, was used to characterize the

crystallographic structure, chemical composition, and physical properties of AuCu nanostructures. A Cu K_α radiation source was employed.

Figure 3-10 Bruker/Siemens D5000 X-ray diffraction (XRD)

X-ray diffraction (XRD) is a versatile, non-destructive technique that reveals detailed information about the chemical composition and crystallographic structure of natural and manufactured materials. These techniques are based on observing the scattered intensity of an x-ray beam hitting a sample as a function of incident and scattered angle, polarization, and wavelength or energy. About 95 % of all solid materials can be described as crystalline. When X-rays interact with a crystalline substance (Phase), one gets a diffraction pattern. The X-ray diffraction pattern of a pure substance is, therefore, like a fingerprint of the substance. The powder diffraction method is thus ideally suited for characterization and identification of polycrystalline phases.

3.4.4 SEM

A Hitachi S-3600N extra-large chamber variable pressure Scanning Electron Microscope (VP-SEM) with an EDAX EDS system, as shown in **Figure 3-11**, located in LSU Materials Characterization Center (MC^2), was used to characterize the nanowires/nanotubes after electrochemical etching.

Figure 3-11 Variable pressure Scanning Electron Microscope (VP-SEM Hitachi S-3600N)

In the SEM, an incident electron beam (primary electrons) excites free electrons inside a specimen and the excited electrons (called the secondary electrons) are subsequently emitted from the specimen surface. The quantity of these secondary electrons, which are collected by a detector, changes with the location of the surface and contribute to variations in the image contrast. A protruding site produces more secondary electrons and thus appears white, whereas a flat region emitting fewer or zero electrons shows up black. As a result, surface irregularities can be seen as black-white images. The accelerating voltage used was 20~30 kV.

SEM specimens were in a vacuum environment. The acrylic resin and alumina materials used in this study can also be examined if the surface is coated with a thin conducting film, such as gold or gold-palladium. Furthermore, materials giving low-contrast will provide better images in terms of sharpness and resolution after being coated with a gold or gold-palladium film. In the work presented here, a two-minute sputtering time was sufficient to obtain a continuous coating film. The sputtering machine used was a Technics Hummer II Sputter Coater, located in Department of Geology and Geophysics, LSU.

3.4.5 TEM

Detailed nanostructure with size below 50 nm was examined with a JEOL 100-CX transmission electron microscopy (TEM), as shown in **Figure 3-12**, located in Socolofsky Microscopy Center in Department of Biological Sciences, LSU.

Figure 3-12 Transmission Electron Microscope (JEOL 100 CX TEM)[67]

TEM is able to resolve atomic features. The preparation procedures of nanowire specimens for the TEM includes: dissolving the membrane, rinsing by distilled water and then centrifugalizing the suspension three times. Finally a drop of the suspension was placed on a holey carbon grid film and allowed to dry.

When trying to distribute the magnetized Au/CoAu nanowires on the carbon grid for TEM analysis, due to the tiny magnetic property, these nanowires tend to stay together and tamper with the uniform distribution. A particular metal-stabilizing hydrophilic compound was employed, which is called sulfobetaine. This colloidal dispersion in water, or a hydrosol, can be made by attaching an SO^{3-} group to the end of one of the hydrocarbon chains of each NR^{4+} ion to make it hydrophilic or water attracting, as shown in **Figure 3-13**.

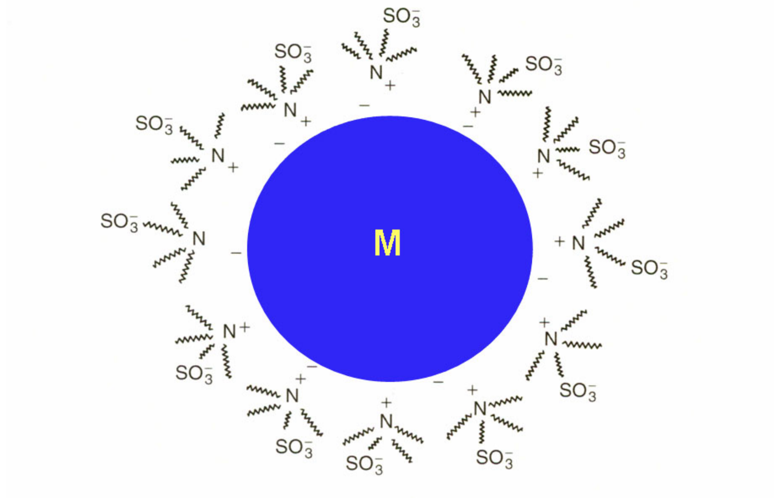

Figure 3-13 Metallic colloidal particle stabilized by sulfobetaine compounds related to NR$_4$X, but with an SO3$^-$ group at the end if one of the alkyl chains R[68]

3.4.6 Au Sputtering System

When preparing and processing samples in this work, pure Au thin films were widely employed. This Au sputtering system was a Technics Hummer II Sputter Coater, as shown in **Figure 3-14**, located in Department of Geology and Geophysics, LSU. A schematic

demonstration of a sputtering system is shown in the middle of **Figure 3-14**. A sputtering system is a vacuum chamber, which after it is pumped out, is re-filled with a low-pressure argon gas. A high voltage ionizes the gas, and creates what is known as the Crookes dark space near the cathode, which in our case, consists of a metal target made out of the metal we want to deposit. Almost all of the potential of the high-voltage supply appears across the dark space. (The glow discharge consists of argon ions and electrons which have been stripped off of them. Since there are about equal number of ions and electrons, the net charge density is about zero, and hence by Gauss' law, so is the field.)

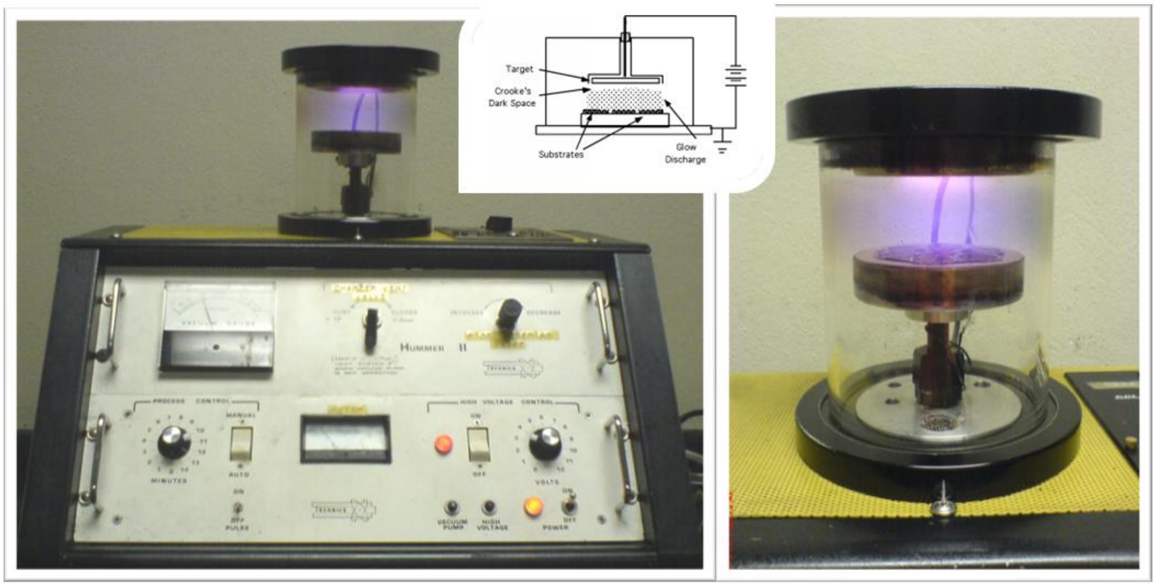

Figure 3-14 Technics Hummer II sputter deposition system: (Left) overview, (Right) Chamber with plasma on, and (Middle top) schematic demonstration of a sputtering system

3.4.7 Magnetic Measurements

The giant magnetoresistance (GMR) effect and coercivity were measured with a 9-Telsa quantum design physical properties measurement system (PPMS 6000) in Department of Physics and Astronomy, LSU, with an excitation current ranging between 0.1-1 mA and a magnetic field in between -1 T to 1 T. The GMR were measured at various temperatures, including room temperature, 77 K, and 10 K. **Figure 3-15** shows two pictures of the PPMS 6000 GMR

measurement setup, (a) overview of this system, and (b) Pt. contact on membrane containing nanowires. When measuring the CPP GMR, the magnetic field was perpendicular to the electric current passing through the nanowires, the magnetic field being parallel to the layers. The multilayered nanowires showed fairly large electrical resistance, depending on the number of wires connected in parallel.

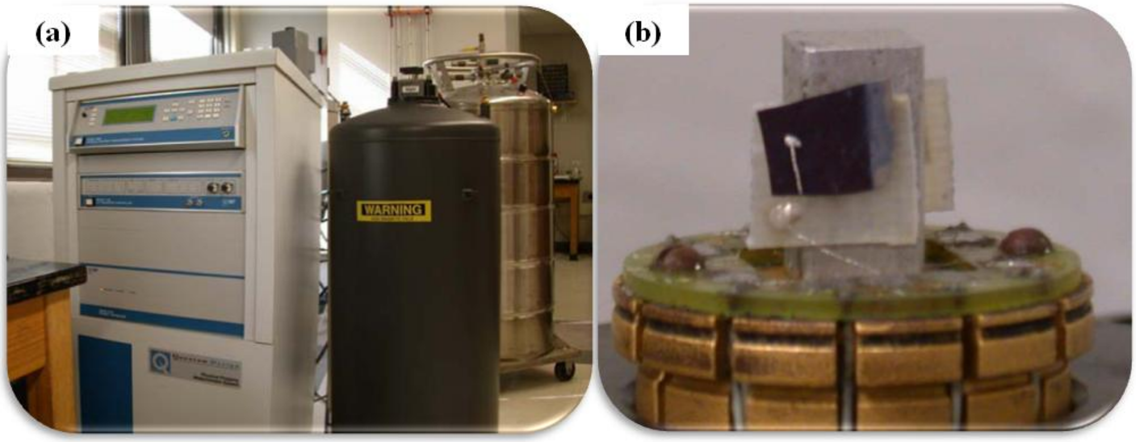

Figure 3-15 GMR characterization system: (a) overview of PPMS 6000 system, and (b) Pt. contact on membrane containing nanowires[69]

CHAPTER 4 RESULTS AND DISCUSSION

In a previous study by Guan[4, 23], a process of using a non-cyanide single bath to electrodeposit AuCo alloys and multilayers was characterized. In the AuCo sulfite electrolyte, the cobalt concentration was kept in great excess compared to gold in order to obtain alloys rich in cobalt at a high applied current density or potential, to obtain a gold deposit at a low applied current density or potential, and to make it possible to fabricate multilayers. The electrolyte stability, alloy compositions, current efficiencies and partial current densities were examined using a rotating disk electrode. The electrolyte for multilayer plating consisted of 0.67 M citric acid and 0.00042 M Au with pH of 6.15. When electrodepositing multilayered thin films, the Au content reaches 99.5 wt. % and the Co content is higher than 98.7 wt. % when the current density is lower than -1 mA/cm^2 and higher than -100 mA/cm^2, respectively.[23]

4.1 Electrodeposition of Nanowires

A modified Au/Co electrolyte for nanowire deposition was developed. It had more concentrated Au ions compared to the previous study in order to compensate for the longer diffusion distance in anodic aluminum oxide (AAO) or polycarbonate (PC) membrane templates. As before, the cobalt concentration was kept in great excess compared to the gold concentration in order to obtain alloys rich in cobalt and to make it possible to fabricate multilayered structures. In this AuCo electrochemical system, citric acid ($C_6H_8O_4 \cdot H_2O$) was used as an additive. The role of the citrate is twofold: to help maintain the pH at the electrode surface and to prevent precipitation of metal salts via complexation.[70] Details of this electrolyte were listed in **Table 3-1**.

Galvanostatically controlled electrodeposition was applied to obtain multilayered nanowire structures. The proper current densities for Au and Co electrodeposition were determined from a polarization curve (current verses applied potential) in a stationary electrode, as shown in **Figure 4-1**. The potential sweep range was from the open circuit potential (OCP), where the current is zero, to -2 V vs. SCE. The sweep rate was 2 mV/s and ohmic drop was corrected in this polarization curve. The membrane type was AAO with a pore size of 0.02 μm, and the Au-Co electrolyte composition was shown in **Table 3-1**.

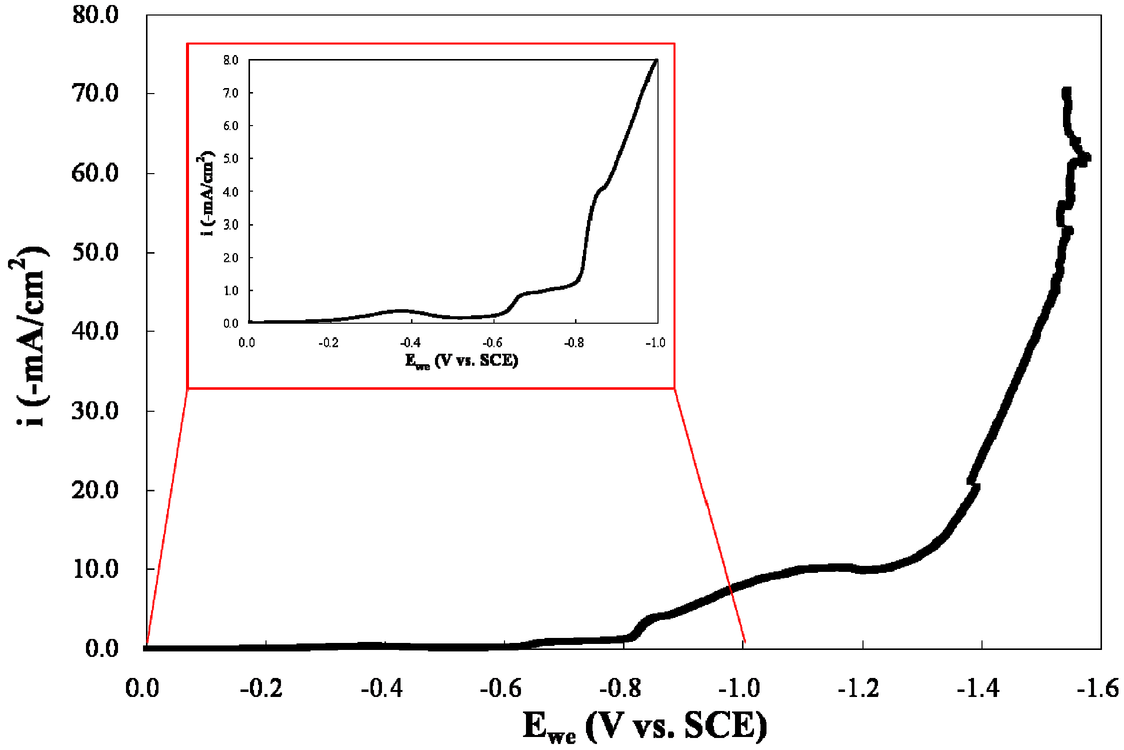

Figure 4-1 Polarization curve of Au-Co electrolyte for nanowire plating on 0.02 μm AAO membrane, sweep rate 2 mV/s

In this polarization curve, at potentials between OCP and -0.6 V vs. SCE, the reduction of Au (I) ions is the only main reaction and elemental Au will be deposited. When potentials are positive than -0.35 V vs. SCE, kinetics (or charge transfer), controls the Au reduction reaction. The rate of the reaction is then dependent upon the potential and concentrations of the species at

the surface of the electrode. As the potential becomes more negative, the limiting current plateau of the Au reduction reaction is reached which is characterized by the relatively flat portion of the polarization curve at steady state. Here the limiting current plateau of Au reduction is in the range of -0.35 to -0.6 V vs. SCE. As the potential becomes more negative than -0.6 V vs. SCE, the Co ions start to be reduced and as a result a CoAu alloy will be deposited. At even more negative potentials (-0.8 V vs. SCE) the current begins to increase significantly, indicating the onset of hydrogen evolution. Even though the main reaction rates are unchanged the current efficiency of the reduction system is lowered by the addition of the side reaction. It is therefore most desirable to operate in the region which minimizes other unwanted reactions.

Based on the polarization curve, a series of current densities were examined for electrodepositing AuCo alloy nanowires in anodic oxidized alumina (AAO) membranes with a pore size of 0.02 μm from the bath containing 0.00125 M Au (I). The average length of those AuCo alloy nanowires was 10 μm, which was calculated by the Faraday equation. As for each nanowire sample, the measured composition was an average value analyzed by XRF. The summary of the composition of those alloy nanowires as a function of current density was shown in **Figure 4-2**. The composition varies with the applied current density. As expected, at low current densities, nearly pure Au nanowires are deposited. In contrast, Co-rich CoAu alloy nanowires are deposited at high current densities.

Figure 4-3 shows two representative examples of the resulting nanowires deposited at a constant current density of -0.2 mA/cm^2 in anodic oxidized alumina membranes (Whatman® Anodisc®) with pore sizes of (a) 0.02 μm and (b) 0.1 μm. For both of them, the nanowires are 25 μms tall and well formed. The average composition of these nanowires were 92.6 Au wt % and 7.4 Co wt %. Since the AAO membrane has an average thickness of 60 μm, if longer deposition

was applied, the nanowires deposited in it could have a length as much as 60 µm, which means a wide range of aspect ratio could be achieved.

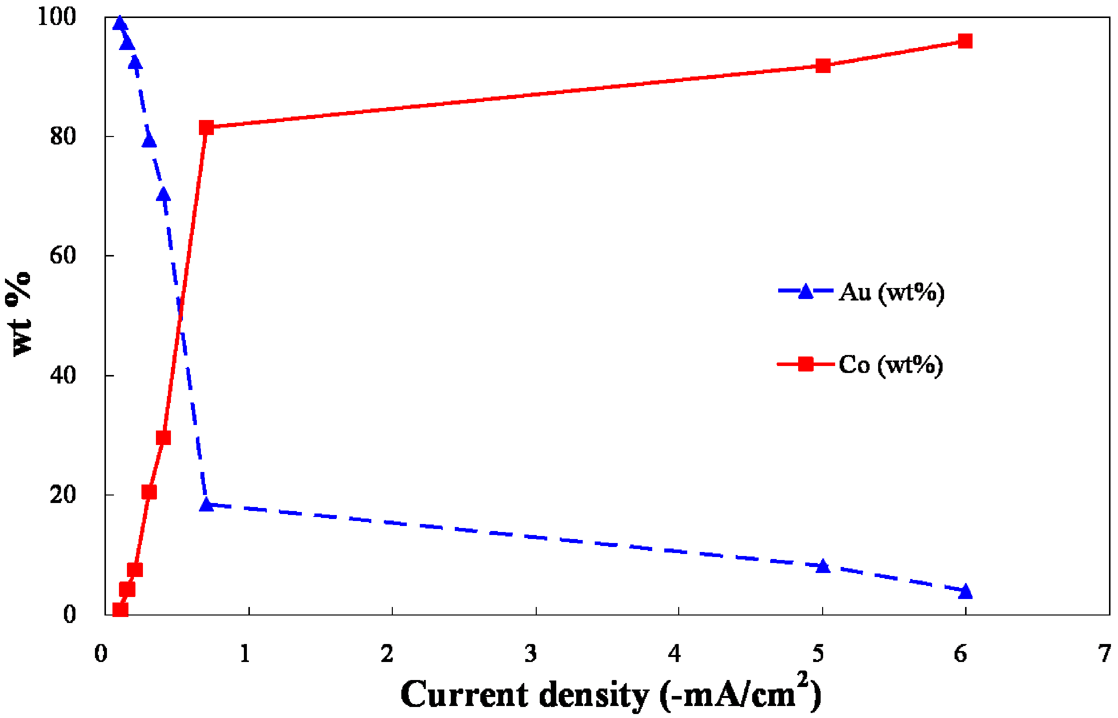

Figure 4-2 Alloy composition change in galvanostatic plated AuCo nanowires in the range of low current densities

Multilayered nanowires were deposited at -0.2 and -6 mA/cm^2 in a pulsed fashion. **Figure 4-4** shows transmission electron microscope (TEM) pictures of two different nanowires deposited with different Co layer deposition times: (a) 8 s; and (b) 24 s. The Au layer was deposited for 180 s in both cases. The Au layer thickness was 25 nm, and the Co layer thickness was 12 nm and 36 nm for the Co deposition times of 8 and 24 s, respectively. Therefore, the electrodeposition rate of Au with the current density of -0.2 mA/cm^2 was 0.14 nm/s, and the electrodeposition rate of Co with the current density of -6 mA/cm^2 was 1.5 nm/s. It is apparent from **Figure 4-4** that the metal layers are continuous and reasonably flat, with the interface perpendicular to the long axis of the wire. It is also noticed that the wire diameter is several times larger than the pore diameter quoted by the manufacturer (20 nm), and in fact, is close to 260nm.

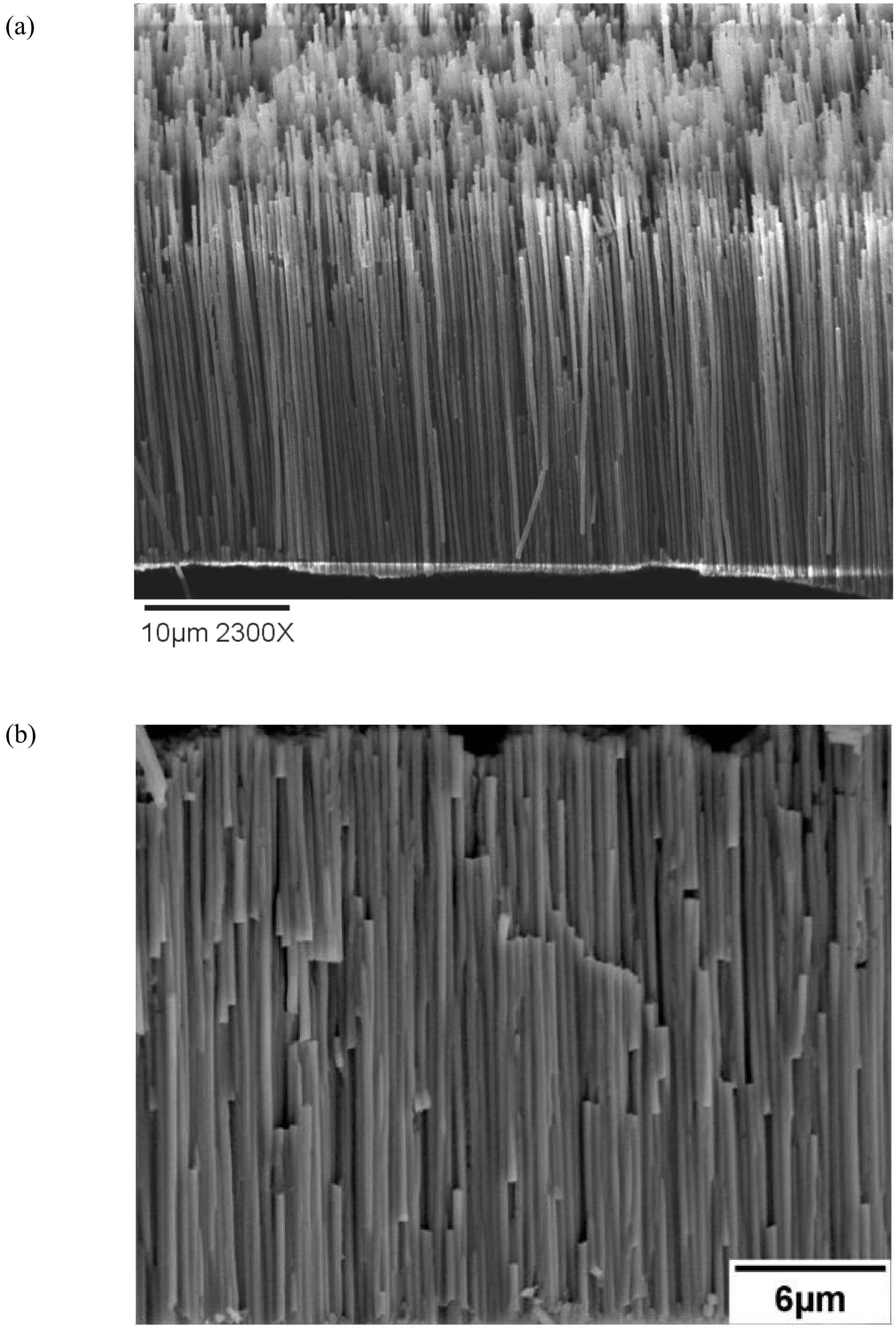

Figure 4-3 SEM images of AuCo alloy nanowires electrodeposited in AAO membranes with two different pore seizes: (a) 0.02 µm, (b) 0.1 µm

Based on the deposition rate of Au and CoAu alloy, another multilayered Au/Co nanowire sample with different layer sizes was electrodeposited in a 0.2 μm AAO membrane. The deposition times were 180 s for Au layer and 33 s for CoAu layer, leading to a 25 nm thick Au layer and 50 nm thick CoAu alloy layer, respectively. A high resolution SEM image of one single nanowire was shown in **Figure 4-5.** Due to the limitation of SEM, the multilayered structure was not as obvious as the results from TEM.

According to the data supplied by the manufacturer and confirmed by our own TEM studies, many pores of diameter close to quoted value (20 nm) join to form one much larger pore within around 1 μm of the surface of the membrane that the manufacturer's recommend should be uppermost for filtration applications. The change in pore diameter close to the filtration side is a consequence of a reduction in the anodization potential during manufacture. Away from this filtration surface, the pores are straight, uniform, and parallel. When sputtering Au on one side of the membrane as the contact layer for nanowire electrodeposition, the filtration side, which looks much flatter and shinier under light, should face up to the Au target. In such a way, uniform and parallel nanowires arrays can be electrodeposited and released easily for further analysis and processing. **Figure 4-6** shows a bifurcating Au/CoAu multilayered nanowire structure deposited in 0.02 μm AAO membrane. The stem diameter was 365 nm, and the branch diameter was 220 nm. Compared to previous **Figure 4-4**, the average nanowire diameter ranges from 200 to 400 nm, which is much bigger than the manufacture specification of 20 nm on the filtration side.

Based on a previous investigation[23], the nanoporous template method can be used to fabricate both AuCo alloy and multilayered nanowires with various dimension and compositions. Compared with other methods, such as electron beam techniques and nanosphere lithography, the nanoporous template methods have three advantages: first, the alumina template methods are

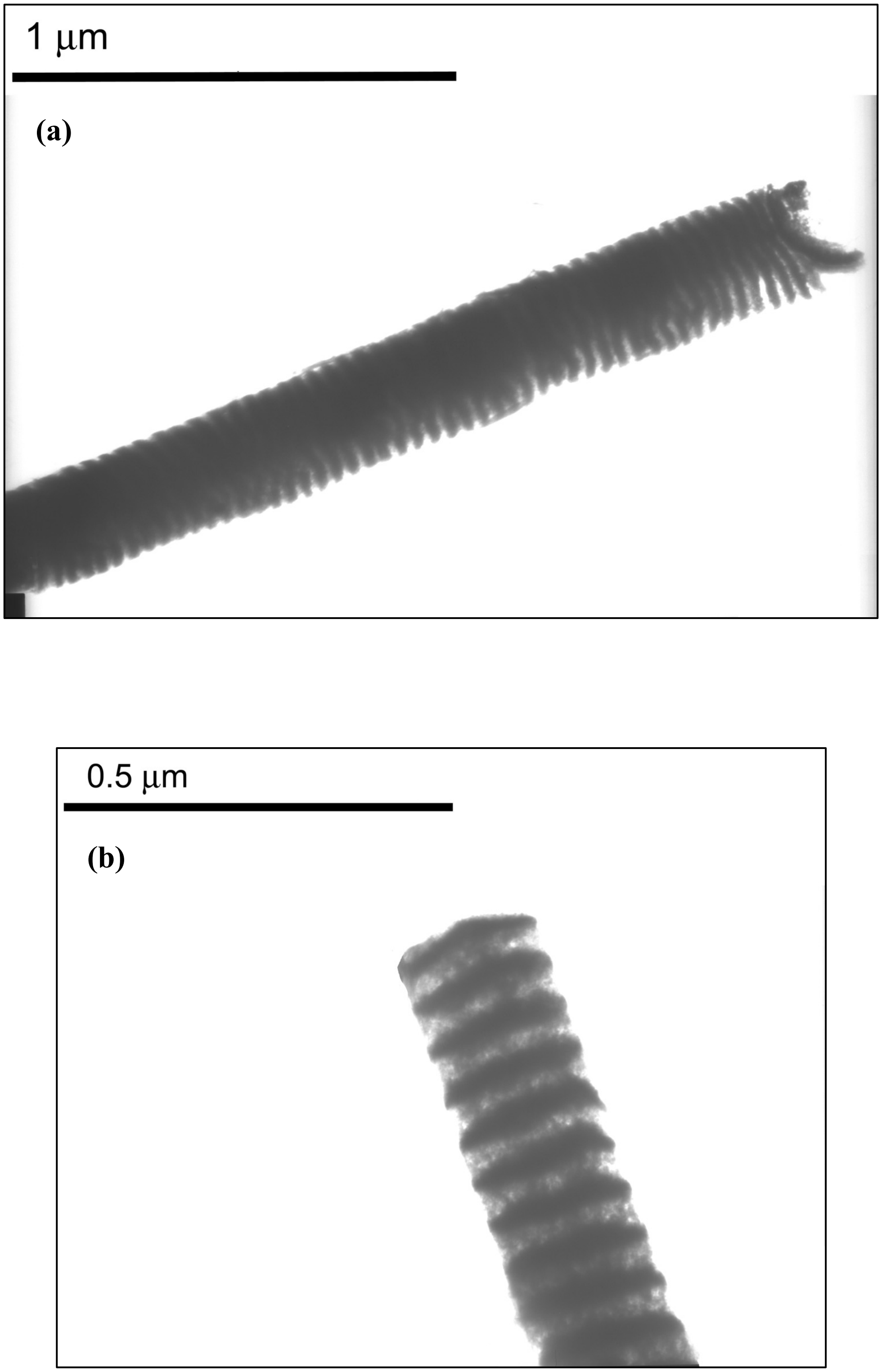

Figure 4-4 TEM images of multilayered Au/CoAu nanowires deposited in 0.02 µm AAO membrane with various deposition times for CoAu layer: (a) t_{Au} 180 s / t_{Co} 8 s, and (b) t_{Au} 180 s / t_{Co} 24 s

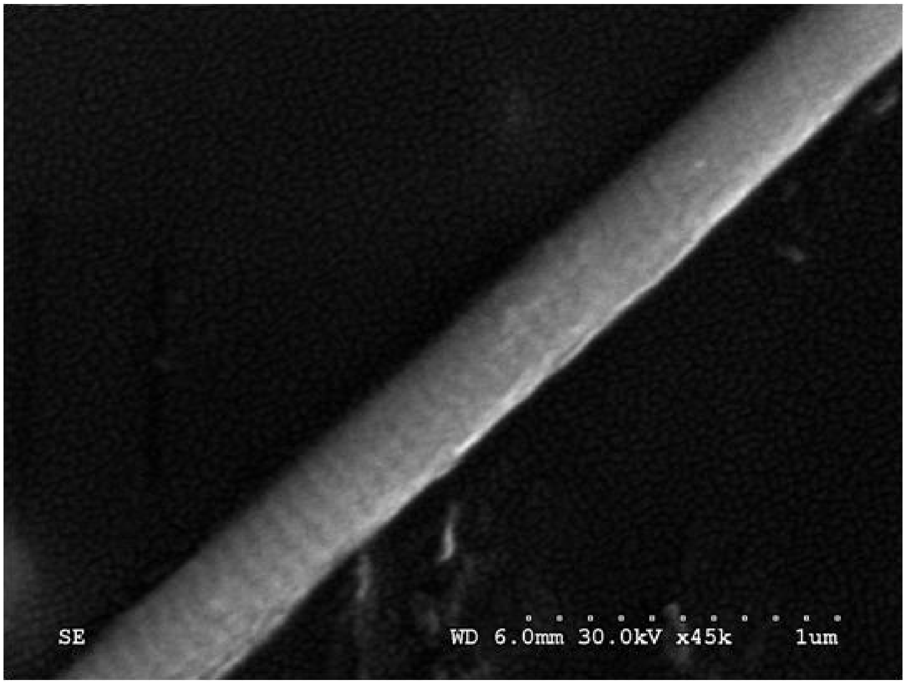

Figure 4-5 High resolution SEM image of a multilayered Au/Co nanowire deposited in 0.2 μm AAO membrane with deposition times of 180 s for Au layer and 33 s for CoAu layer

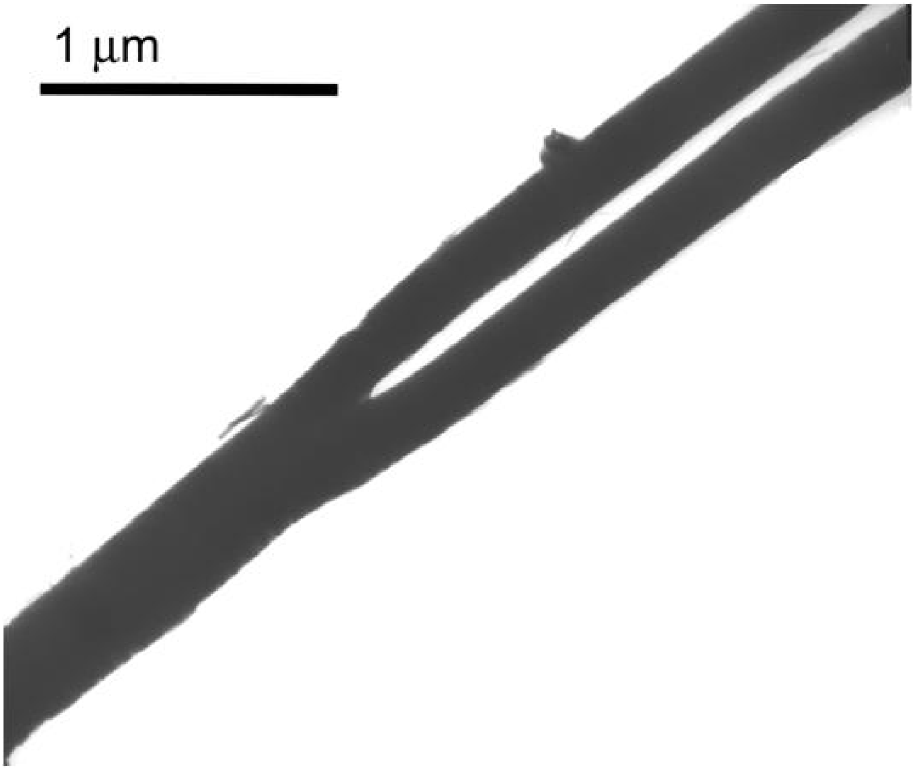

Figure 4-6 TEM image of a bifurcating Au/CoAu multilayered nanowires deposited in 0.02 μm AAO membrane

scalable and parallel, providing a method to fabricate large, ordered nanowire arrays. Second, the nanowire height is independent of the wire diameter allowing high aspect ratio wires to be fabricated. Nanowire diameter and height are controllable by varying the electrochemical conditions. In addition, the electrochemical method does not require expensive instrumentation, high temperature or low vacuum pressures.

However, in our practical electrodeposition process, there is always some unexpected phenomenon. For example, when trying to fabricate three series of multilayered Au/CoAu nanowires with average height of 30 μm in 0.1 μm AAO membranes, the first two series, Au 25 nm / CoAu 50nm and Au 25 nm / CoAu 150nm, could be deposited successfully. While, the third series with same average height of 30 μm, but larger CoAu layer size of 250 nm or above, cracked during the process of electrodeposition. Those cracks were shown in **Figure 4-7**.

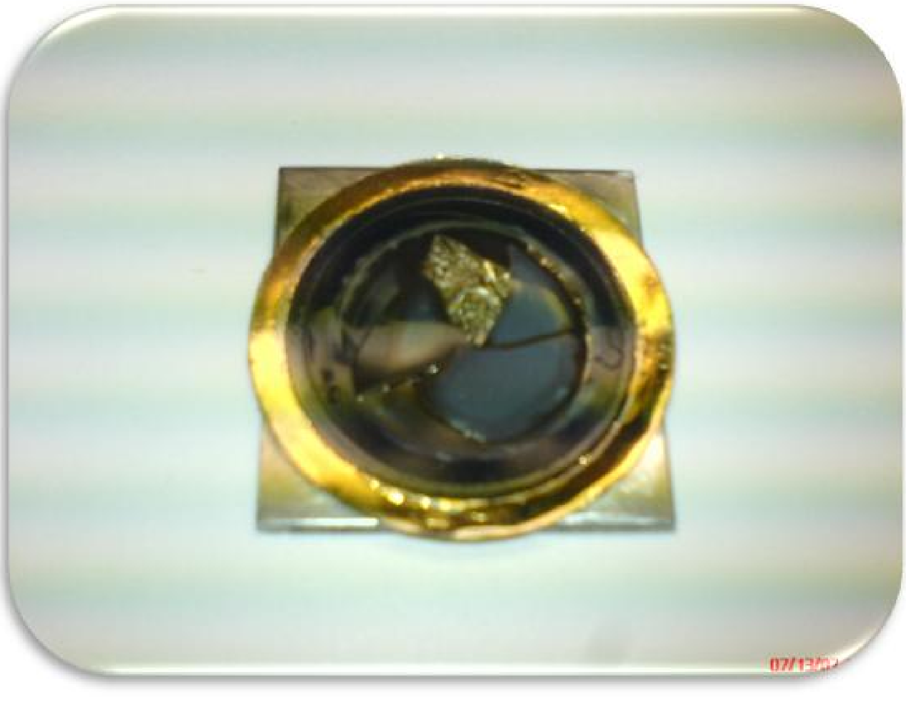

Figure 4-7 Cracked AAO membrane when depositing Au 25 nm / CoAu 250 nm multilayered nanowires

This cracking of the deposit is believed to be associated with the internal stress of the electroplated gold layer. There are two types of stresses that need to be considered, tensile stress and compressive stress. Tensile stress is associated with the coalescence of islands that have nucleated on a substrate. Islands of deposited metal, in an effort to minimize surface energy, tend to coalesce by joining together (sometimes referred to as "zipping"), creating elastic strain. It is thought that compressive stress results during deposition when adatom incorporation into the lattice at the grain boundaries is favored.

Kelly *et al.*,[71] studied the effects of adding an arsenic additive on the gold microstructure and residual stress from unsparged solutions of Techni gold 25E with a pH of 6.5. According to their report, Au films produced without and with arsenic have tensile and compressive stress, respectively. For both electrolytes, stress generally becomes less tensile (or more compressive) with increasing current density. In the absence of arsenic, pulse plating does not appreciably change the film stress. Pulsing with arsenic does lower the measured compressive stress close to zero. The primary microstructural effect of the arsenic is a reduction of the twin density. An adsorbed layer of arsenic ions is involved since ppm levels are sufficient to induce such changes in film stress. However, considering its toxic property, arsenic additive is not a preferred component in our research.

Codeposition of hydrogen can also cause cracks in a deposit. A tensile macrostress can develop when hydrogen diffuses onto the substrate or previously deposited layers causing them to expand, or when hydrogen diffuses out of a layer of the deposit allowing it to shrink.[4] In some circumstances, when micropores form during deposition, hydrogen then diffuses into them causing them to expand and resulting in a compressive macrostress. Improving the current efficiency and removing the codeposition of hydrogen is an effective way to ameliorate the multilayer thin film structures.

Discovered in the previous study,[23] the current efficiency for this Au/Co electrodeposition system was low. As a result, codeposition of hydrogen could be the main reason for cracking of longer nanowires. The vendor of the Au solution did not provide any information about the additives. Therefore in the following research, the maximum length of nanowires is going to be controlled under 30 μm.

4.2 Electrodeposition of Nanotubes

Using the same concentrated Au/Co electrolyte and a stationary working electrode cell set-up, nanotubes were also electrodeposited in nanoporous templates with larger pore sizes. Polycarbonate (PC) filtration membranes (from Poretics®, Osmonics) with three different pore sizes (0.4, 1.0, and 2.0 μm) were examined. The thickness of this PC membrane is in the range of 6 ~ 10 μm. Before electrodeposition, a Au layer was sputtered on the reverse side of the membrane, serving as a conductive substrate. All the multilayered Au/CoAu nanotubes were electrodeposited with a two galvanostatic, square-wave pulsed plating: -0.2 mA/cm^2 for the Au layer and -6 mA/cm^2 for the Co layer with variable times.

Figures 4-8, **4-9 and 4-10** show SEM images of Au/CoAu multilayered nanotubes electrodeposited in PC membranes with three different pore sizes, i.e. 0.4, 1.0, and 2.0 μm respectively. For all of them, the deposition times were 33 s for the Co-rich CoAu layer and 180 s for the Au layer. The overview image of those nanotubes in **Figure 4-9** showed that the nanotube length was about 8 μm, which is in the range of the membrane thickness of 6 ~ 10 μm. The inset cross section view of nanotubes in **Figure 4-9** indicated that both the inner surface and outer surface of the nanotube were very smooth. The inset top view of nanotubes in **Figure 4-10** shows that the outer diameter of the nanotube was 2.4 μm, which is a little bit larger than the specified pore diameter of 2 μm, and the tube wall thickness was 275 nm.

In our previous study,[4] nanotubes were fabricated by orienting the electrode so the tubes grew down. Hydrogen bubbles were purposely trapped to create the tube. The problem that was encountered was that the tubes were not smooth and appeared rough and pitted. Here a larger diameter membrane is used to promote tube formation in an upward facing orientation. The quality of the tubes' morphology was considerably improved.

Various membranes with a wide range of pore diameters (0.01, 0.1, 0.2, 0.4, 1.0, and 2.0 μm) were used to electrodeposit the multilayer under the same conditions. It was found that pore size plays an important role in determining whether nanowires or nanotubes are formed. Membranes with pore sizes reported by the manufacturer that are smaller than or equal to 0.2 μm will give nanowires, while membranes with pore sizes greater than or equal to 0.4 μm result in nanotubes. Details are summarized in **Table 4-1**, which was confirmed by previous SEM images in **Figure 4-3** to **Figure 4-10**.

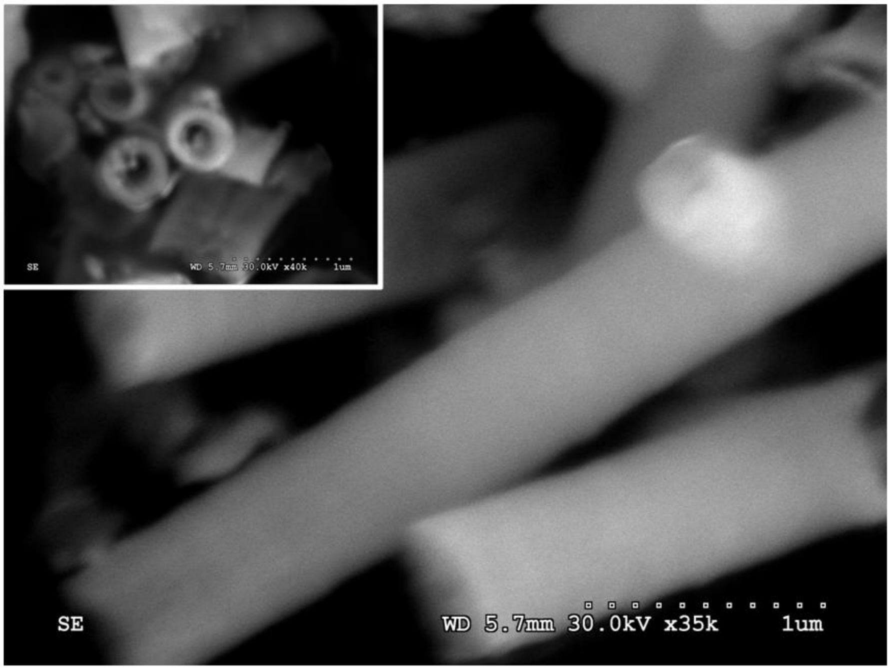

Figure 4-8 SEM images of Au/CoAu multilayered nanotubes fabricated in polycarbonate (PC) membrane with pore size of 0.4 μm

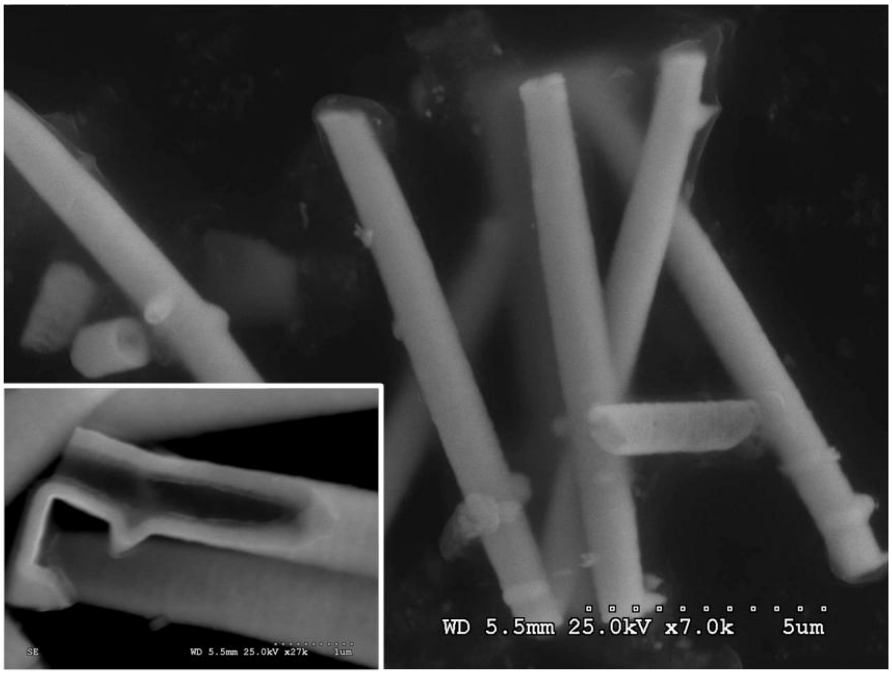

Figure 4-9 SEM images of Au/CoAu multilayered nanotubes fabricated in polycarbonate (PC) membrane with pore size of 1.0 μm

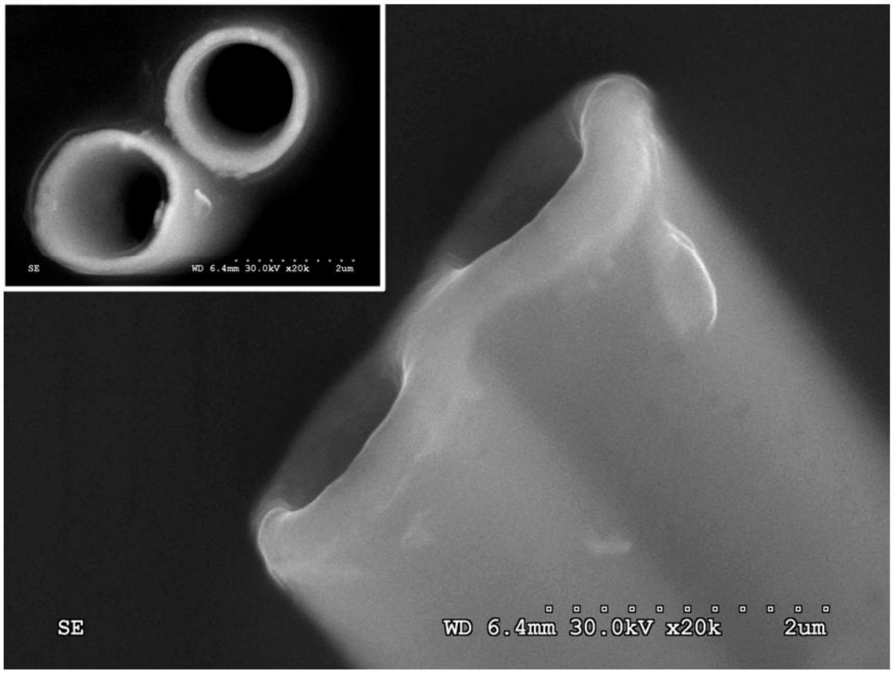

Figure 4-10 SEM images of Au/CoAu multilayered nanotubes fabricated in polycarbonate (PC) membrane with pore size of 2.0 μm

Table 4-1 Nanowires/nanotubes distribution with various pore sizes

	AAO membrane			PC membrane		
Pore Size (μm)	***0.02***	***0.1***	***0.2***	***0.4***	***1.0***	***2.0***
Nanowires	✓	✓	✓			
Nanotubes				✓	✓	✓

4.3 Magnetic Property of Au/CoAu Nanostructures

4.3.1 Giant Magnetoresistance (GMR)

The giant magnetoresistance (GMR) effect refers to a very large change in electrical resistance that is observed in a ferromagnet/paramagnet multilayer structure, which was first discovered in France in 1988. The resistance change occurs when the relative orientations of the magnetic moments in alternate ferromagnetic layers change as a function of applied magnetic field. GMR is defined as $(R_H-R_0)/R_0*100$, where R_H is the resistance in an external field H, and R_0 is the resistance when the external field is zero. The effect is most usually seen in magnetic multilayered structures, where two magnetic layers are closely separated by a thin nonmagnetic spacer layer a few nm thick. It can also occur in an unlayered alloy films, nevertheless in most cases, with a much smaller value. To date, several conventional techniques have been used to produce magnetic multilayers, including molecular beam epitaxy, electron-beam evaporation, ion-beam sputtering, magnetron sputtering, and electrodeposition. The primary industrial applications of GMR effect includes: high density data storage system, computer hard drive, and magnetic RAM. Moreover it can be used in linear position sensor fabrication, angular measurement and current measurement.

4.3.2 CIP GMR

For the last few years, a large number of studies have been devoted to thin film GMR materials with current-in-plane magnetoresistance (CIP GMR) and various applications have been achieved. One of the important impacts of GMR on technology development is the GMR read-out heads of hard disks, which have revolutionized techniques for retrieving data from hard disks and have accelerated the trend of hard disk miniaturization in the last few years. In particular, hard disks have shrunk from a bulky box under your desk to a slender, portable one which is crucial to slim laptops computers and music players. Because of this revolutionary impact, the Nobel Prize in Physics 2007 was awarded to Albert Fert and Peter Grunberg for their discovery of giant magnetoresistance almost twenty years ago.[72] The use of GMR can be regarded as one of the first major applications of nanotechnology.

GMR also plays a major role in various magnetic bioMEMS sensors for the development of a new generation of electronics.[73, 74] For example, in 2002, Schotter *et al.*[75] designed magnetoresistive biosensors with sensor elements small enough to cover the entire area of a single probe DNA spot. The sensitivity of the GMR biosensor was more than two orders of magnitude higher that of the established fluorescence detection. In 2004, Bruckl *et al.*[76] designed magnetoresistive biochips, which are capable of detecting even single molecules (e.g. DNA) by functionalized magnetic markers.

In our previous study, two series of Au/CoAu multilayers were electrodeposited on Cu (100) foil for the investigation of current-in-plane giant magnetoresistance (CIP GMR) behavior with film thickness at room temperature. The plating current densities for each bilayer were -1 mA/cm^2 for the Au layer and -100 mA/cm^2 for the Co-rich CoAu alloy layer with variable times.

The GMR measurement was performed with the multilayer on the Cu foil, which contributes to a short circuit for the in-plane current flow, as shown in **Figure 4-11** at low fields. Therefore, a much higher magnetic field was needed for the demonstration of GMR behavior. There was no MR at low field due to the shunting of the current through the copper substrate, as expected.

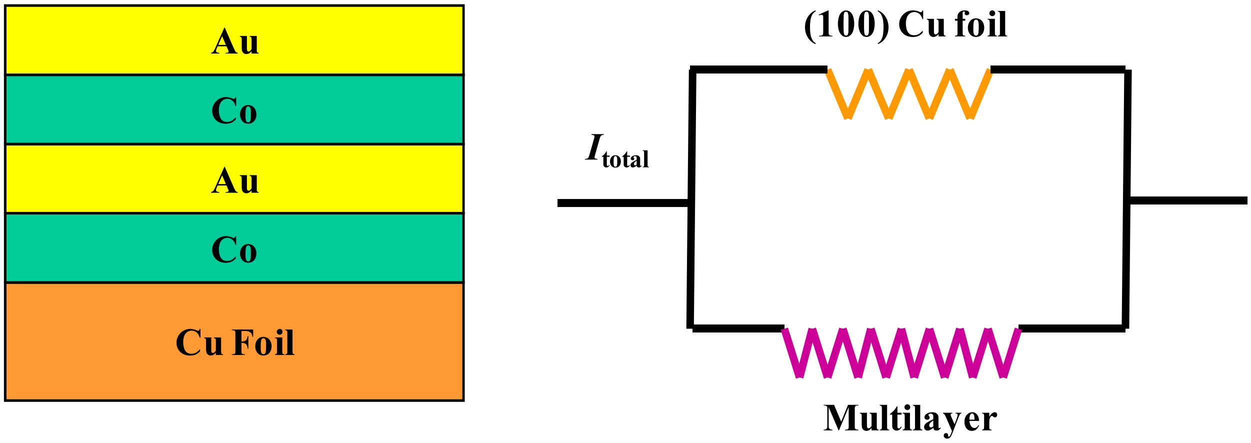

Figure 4-11 Schematic of GMR on Cu foil substrate

Figure 4-12 shows that the magnetoresistance varies with Co-rich CoAu layer thickness. The Au layer thickness was fixed at 3 nm by maintaining the plating time while the Co-rich CoAu layer plating time varied from 2 to 5 nm. The Au/CoAu multilayers deposited on Cu foil exhibited a change in resistance, with large magnetic field. Also, the observed GMR is positive when the Co-rich layer is thinner than 4 nm. Increasing the Co-rich CoAu layer thickness, the GMR changes from positive to negative with more than 13 % GMR. This sample was comprised of 3 nm Au layer and 5 nm Co layer, having 925 bilayers.

In a second series of experiments the Au layer thickness was varied. **Figure 4-13** shows that the magnetoresistance varies with Au layer thickness. A similar phenomenon was observed in the second sample series. The Co-rich CoAu layer thickness was fixed at 4 nm by keeping the plating time constant while the Au layer plating time varied from 1.5 to 4 nm. The GMR is

positive when the Co-rich CoAu layer is less than 3 nm. While for the sample consisting of 4 nm Au layer / 4 nm CoAu layer and having 925 bilayers, the GMR changes from a positive to negative value with a GMR of more than 7 % at a magnetic field of 9 Tesla.

In both **Figures of 4-12** and **4-13**, GMR transitions from a positive to negative value depend on the layer thicknesses. Both the Au and CoAu layer thicknesses affect the GMR. The origin of GMR is due to the antiferromagnetic (AF) coupling of two adjacent ferromagnetic Co layers separated by a nonferromagnetic Au layer. When the external magnetic field is applied and increased, the resistance will decrease. The observed positive magnetoresistance is called positive inverse magnetoresistance (IMR), which means a smaller resistivity for an antiparallel arrangement of the magnetizations of successive magnetic layers.

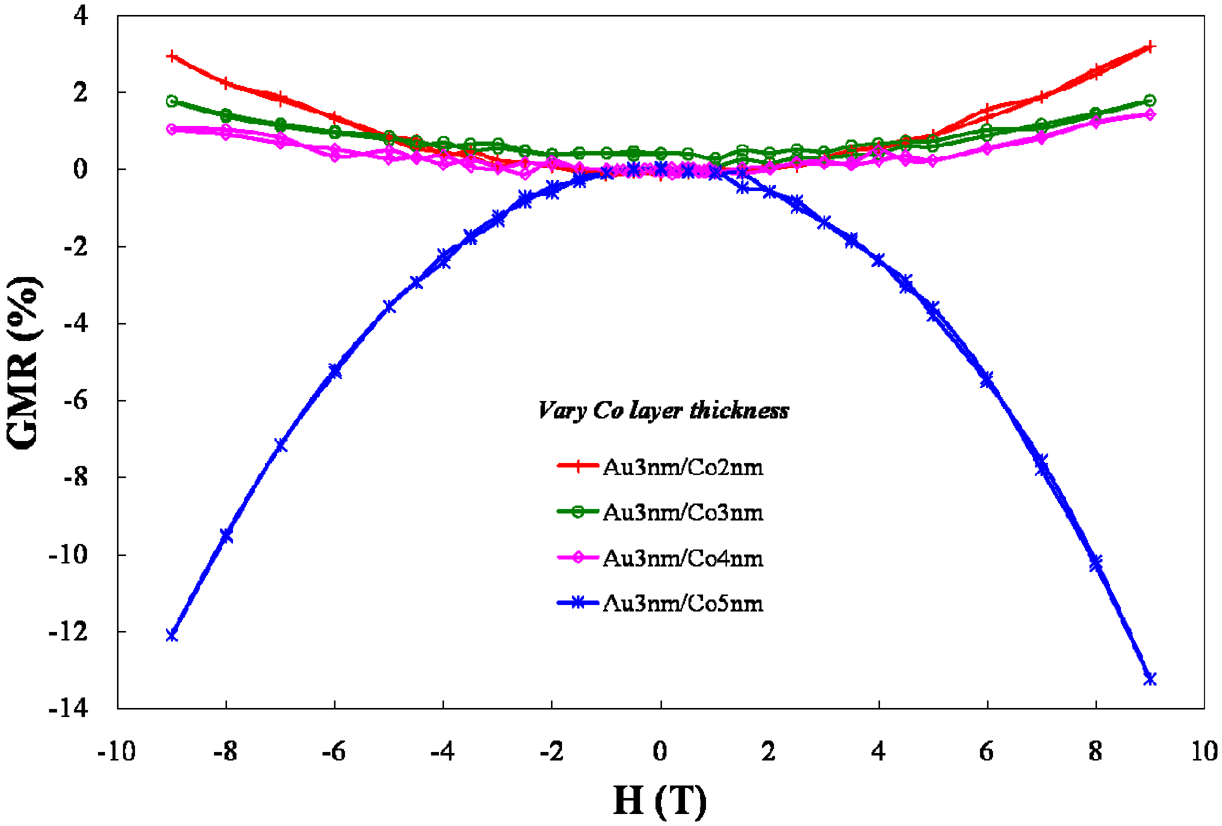

Figure 4-12 GMR results of Au/CoAu multilayer films on Cu foil substrate, with variable CoAu layer thickness

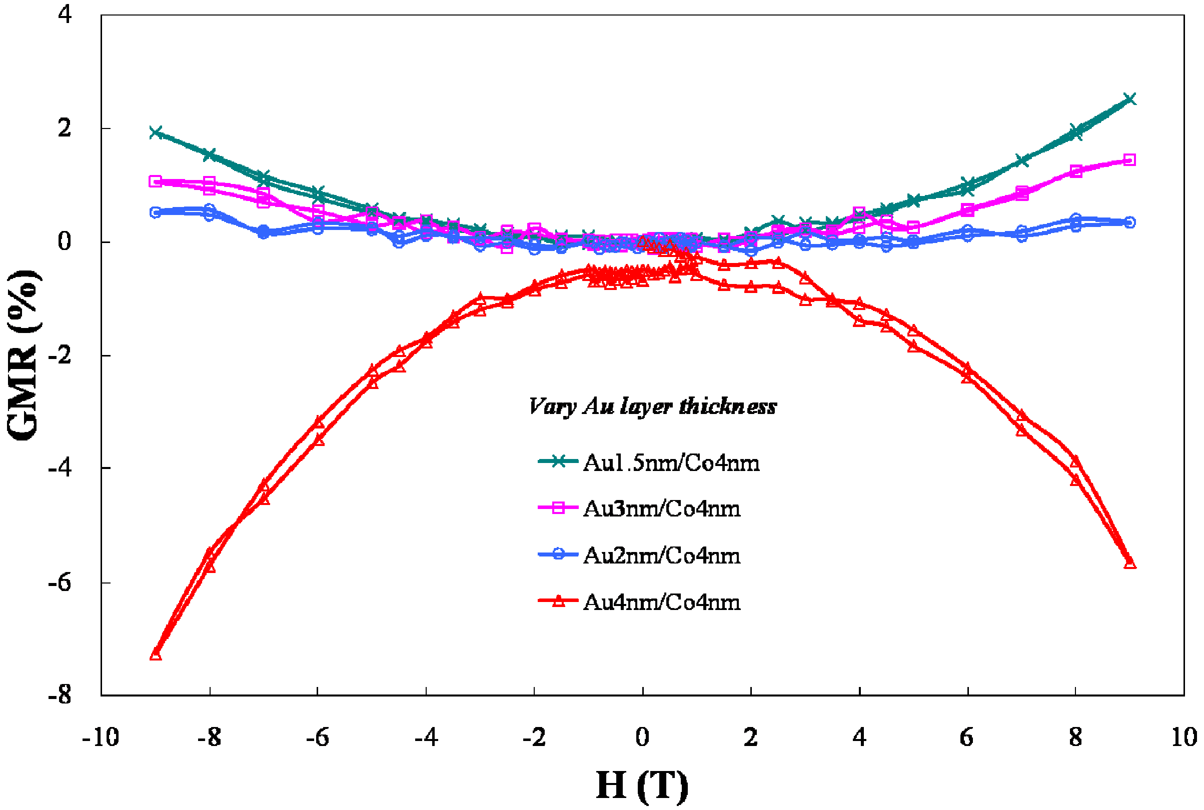

Figure 4-13 GMR results of Au/CoAu multilayer films on Cu foil substrate, with variable Au layer thickness

Such an IMR effect has been discovered in different systems. George *et al.*[77] found that MR was positive and inverse at low magnetic field, and negative and direct at high field in Fe/Cu multilayers doped with thin Cr layers. This behavior was attributed to the magnetization misalignment of the two Fe layers separated by Cr. Dinia *et al.*[78] reported inverse magnetoresistance from ferromagnetic Fe layers separated by a semiconducting (Si, Ru) layer. This reversed magnetoresistance is due to the superparamagnetic interfaces and is attributed to the difference of the electronic nature of the Fe/Si interfaces and Fe/Ru interfaces.

Rahmouni *et al.*[79] observed inverse MR in Co/Ru/Co and doped Co/Ru/$Co_{0.9}2Ru_{0.08}$ sandwiches and ascribed this behavior to the competition between bulk and interface spin-dependent scattering which contribute to negative and positive (inverse) MR, respectively.

Similarly, Zhao *et al.*[80] found when a nano-nitride-layer (NHL) is doped at the inner interfaces of the core Co/Cu/Co sandwich, an inverse GMR was observed. They also ascribed this inverse MR to the competition between the positive bulk and negative interfaces spin asymmetry.

4.3.3 CPP GMR

Due to the high aspect ratio of a nanowire, the GMR property can be easily measured in a current perpendicular to the plane of the layer (CPP GMR). Recently, current-perpendicular-to-plane GMR has been proven to show larger magnetoresistance changes in Co/Cu,[10] CoNi/Cu[81] and NiFe/Cu[11] systems. Compared with the above CIP GMR from multilayered thin films, CPP GMR from multilayered nanowires exhibits more advantages. In the CIP configuration, the characteristic length, the electron mean free path, is about 2 nm, which makes the layer thickness very critical. Comparatively, the characteristic length in the CPP configuration, spin-diffusion length, is about 20 nm, leading to easier fabrication due to the larger layer thickness. Most important, this leads to a larger resistance that enables higher accuracy measurement.

Due to the larger resistance and higher accuracy, multilayered nanowires/tubes have found applications in biological detection by means of a GMR sensor, which provides a robust, inexpensive sensing technique with high sensitivity and considerable scope for quantitative signal data, enabling magnetoresistive biochips to meet specific diagnostic needs that are not met by existing technologies.

In this investigation of the current-perpendicular-to-plane giant magnetoresistance (CPP GMR), multilayered Au/CoAu nanowires with various layer thicknesses were electrodeposited. The CoAu layer was deposited at -6 mA/cm^2, and the Au layer was deposited at –0.2 mA/cm^2 in the non-cyanide Au/Co electrolyte. The layer thickness was controlled by varying the deposition time. The magnetoresistance changes as a function of external magnetic field of two series of

Au/CoAu nanowires at room temperature were shown in **Appendix A**. However, the magnetoresistance behaviors were noisy and irregular and the resistances are time dependant, not characteristic of GMR.

One of the possible reasons that GMR was not observed could be that there are multi-magnetic domains formed inside a single magnetic layer, which will ruin the antiferromagnetic coupling for the GMR. Also, the irregularity of pore size distribution and bifurcating structure in AAO membrane (**Figure 4-6**) will result in overlapping pores, which favors the multi-domain formation. Another possible reason could be attributed to the non-distinct interface between Au and Co layers inside nanowires. Even Au/Co multilayered films prepared by ion-beam sputtering also showed rather diffuse interfaces at which there appeared significant intermixing of Co and Au species. When these multilayers were annealed at 275 °C, the miscible Co and Au atoms tend to segregate, markedly sharpening the composition profile.[82]

In general, electrodeposited multilayers that exhibit large GMR use copper, not gold, for the non-ferromagnetic layer. For example, Myung *et al.*[15] used a sequential dual bath technique to electrodeposit Co 4.5 nm / Cu 5 nm multilayers, which showed a maximum GMR of 2.5 % at room temperature. Liu *et al.*[46] examined the Co/Cu multilayered nanowires and found 11 % CPP GMR at room temperature and 22 % at 5 K. Therefore, in this study, copper sulfate was added to the electrolyte to deposit some copper with the gold. The electrolyte contained $CoSO_4{\cdot}7H_2O$ 0.4 M, $CuSO_4{\cdot}5H_2O$ 0.008 M, $KAuCl_4$ 0.0006 M, $Na_3C_6H_5O_7{\cdot}2H_2O$ 0.1 M, and H_3BO_3 0.1 M at pH 5.0.

AuCu/CoAuCu multilayered nanowires were potentiostatically pulse plated from this AuCuCo electrolyte in AAO membranes with a pore size of 0.02 μm. The AuCu layer was electrodeposited at -0.5 V vs. SCE for 140 s and the CoAuCu layer was deposited at -1.6 V vs.

SCE for 4 s with bilayer number of 631. The estimated layer sizes were 5 nm for AuCu layer and 17 nm for CoAuCu layer. **Figure 4-14** shows the CPP GMR behavior of this AuCu/CoAuCu multilayered nanowire. Obviously, the addition of the Cu component improved the CPP GMR considerably to a much bigger value of 5-6 % and resulted in a better GMR behavior. While the electrolyte used here is necessary for Au plating, it is not the best choice for Cu, although larger GMR values can be obtained with CuCo from different electrolytes. On the other hand, CuCo electrolytes are generally at low pH values, which would cause precipitation of the Au ions and thus cannot be used.

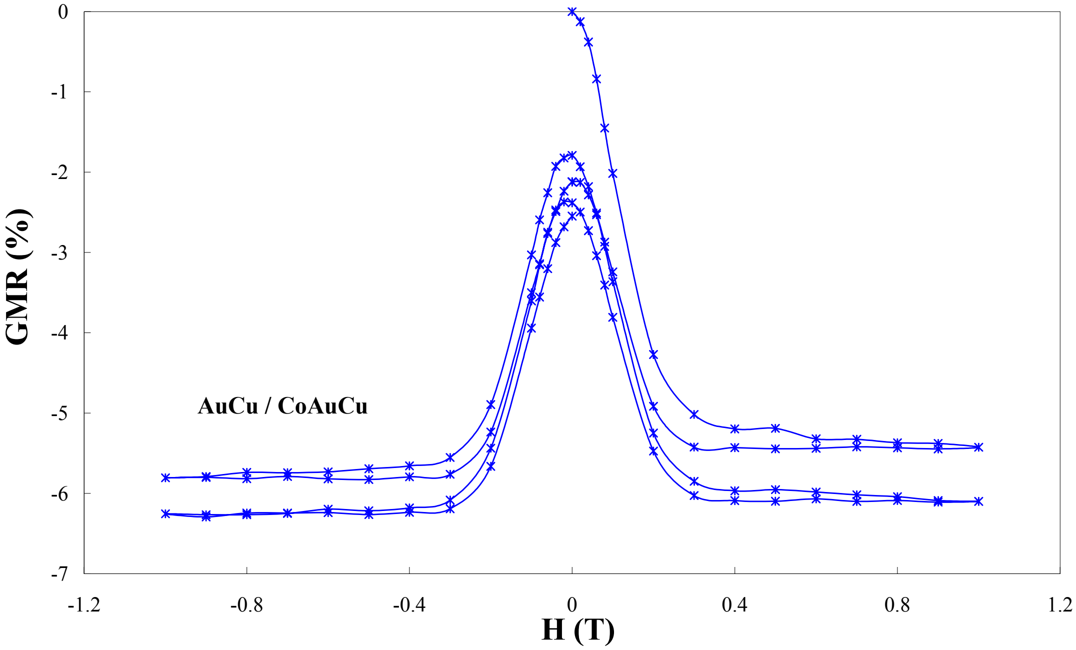

Figure 4-14 CPP GMR of (AuCu 140 s / CoAuCu 4 s) × 631 multilayered nanowires electrodeposited in 0.02 μm AAO membrane

4.3.4 Annealing Effects on GMR

As previously discussed in **Section 4.3.1** and **4.3.2**, a maximum CIP GMR of negative 13 % was observed in Au 3 nm / CoAu 5 nm multilayered thin films and no significant GMR values were observed in those Au/CoAu multilayered nanowires. The possible reasons could be

that the layer interface is not distinct in layer composition and that a gradient occurs. Den Broeder *et al.*[83] found that Au/Co multilayered thin films prepared by ion-beam sputtering (IBS) showed rather diffuse interfaces at which there appeared significant intermixing of Au and Co species. When the multilayers are annealed at 275 °C in a reducing H_2/N_2 atmosphere, the miscible Co and Au atoms tend to segregate, markedly sharpening the composition profile.

There have been other studies in the literature on the effect of annealing multilayered thin films. For example, Hylton *et al.*[84] found that post-deposition annealing is required to obtain GMR for NiFe/Ag discontinuous multilayer. For a wide range of NiFe and Ag thickness, no giant magnetoresistance was observed in the unannealed films. After annealing at atmospheric pressure in a mixture of 5 % H_2 and 95 % Ar in a rapid thermal processing oven at a temperature range between 300 and 400 °C for 10 min, a large, negative magnetoresistance was observed of order 4 to 6 % in applied fields of 5 to 10 Oe at room temperature. A possible mechanism to explain the onset of GMR after annealing is the diffusion of Ag along the columnar grain boundaries. This diffusion effectively breaks up the NiFe layers into grains that interact magnetostatically. An antiparallel magnetostatic coupling in the absence of an external magnetic field produces a maximum resistance; the resistance then decreases as a magnetic field is applied and the magnetic moments of the grains become aligned.

The effect of annealing treatment on the Au/CoAu multilayered thin films and nanowires was investigated to examine if there is an improvement in GMR. Two multilayered thin film samples which exhibited nice CIP GMR were examined: Au 3 nm / CoAu 5 nm with negative 13 % GMR, and Au 4 nm / CoAu 4 nm with negative 7 % GMR, as shown in **Figure 4-16** and **4-17**.

The annealing process was carried out in a mixture of 5 % H_2 and 95 % Ar in a Lindberg/Blue tube furnace, shown in **Figure 4-15**, with a collaboration between our group and Dr. Young's group in the Department of Physics and Astronomy. The quartz boat containing the GMR samples was placed in the middle of the furnace to avoid temperature gradients. The annealing temperature was set as 300 °C. Before heating, H_2 and Ar mixture gas flow was first used to flush the quartz tube at room temperature to remove any traces of air. The temperature was then ramped at 2 °C per minute and the samples were annealed at 300 °C under continuous flow of H_2 and Ar mixture gas. An estimated time of 30 min is expected to segregate the Co and Au atoms at the layer interfaces and sharpen the composition profile. Later the heating was automatically shut off and the samples were allowed to cool down to room temperature while keeping the flow of the protection gas. Some old Au/CoAu nanowires were also annealed for the improvement of GMR.

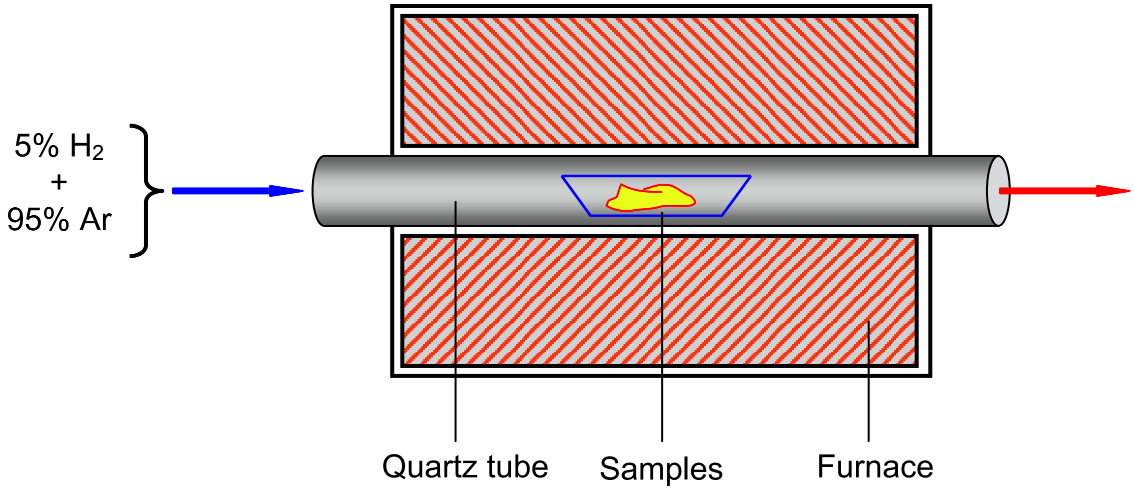

Figure 4-15 Schematic illustration of annealing process in a tube furnace

After the annealing treatment, the CIP GMR properties of those two multilayered thin film GMR samples were measured with the PPMS 6000 system. Results are shown in **Figure 4-16** and **4-17**. However, those CIP GMR results after annealing treatment were not as promising as expected. In **Figure 4-16**, the original CIP GMR of multilayer thin film Au 3 nm / CoAu 3 nm

was negative 13 %, after the annealing treatment, the GMR value became positive 8 %. Similarly, in **Figure 4-17**, the CIP GMR of Au 4 nm / CoAu 4 nm multilayer changed from negative 6 % to negative 1 %.

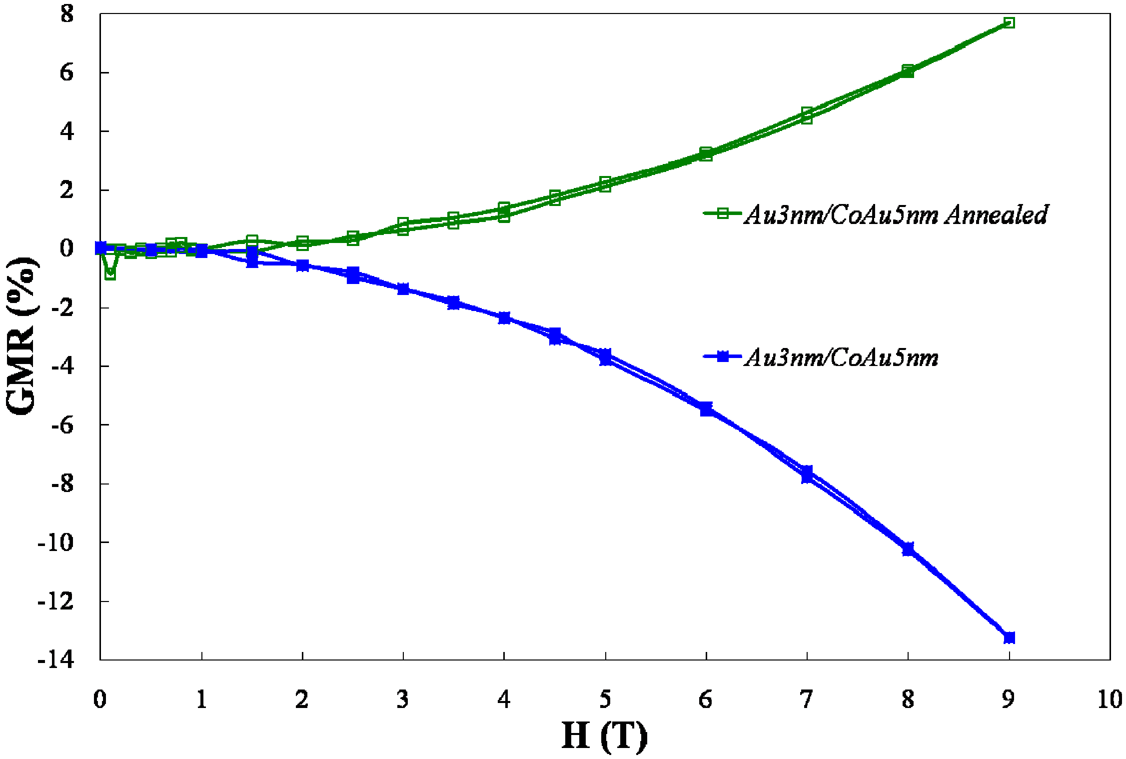

Figure 4-16 CIP GMR of Au 3 nm / CoAu 5 nm multilayers before and after annealing treatment

Even though the results were not as good as the previous literature reported, there are still certain reports disclosed similar unfavorable phenomena. As an example of negative effects of annealing, Vrenken *et al.*[85] investigated the relationship between microstructure and giant magnetoresistance of granular $Au_{80}Co_{20}$ alloys. Subsequent annealing at 300 and 400 °C fundamentally changes the Co particles through spinodal decomposition and loss of coherency between the Co- and Au-rich phases. The particle boundaries become diffuse and the particles even become interconnected which leads to the GMR effects continuously decreases upon annealing with increasing measurement temperature. Similarly, when Evans *et al.*[86] investigated

the CPP GMR of multilayered Cu/CoNiCu nanowires electrodeposited in anodic aluminum oxide membrane, it was found that annealing the deposit would reduce the GMR effect due to interdiffusion and recrystallization phenomena.

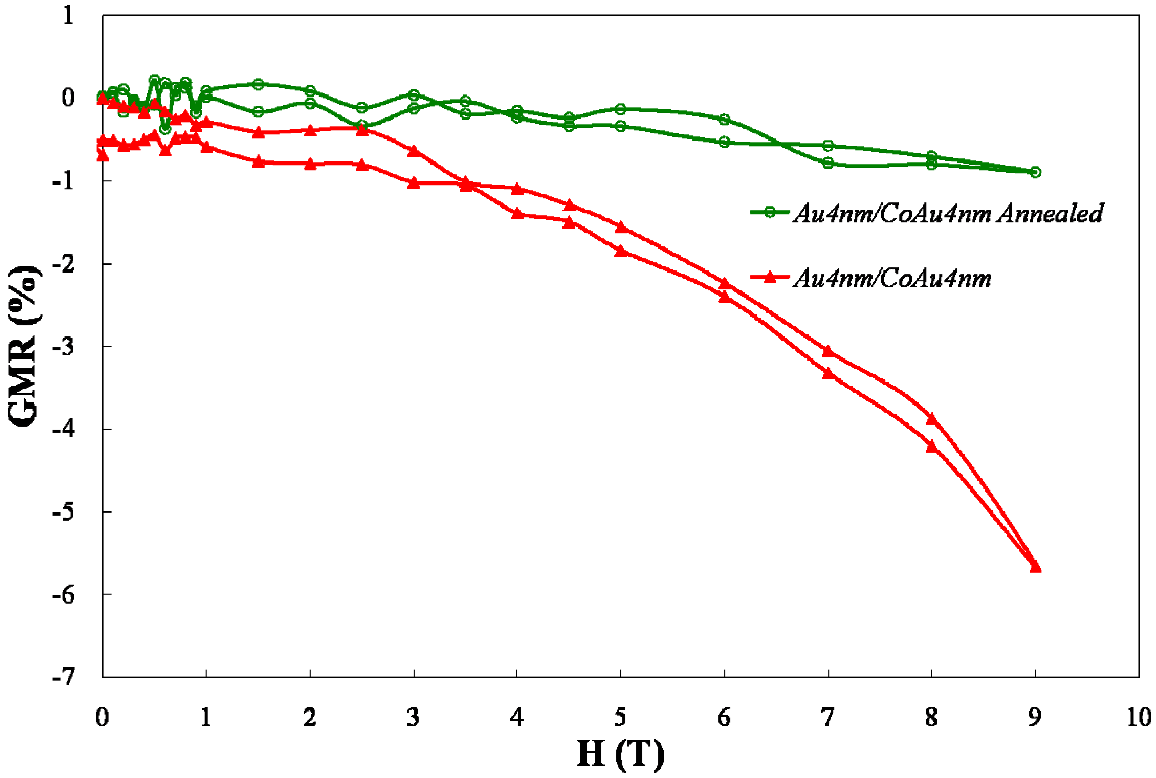

Figure 4-17 CIP GMR of Au 4 nm / CoAu 4 nm multilayers before and after annealing treatment

Further annealing effects on the Au/Co system from X-ray diffraction (XRD) data will be discussed later in the section of selective electrochemical etching of Au/CoAu multilayered nanowires and nanotubes.

4.3.5 Hysteresis Loop

A typical hysteresis loop is schematically shown in **Figure 4-18.** Hysteresis is well known in ferromagnetic materials. When an external magnetic field in one direction is applied to a ferromagnet, the ferromagnet absorbs some of the external field. Even when the external field

is removed, the magnet will retain some field: it has become magnetized. During the process, there is a point where further increases in magnetic field strength will result in no further change in flux density. This condition is called magnetic saturation. The ferromagnet must be driven back to zero magnetization by a magnetizing field in the opposite direction. The amount of reverse driving force (magnetic field) required to demagnetize the material is called coercivity (H_c). If an alternating magnetic field is applied to the material, its magnetization will trace out a loop called a hysteresis loop. The lack of retraceability of the magnetization curve is the property called hysteresis and it is related to the existence of magnetic domains in the material. Once the magnetic domains are reoriented, it takes some energy to turn them back again. This property of ferromagnetic materials is useful as a magnetic "memory", which has been used in audio tape recording and data storage in a computer hard drive. Some compositions of ferromagnetic materials will retain an imposed magnetization indefinitely and are useful as permanent magnets.

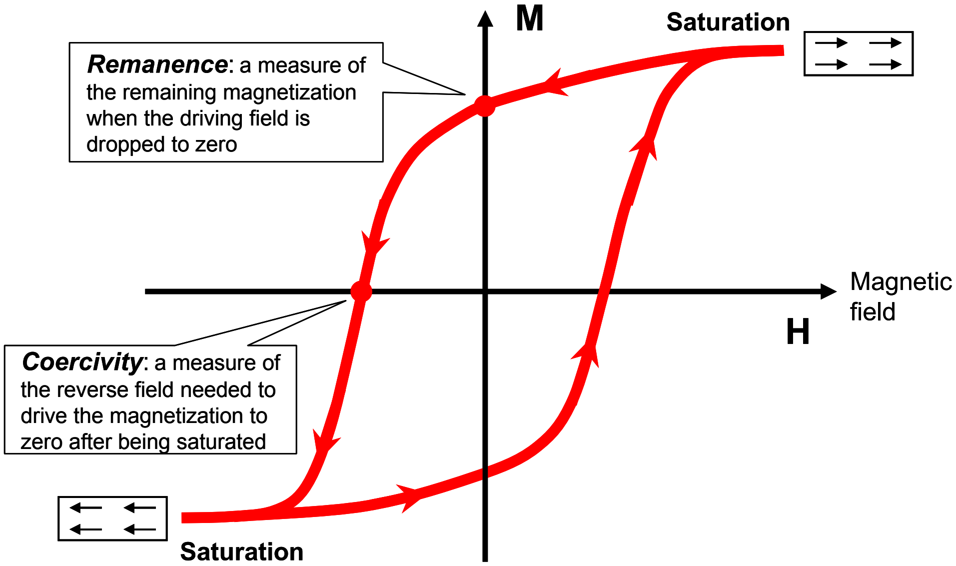

Figure 4-18 Schematic illustration of hysteresis loop

Figure 4-19 shows the magnetic hysteresis loop of electrodeposited multilayered nanowires containing 8 nm Au layer and 8 nm CoAu alloy layer. The electrodeposition

procedure of those nanowires was the same as discussed in **Section 4.1**, having the Au deposited at -0.2 mA/cm^2 for 56 s and the CoAu deposited at -6 mA/cm^2 for 5 s in a pulsed fashion. The total number of bilayers was 4221. The magnetic field was perpendicular to the nanowire arrays. As shown in **Figure 4-19**, the saturation field was 0.6 emu, at which state the material cannot absorb a stronger magnetic field, the remanence was about 0.015 emu and the coercivity was about 70 Oe. Both remanence and coercivity field are low, which is close to other reports. Valizadeh *et al.*[2] reported a low remnant magnetization in the magnetic measurement of Co 12 nm/Au 4 nm nanowires for fields applied parallel and perpendicular to the film plane. And Velu *et al.*[8] reported a coercivity field H_c of a few 100 Oe for perpendicular magnetic Co/Au sandwiches, which is higher than the result of 70 Oe in our study.

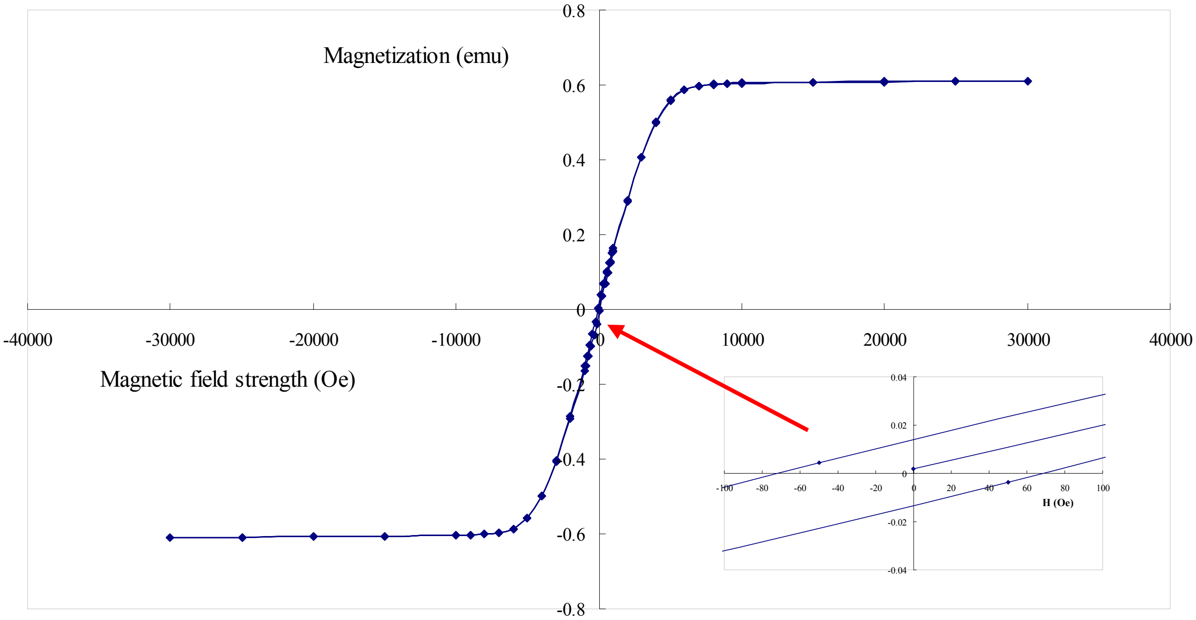

Figure 4-19 Hysteresis loop of Au/Co multilayered nanowires

4.3.6 Conclusion to Magnetic and Magnetoresistance Properties

The magnetic and magnetoresistance property of Au/CoAu multilayered thin films and nanowires were investigated. Au/CoAu multilayered thin film samples comprised of Au 3 nm /

CoAu 5 nm and Au 4 nm / CoAu 4 nm exhibited maximum CIP GMR values of negative 13 % and negative 7 % at a magnetic field of 9 Tesla, respectively. Positive inverse magnetoresistance (IMR) were also observed in the Au/CoAu multilayered thin films. However, no significant CPP GMR values with Au/Co multilayered nanowires were observed. In order to improve the GMR properties, annealing treatment was examined. Nevertheless, the results showed that annealing did not favor GMR enhancement.

4.4 Electrochemical Etching Conditions

4.4.1 Potential-pH Conditions of Au and Co

A schematic of a Pourbaix diagram is given in **Figure 4-20**, which exhibit sufficient detail for most purposes related to corrosion. Areas on the Pourbaix diagram are often labeled passive, corrosion and immune, as indicated. However, these are only estimates based on a metal-water system, without other ions in the solution, actual rates cannot be derived from the diagrams. Corrosion is possible in areas of the Pourbaix diagram where soluble ions of the metal are stable. The metal is possibly resistant to corrosion or passive in areas where an oxide is stable. In areas where only the reduced form of the metal is stable, the metal is thermodynamically immune to corrosion. Potential can be located in the area of immunity by cathodic protection.

In regions where an oxide film is stable, the metal may be passive. Passivity is the characteristic of corrosion resistance due to a protective surface film, although corrosion is favored thermodynamically. The diagram cannot predict how rapidly the film may form or how low the resultant corrosion rate may be. Where a soluble ion is stable, corrosion is possible. In the areas of the diagram where the reduced form of the metal is stable, the metal is immune to corrosion.

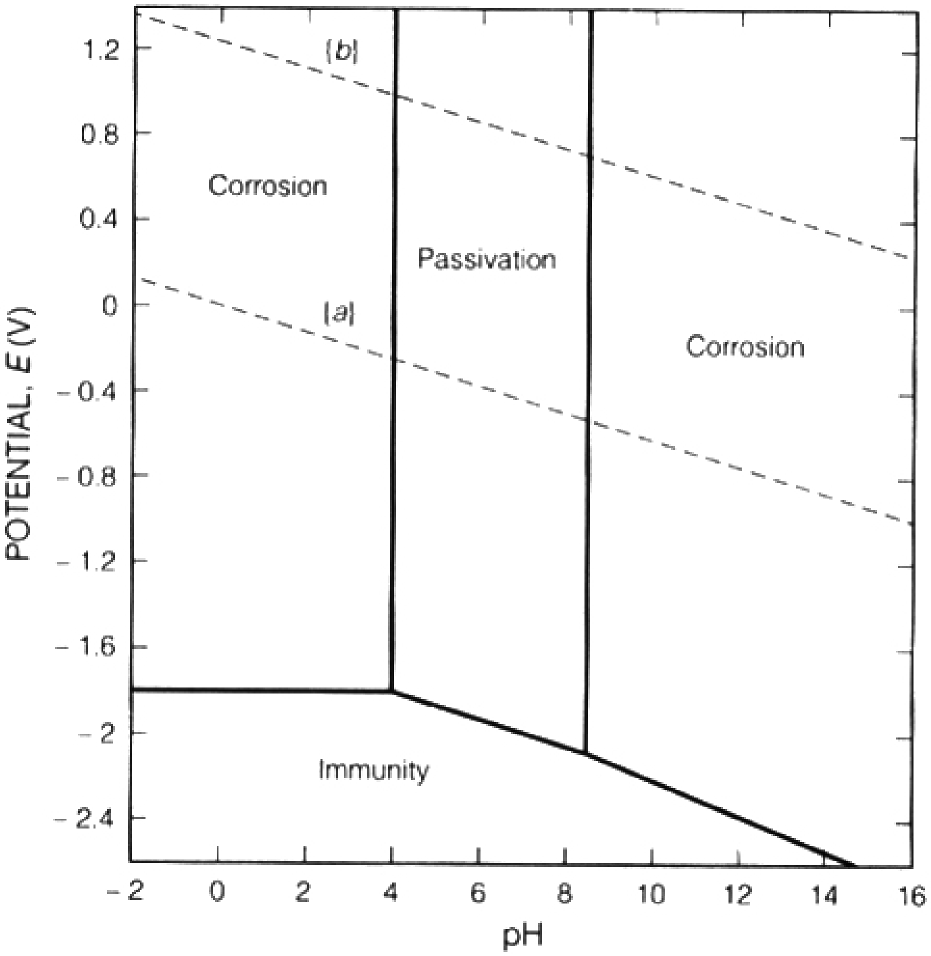

Figure 4-20 A schematic illustration of a Pourbaix diagram[87]

The potential-pH (Pourbaix) diagram for the gold-water system at room temperature is shown in **Figure 4-21**. Note that the reversible potential for the oxidation of pure gold is greater than the reversible potential for the oxygen reduction (line "b") for all pHs, thus from a thermodynamic perspective, gold is stable at room temperature in pure water. At room temperature, gold is not attacked by acids unless they are both complexing and oxidizing. However, gold can be attacked by very oxidizing systems whose reduction potentials are high, for example, above 1.4 V (vs. NHE) for pH=0. In the study of selective electrochemical etching of Au/Co system, this corrosion zone should be avoided to keep the Au layer unattacked, while etching the Co layer. Proper electrolyte and electrochemical conditions have to be examined.

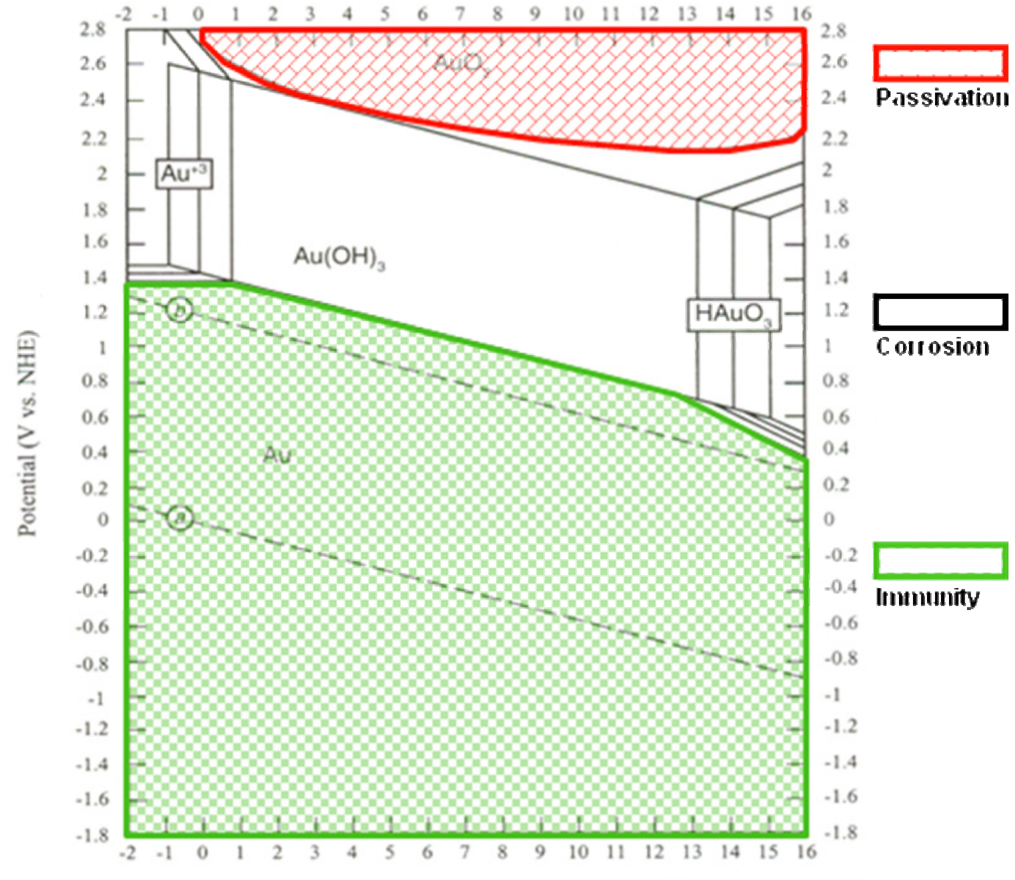

Figure 4-21 E-pH (Pourbaix) diagram for the system Au-water at room temperature[88]

Figure 4-22 shows a potential-pH equilibrium diagram for the cobalt-water system at room temperature and indicates the theoretical conditions of corrosion, immunity and passivation of cobalt without complexing agents. This diagram indicates the conditions of thermodynamic stability of cobalt and derivatives of it which can exist in the presence of water or aqueous solution free from substances with which cobalt can form soluble complexes or insoluble salts. Cobalt forms soluble complexes with ammonia, citrate, chlorides, cyanides and sulphocyanides.

According to **Figures 4-22**, the corrosion resistance of cobalt in non-complexing solutions depends on the pH and the presence of oxidizing agents: cobalt is not corrodible in neutral or alkaline solutions free from oxidizing agents, slightly corrodible in acid solutions free from oxidizing agents and very corrodible in acid or very alkaline solutions containing oxidizing

agents. Neutral or slightly alkaline oxidizing solutions cover it with a layer of oxide. Cobalt is easily protected cathodically for instance by lowering its electrode potential to a value below -0.5 V (Vs. NHE) in acid or neutral solution. Therefore, in order to electrochemically etch the Co layer in the Au/Co system, the electrolyte pH should be lower than 9, and the electrode potential should be more positive than -0.5 V (vs. NHE), as indicated in corrosion zone in **Figure 4-22**. Since the E-pH diagrams are based on the reactions of pure metals in water, they are only an estimate for the metal alloy system investigated here.

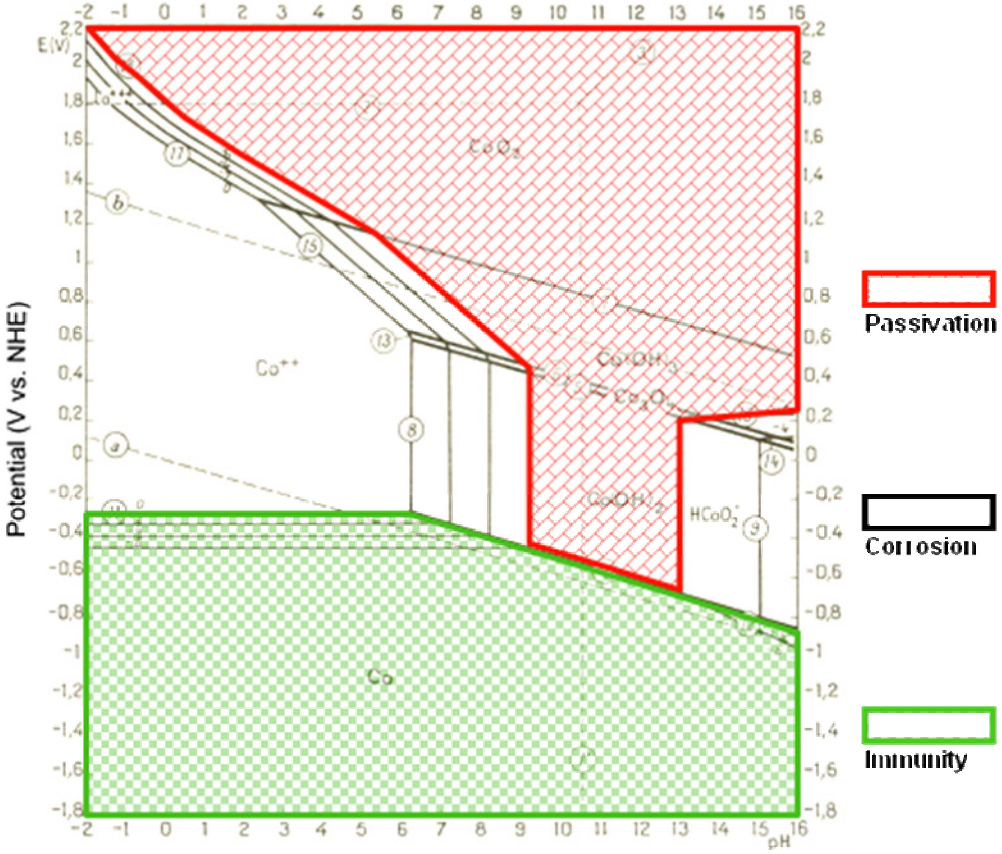

Figure 4-22 E-pH (Pourbaix) diagram for the system Co-water at room temperature[89]

4.4.2 KCl Electrolyte and Polarization Behaviors of CoAu and Au

In industry, electrochemical etching is widely employed as a tool to machine very hard and tough alloys (e.g. those based on Ti and Fe-Co-Ni-Cr) to produce components which are

able to perform a function reliably but also having minimum weight, such as aerospace propulsion and power generation sectors. Usually this specification often leads to components of very complex shape. The alloys which must be employed cause problems in conventional machining because of the low rate of metal removal, the short tool life and overheating. Electrochemical etching, also called anodic dissolution, can avoid those problems completely. [90]

Electrochemical etching relies upon a high local current density and control of the anodic dissolution so that passivation does not occur. In industry, these requirements result in the use of highly conducting electrolytes containing depassivating species (Cl^- or complexants), a small interelectrode spacing, and high flow rate of electrolyte. The last feature is also important in transporting insoluble compounds away from the work piece and in cooling. When electrochemically etching nanoscaled Au/CoAu multilayered wires or tubes, optimizing the electrolyte will be much easier and practical than adjusting the interelectrode spacing under nanometer scale. Ideally, the nanowires will be etched at 100 % current efficiency, and the rate of removal being described by (and limited by) Faraday's law.

In the electrochemical engineering industry, chloride is well known for its depassivation ability. For example, chloride restricts the stability of oxidized chromium films, leading to localized corrosion by film breakdown in the Fe-Cr and Fe-Cr-Ni stainless steels.[87] Due to this outstanding depassivation effects and low cost, a low concentration of chloride (i.e. NaCl and KCl) is a common constituent of many electrochemical etching baths. Higher current efficiency and faster etching rate in the anodic dissolution process could be achieved. Therefore in this research, a neutral potassium chloride solution is chosen as the electrochemical etching electrolyte for the fabrication of Au/CoAu nanostructures.

When looking for a proper electrolyte for the electrochemical etching process, ion conductivity (i.e. the reciprocal of resistivity) is one of the important properties used to characterize the electrolyte. A plot of conductivity vs. bulk concentration appears in **Figure 4-23**. For soluble compounds, such as H_2SO_4, KOH and CH_3COOH, conductivity reaches a maximum, but then decreases due to association and viscosity effects. But potassium chloride (KCl) reaches its solubility limit (35.5 grams KCl per 100 mL water at 20°C, equivalent to 4.7 M) before other effects limit conductivity. Therefore, this sets up an upper bound to possible solutions that are to be examined. Consequently, a series of unsaturated KCl solutions with four different concentrations (2.0, 1.5, 1.0, and 0.5 M) were investigated in this research.

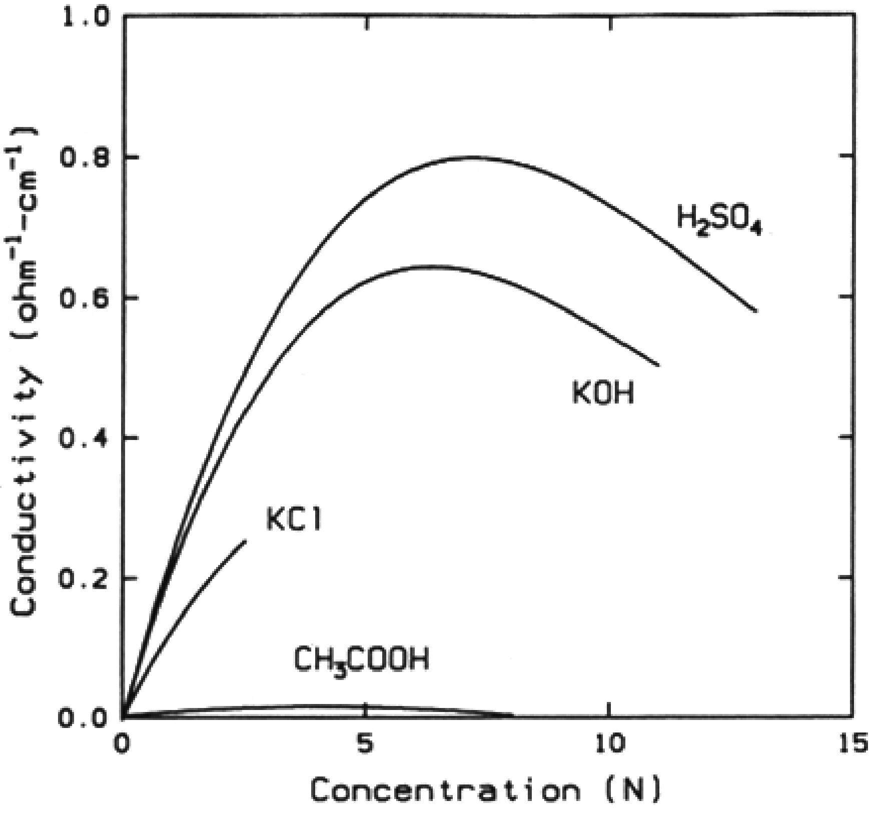

Figure 4-23 Ionic conductivity as a function of concentration at 25 °C[91]

In order to determine the proper potential range for Co selective electrochemical etching in Au/CoAu multilayered nanowires and/or nanotubes, anodic polarization curves was obtained

in those four KCl solutions with copper rotating disk electrodes (RDE) at a rotation rate of 1600 rpm, shown in **Figure 4-24 (a) – (d)**. To prevent the co-anodization of copper in the process of polarization, a thick layer of pure Au was sputtered on the top surface of the Cu RDE as a substrate layer. Then, in a non-cyanide single bath, Co-rich CoAu alloy layer for anodic polarization was galvanostatically electrodeposited at -50 mA/cm^2 for 420 s leading to an average composition of 98.1 Co wt % and 1.9 Au wt %. Details were discussed in **Section 4.1**.

As shown in **Figure 4-24**, the Co-rich CoAu alloy shows an active-passive behavior of metal-dissolution in those four KCl electrolytes. The corrosion rate is plotted on a log scale to accommodate these broad changes with oxidizing potential. For example, **Figure 4-24 (a)** reflected the detailed current response as a function of the working electrode in a 2 M KCl solution. As the electrode potential increases to more positive values from the open circuit potential (OCP = -0.592 V vs. SCE), the metal dissolution rate (or corrosion rate which is measured by anodic current density) increases, (active region). At a potential value of -0.089 V vs. SCE, which is noted as the primary passive potential (E_{pp}), the corrosion reaches a peak value of 57.38 mA/cm^2, which is noted as critical anodic current density (i_{crit}). After that, the corrosion rate decreases slightly as a passive film forms on the electrode surface and becomes stable. It is slightly passivated. At still more positive potentials (E_t = 0.047 V vs. SCE), the passive film on the Co breaks down, and the anodic current increases once again in the transpassive state.

The origin of passivity can be due either to oxide formation or salt film precipitation on the surface. In both cases, an increased barrier to dissolution results upon an increase in potential. The increased kinetic barrier upon anodic polarization contrasts with the exponentially decreased barrier which develops during anodic polarization of an active metal. The electrochemical parameters that characterize passivity (E_{corr}, E_{pp}, E_{t}, i_{corr}, i_{crit} and i_{p}) depend on both the metal and the environment to which it is exposed.

With the same copper rotating disk electrode sputtered with a thick layer of gold as a substrate, three other different KCl concentrations (1.5, 1.0, and 0.5 M) were examined, and the corresponding anodic polarization curves are shown in **Figure 4-24 (b), (c), (d)**. For each, the Co-rich CoAu alloy layer was electrodeposited with same current density for same amount of time. Comparing those four anodic polarization curves in **Figure 4-24**, electrochemical etching of Co-rich CoAu alloy in different KCl concentrations exhibits similar active-passive behavior. CoAu alloy experienced three states in the process of working potential scanning from open circuit potential to a much positive value, i.e. active, passive, and transpassive sates consequently.

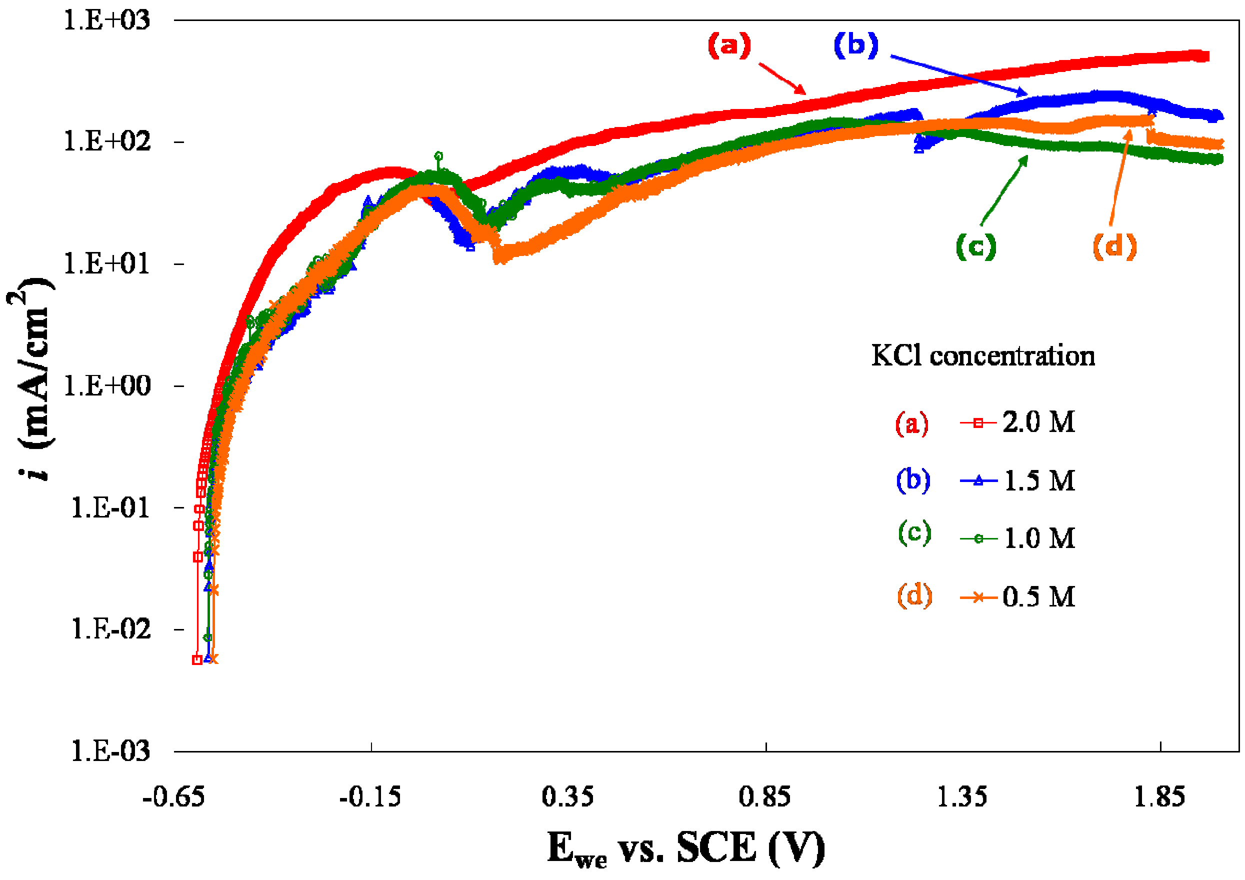

Figure 4-24 Anodic polarization curves of Co-rich CoAu alloy in KCl solutions with four different concentrations: (a) 2 M, (b) 1.5 M, (c) 1.0 M, and (d) 0.5 M with rotating disk electrode at 1600 rpm

Figure 4-24 shows a change in the open circuit potentials (OCP), primary passive potentials (E_{pp}), and critical anodic current densities (i_{crit}). Decreasing the concentration of KCl electrolytes from 2.0 M to 0.5 M did not change the open circuit potential much significantly. OCP shifted slightly from -0.592 V vs. SCE to a more negative value of -0.551 V vs. SCE; the difference between them was only 0.041 V. On the contrary, the primary passive potential and the anodic critical current density did change dramatically under the influence of KCl concentration change. For example, the primary passive potential shifted from a negative value of -0.089 V vs. SCE to a positive value of 0.031 V vs. SCE, the potential change was up to 0.12 V; and the anodic critical current density decreased from 57.38 mA/cm^2 to a much lower value of 39.78 mA/cm^2, the current density change was up to 17.6 mA/cm^2. Details are summarized in **Table 4-2**. Considering the purpose of this research is to realize the selective electrochemical etching of Co-rich CoAu alloy from Au/CoAu multilayered nanostructures with high efficiency and accuracy, the passivation state of CoAu alloy has to be avoided, which means higher i_{crit} and more negative active E_{pp} are preferred. Therefore, a KCl solution with 2 M concentration was chosen initially for better electrochemical etching of Co-rich CoAu alloy.

Table 4-2 Open circuit potentials, primary passive potentials and critical anodic current densities during the electrochemical etching of Co-rich CoAu alloys in KCl electrolytes

KCl conc. (M)	*OCP (V vs. SCE)*	*E_{pp} (V vs. SCE)*	*i_{crit} (mA/cm^2)*
2.0	-0.592	-0.089	57.38
1.5	-0.564	-0.016	47.07
1.0	-0.565	0.011	51.74
0.5	-0.551	0.031	39.78

During the anodic polarization process, we noticed the color of the KCl solution always changed from transparent at the beginning when no potential was applied to a light blue color

after the potentials was scanned from open circuit potential to 2 V vs. SCE. After each run, not only the Co-rich CoAu alloy layer on the top of rotating disk electrode was etched away completely, but also the underneath sputtered Au layer used as a protection substrate for CoAu alloy etching disappeared too. Furthermore, the copper disk electrode was also partially etched, leading to a rough surface. Usually, a solution containing $(CoCl_4)^{2-}$ is blue color and a diluted copper(II) chloride solution is also light blue. To distinguish the anodic dissolution behavior of Co-rich CoAu alloy from background noise, a similar anodic polarization process was applied to an original copper rotating disk electrode sputtered with pure Au protection layer.

The working potential was scanned from the open circuit potential to 2 V vs. SCE with a sweep rate of 2 mV/s and the current response is shown in **Figure 4-25**. Similar to the Co-rich CoAu alloy dissolution behavior, this substrate shows an active-passive behavior as well. The corrosion starts from a more positive open circuit potential (-0.252 V vs. SCE), and then, after passing the primary passivation potential (E_{pp}) of -0.043 V vs. SCE, reaches a slight passivation region and stays for a short moment. Right above the transpassive potentials (E_t = -0.027 V vs. SCE), the current increases once again till the end of the potential scan. Finally by the end of potential sweeping to a high positive potential of 2 V vs. SCE, the top Au layer was already dissolved completely and the bottom Cu disk was partially etched, left a rough surface and a light blue solution. This light blue color was believed to be the color of diluted copper(II) chloride solution.

Due to the limitation of Au sputter deposition system, this sputtered Au layer was not thick enough, and consequently cannot isolate the bottom copper disk from getting in touch with the KCl electrolyte entirely. Considering the standard electrode potential (E^o) of Cu^{2+}/Cu is only 0.340 V vs. NHE, equivalent to 0.099 V vs. SCE, it was very easy for some uncovered Cu substrate to be etched and further demolishing the top sputtered Au layer. Especially when the

working potential reached the standard electrode potential (E^o) of Au^{3+}/Au (1.52 V vs. NHE, equivalent to 1.28 V vs. SCE), the sputtered pure Au layer started dissolving too. Both the dissolution process of Cu and Au becomes even intense when the potential became further positive till the end of this experiment. Therefore, the anodic dissolution of this substrate in **Figure 4-25** is a mixture involved two anodic dissolution of metal (i.e. sputtered pure Au layer and the copper rotating disk), and some side reactions, for example, water hydrolyzing.

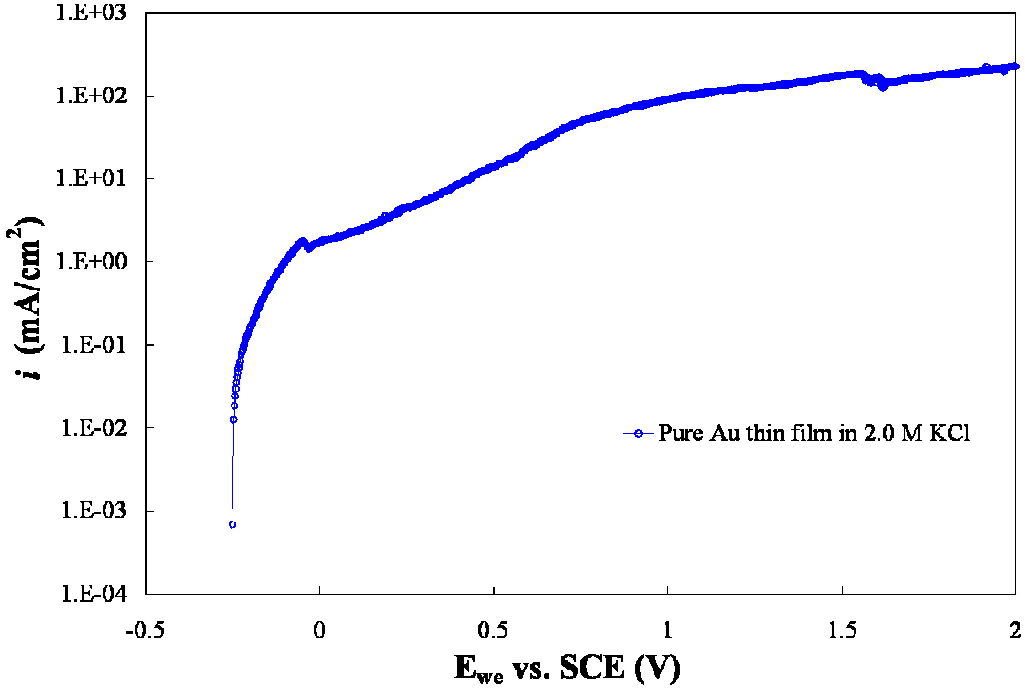

Figure 4-25 Anodic polarization curve of sputtered pure Au thin film on a copper rotating disk electrode (RDE) in 2 M KCl electrolyte at 1600 rpm

Even though the shape of the anodic polarization curve in **Figure 4-25** looks alike to the one in **Figure 4-24 (a)**, due to the log scale of current density axis, they are totally different. For example, in 2 M KCl etching electrolyte, the open circuit potential (OCP) of sputtered Au thin film substrate (-0.252 V vs. SCE) is more positive than that of Co-rich CoAu alloy (-0.592 V vs. SCE). When the applied working potential was lower than -0.252 V vs. SCE, only the Co-rich CoAu alloy can be electrochemically etched, no substrate was attacked. When the working

potential became more positive than -0.252 V vs. SCE, the substrate started to be etched too, but with a lower etching rate up to two or three orders smaller than that of the CoAu alloy etching. Therefore the sputtered Au later could delay the etching of Cu disk and help us to investigate the etching behavior of Co-rich CoAu alloy. By subtract the current response in **Figure 4-25** as background noise from the one in **Figure 4-24 (a)**, an anodic polarization curve of Co-rich CoAu alloy only was plotted in **Figure 4-26**.

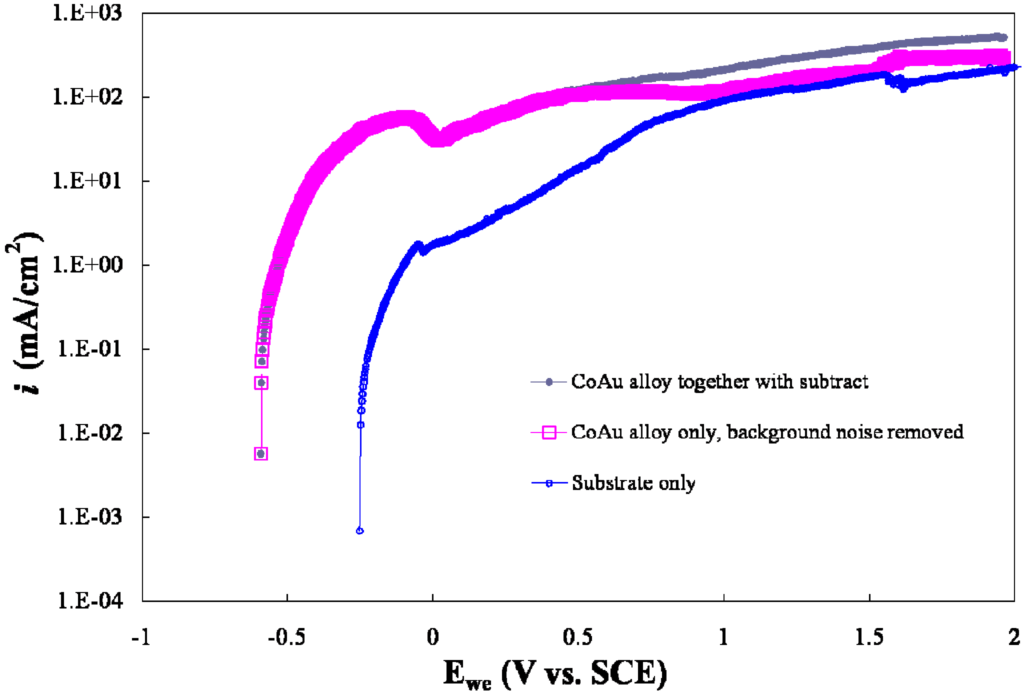

Figure 4-26 Anodic polarization curves of Co-rich CoAu alloy after the background noise being removed on a rotating disk electrode (RDE) in 2 M KCl electrolyte at 1600 rpm

In order to achieve the goal of selective etching of the Co-rich CoAu alloy layer from multilayered Au/CoAu nanostructures, next, the exact behavior of electrochemical etching of pure Au was further invested. A pure bulk Au rotating disk electrode from Pine Research Instrumentation was used in the experiment. Similarly, the anodic polarization was scanned from open circuit potential to 2 V vs. SCE, and the current response were plotted both in a log scale and in a normal scale as a function of working potential, shown in **Figure 4-27 (a)** and **(b)**.

Compared to the Co-rich CoAu alloy, the open circuit potential of this pure Au electrode in 2 M KCl electrolyte shifted to a more positive position, as far as 0.041 V vs. SCE due to its nobility. In the potential range from OCP to 0.81 V vs. SCE, the current response was almost zero. But the current will never be zero with the potential is changing, even when there are no electrochemical reactions, due to the capacitive double layer effect. Beyond potentials of 0.81 V vs. SEC, the side reactions of water electrolysis and chlorine evolution will occur consecutively. The standard potentials of the reactions (i.e. H^+/H_2O = 0.988 V vs. SCE, Cl^-/Cl_2 = 1.117 V vs. SCE and Au^+/Au = 1.589 V vs. SCE) can be used as a guideline to identify the regions where the different reactions occur.

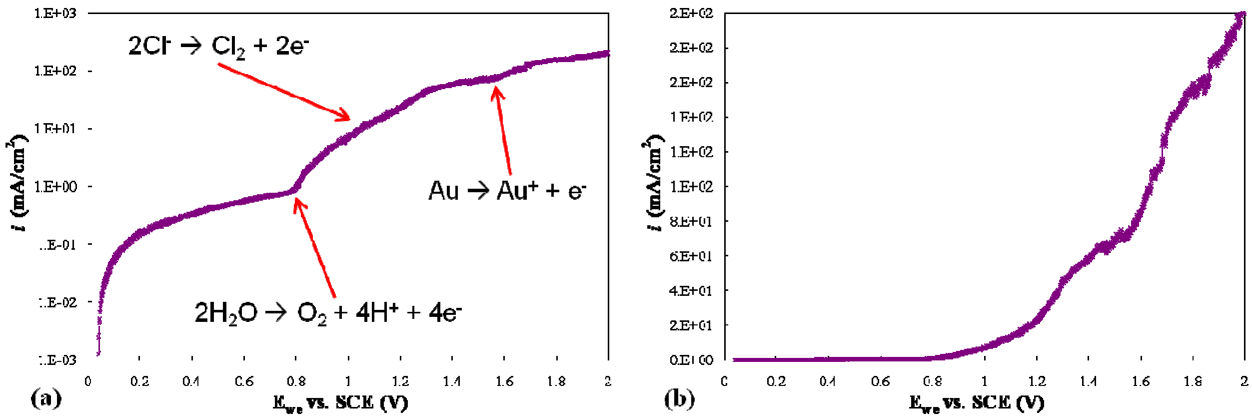

Figure 4-27 Anodic polarization curve of a pure bulk Au rotating disk electrode in 2 M KCl electrolyte at 1600 rpm: **(a)** current density plotted in a log scale, and **(b)** current density plotted in normal scale

When comparing **Figure 4-26** and **4-27** together into **Figure 4-28**, it was found that: in the 2 M KCl electrolyte, even though both Co-rich CoAu alloy and pure Au have different metal-dissolution behaviors, the rate of dissolution for the Co-rich layer is at least two orders of magnitude higher than the dissolution of Au in the range of -0.60 ~ 0.04 V vs. SCE, which established the anodization conditions of selective electrochemical etching of Au/CoAu nanostructures.

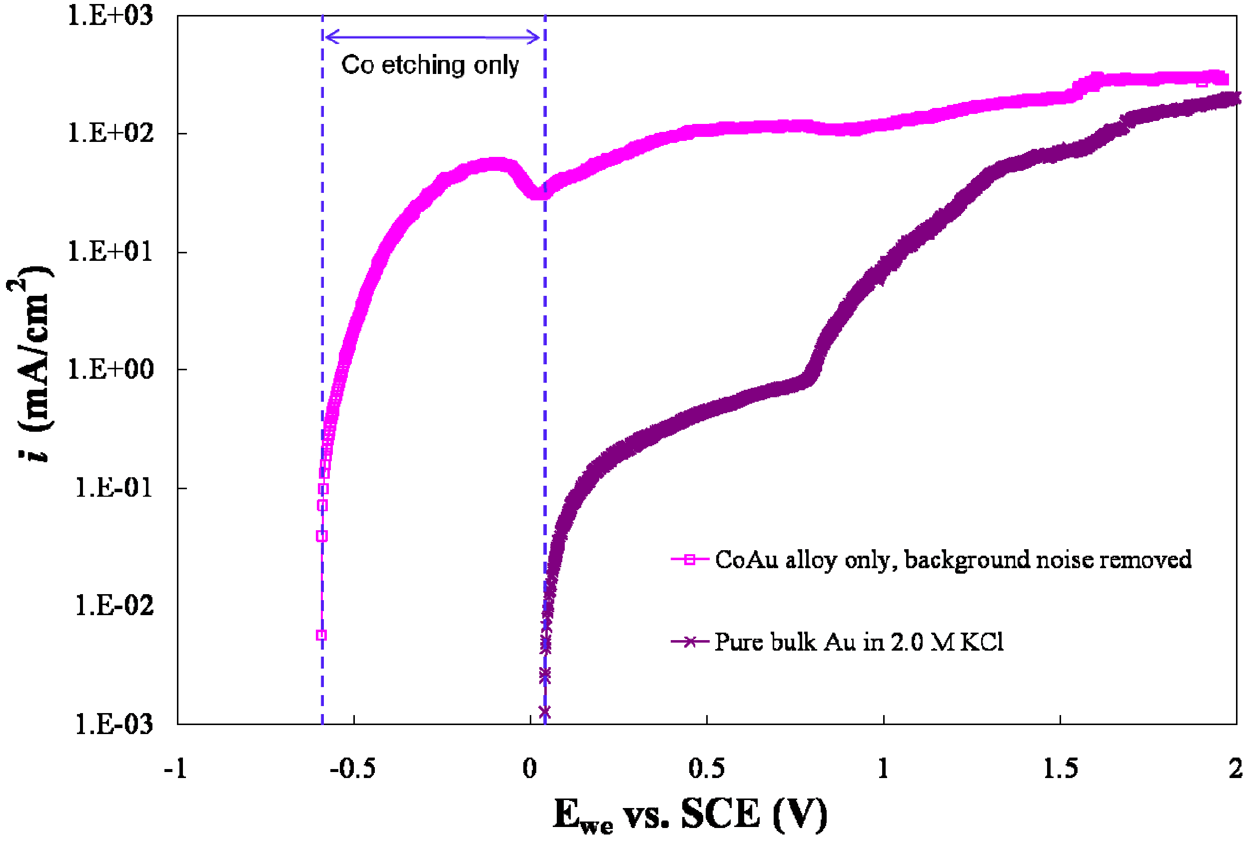

Figure 4-28 Compare of anodic polarization curves from rotating disk electrodes (RDE) with Co-rich CoAu alloy thin film (background noise removed), and pure bulk Au RDE in 2 M KCl electrolyte at 1600 rpm

4.5 Electrochemical Etching of Thin Films

Based on the investigation in **Section 4.4** about the 2 M KCl electrolyte and the polarization behaviors of CoAu alloy and pure Au, the selective of etching of the CoAu alloy from multilayered CoAu/Au nanostructures is feasible. But the exact etching conditions (including etching potential, etching efficiency, etc.) need to be determined. In order to apply the etching conditions to the nanowires and nanotubes, in the next part, thin film samples were first employed so as to survey and understand the current response behavior in the electrochemical etching of CoAu alloys.

4.5.1 CoAu Alloy Thin Films

Thin films used for preliminary investigation of electrochemical etching included a series of CoAu alloy thin films with different Co compositions and pure Co thin films. A stainless steel plate (2.5 × 2.5 cm) was employed as the working electrode, on top of which a thick Au layer was electroplated to ensure matrix adhesion and to prevent substrate dissolution during electrochemical etching. Details about Au plating can be found in **Section 3.3.2.3**. Compared with previous nanowire and nanotube structures, electrochemical etching of thin films are easier to handle.

CoAu alloy thin films with composition ranging from Au-rich to Co-rich were electrodeposited in the novel non-cyanide single electrolyte described in **Section 3.1.3**. Galvanostatic plating with three current densities (-0.2, -0.5 and -6.0 mA/cm^2) were applied for 600, 240, and 20 minutes, respectively. To make sure each sample contains the same amount of metal on the surface, the total cathodic charge of each sample, i.e. the product of current and plating time, is equal to each other. Details were summarized in **Table 4-3**. Among those three samples, the composition of the Co-rich CoAu alloy thin film plated at a current density of -6 mA/cm^2 was identical to that of the CoAu layer in Au/CoAu multilayered nanowires in **Section 4.1**.

After electrodeposition, each CoAu alloy thin film was rinsed with deionized water, dried completely, and then weighed on an analytical scale. The three CoAu alloy thin film samples were then electrochemically etched in a 2 M KCl electrolyte potentiostatically. Based on the anodic polarization curves of elemental Au and the Co-rich CoAu alloy in **Figure 4-28**, the potential range of -0.60 ~ 0.04 V vs. SCE was used for selective etching of the Co-rich CoAu alloy. In order to account for small changes in the reversible potential from sample to sample, the

electrochemical etching process was controlled by setting the same overpotential of 0.04 V above the open circuit potential. The current responses were recorded as a function of time, as shown in **Figure 4-29**.

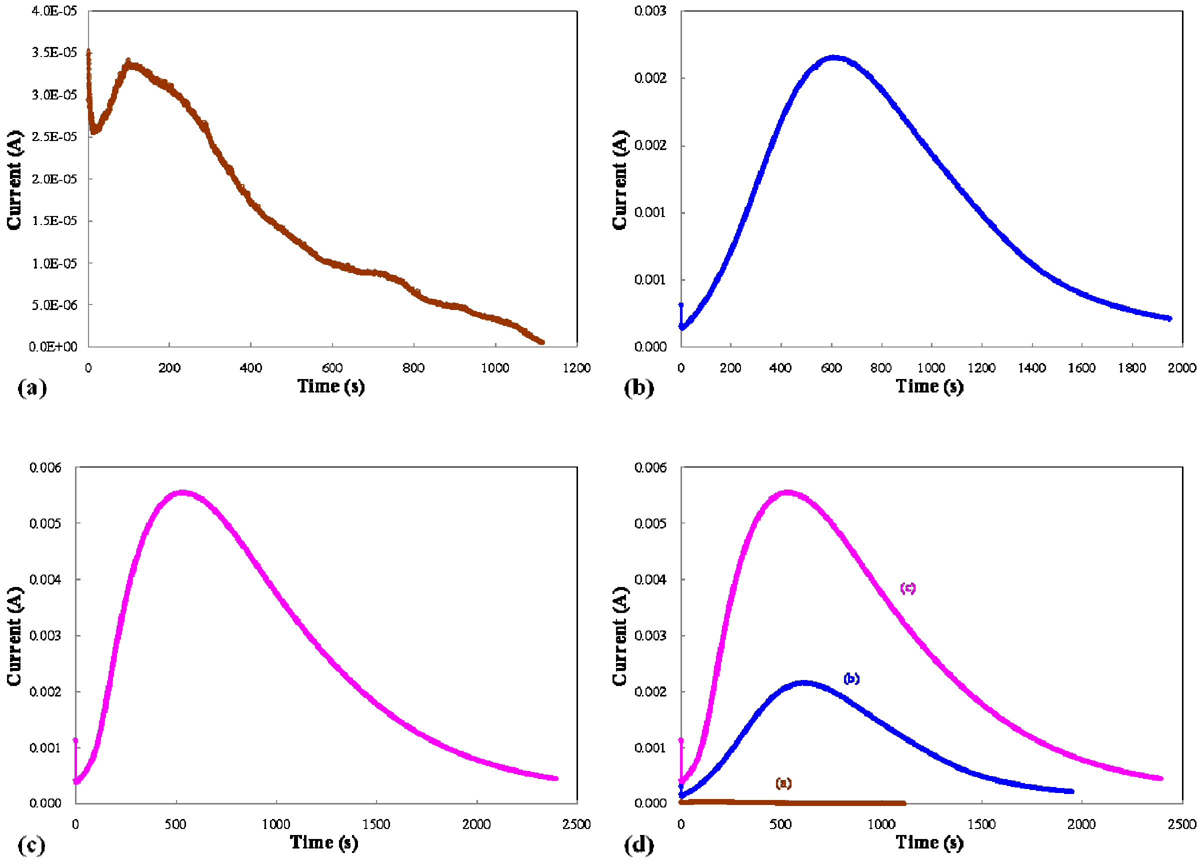

Figure 4-29 Current responses as the function of time during the process of electrochemical etching of CoAu ally thin films with three different compositions on gold electrode: (a) Co7Au93, (b) Co47Au53, and (c) Co96Au4. Plot (d) is the combination of previous (a) (b) (c) in one plot

After electrochemical etching, once again, each CoAu alloy thin film was rinsed, dried completely, and weighed. Based on the change of mass before and after electrochemical etching, and the total anodic charge calculated from the area integration of a plot of current versus time, the electrochemical etching current efficiency were calculated, as shown in **Table 4-3**. Faraday's law, $\int_0^t I dt = \frac{nF\Delta m}{M}$, was employed in the calculation in order to determine the etching efficiency.

Table 4-3 Electrochemical etching efficiency of CoAu alloy thin films plated at different current densities and times

Plating current (mA/cm^2)	***Plating time (min)***	***Composition wt %***	***Etching efficiency (%)***
-0.2	600	Co7Au93	100
-0.5	240	Co47Au53	100
-6.0	20	Co96Au4	96.3

According to **Figure 4-29**, the behavior of the current responses of the three CoAu alloy thin films are similar to each other except for the magnitude of the peak value. For example, in **Figure 4-29 (c)**, right after applying an overpotential of 0.04 V above the open circuit potential, the current decreased dramatically from the double layer charging effect. For example, for the alloy having a composition of 96 wt % Co the current dropped from 1.13 mA to 0.42 mA at the beginning 1 s. Then the current remained stable at 0.42 mA for the next 14 s. As the etching process continued, more Co component dissolved gradually, resulting in a rough surface and enhanced surface area. Consequently, the current increased once again, approaching a maximum value of 5.55 mA. After this peak value, due to the loss of mass, the surface area became smaller and the current started to drop once again until the final end of the etching process. Inspection of the three plots in **Figure 4-29 (a) (b) (c)**, indicates that the higher Co-richness in the CoAu alloy thin film lead to a larger current peak value. The peak values of the current response in **Figure 4-29 (a) (b) (c)** varied dramatically, i.e. (a) 0.03 mA, (b) 2.15 mA, and (c) 5.54 mA. The difference is especially obvious when replotting them into one plot, as shown in **Figure 4-29 (d)**. Even though there are certain minor differences among those current responses, it was observed from **Table 4-3** that all etching efficiencies were 100 % or close to it, which suggests that under the above etching conditions, only Co was etched.

4.5.2 Pure Co Thin Film

Following the same procedure, a pure Co thin film was also electrodeposited at -6 mA/cm^2 for 20 min in an electrolyte which is identical to the one used for Au/CoAu nanowires deposition but no commercial Au solution was added. The pure Co thin film was then electrochemically etched under a same working potential. The current response was plotted in **Figure 4-30**. The current efficiency for the pure Co thin film etching was 100 %, which was a little bit higher than that of the CoAu alloy thin film (deposited at -6 mA/cm^2) etching, i.e. 96.3 %.

Comparing **Figure 4-29 (c)** and **Figure 4-30** the electrochemical etching of the Co-rich CoAu alloy thin film exhibits a more gradual decrease in the current response compared to that of the pure Co thin film. The composition of this CoAu alloy thin film is the same as the CoAu alloy layer in the previous Au/CoAu multilayered nanowires, and a similar current response was observed.

Replotting the two current responses together as a function of square root of time, **Figure 4-31,** shows a very large change in the slope following the maximum. The slope for the CoAu alloy was -0.30×10^{-3} A/s$^{1/2}$, and for the Co deposit it was larger, -1.07×10^{-3} A/s$^{1/2}$. These slopes are referred to as a Cottrell-like slope because it reflects diffusion with semi-infinite boundary conditions away from a flat plate. In the Cottrell equation, it is assumed that the area is not changing. In the experiments here, the material is being etched so that the area is changing, hence, “Cottrell-like”. The difference in the Cottrell-like slopes suggests a higher diffusion resistance in the alloy which may be due to the more porous nature at the etching surface as the Au is left behind from the etched Co region.

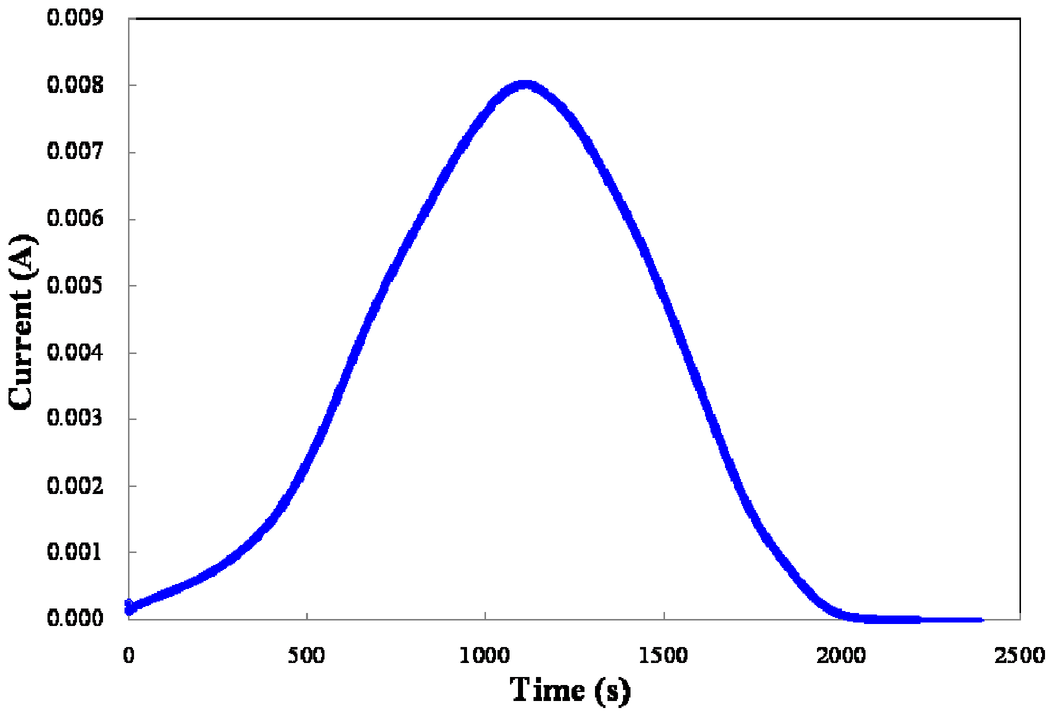

Figure 4-30 Current responses as the function of time during the process of the electrochemical etching of pure Co thin film on gold electrode

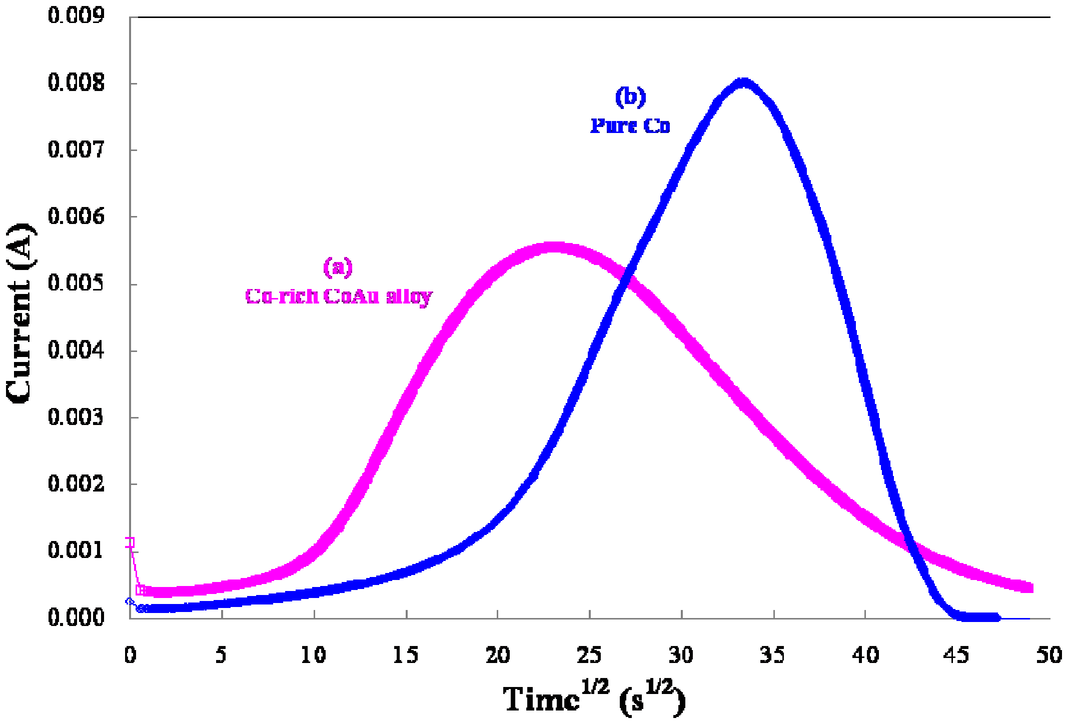

Figure 4-31 Current responses as the function of square root of time during the process of the electrochemical etching of (1) Co-rich CoAu alloy, and (2) pure Co thin films on gold electrode

4.5.3 Conclusion to Thin Film Etching

In conclusion, Co and Co-rich alloy thin films were electrochemically etched in order to determine appropriate conditions for the etching of the nanostructures. A 2 M KCl electrolyte and an applied overpotential of 0.04 V were very effective conditions. The etching efficiency was close to 100 %. Next, the selective etching of Co-rich CoAu layers from multilayered Au/CoAu nanostructures is examined.

4.6 Electrochemical Etching of Nanowires

Nanoparticles are attracting a great deal of attention due to their potential applications in biosensing, optics, electronics, and catalysis. Various nanostructures, including disks, rings, cubes, rods, and wires, have been fabricated through different methods, for example, wet-chemical technique, nanolithography, and vapor phase syntheses. To date, many single-component nanostructures, primarily Au and magnetic nanoparticles, have been extensively studied in the field of biomedical and biotechnological applications including drug delivery, biosensors, chemical and biochemical separation, and for the detection of trace amounts of specific targets, such as bacteria or leukocytes, enzyme encapsulation, and contrast enhancement in magnetic resonance imaging (MRI)[92]. For example, Au nanoparticles coated with naked DNA have been successfully used in DNA delivery by a gene gun.[56] Nie *et al.*[93] introduced the concept of using Au nanoparticles for the detection of DNA hybridization. These single-component nanostructures have proven to be very effective at a large number of tasks.

By controlling the shape of nanowires through electrochemical etching, the nanowires can also be of interest as unique high surface area catalysts. At the limit when one layer of nanowires is completely etched, nanodisks result which can be used for a wide variety of

applications, including drug delivery and biological separations. The Au/CoAu system discussed here is considered a model to develop the methodology for the etching procedure.

Figure 4-32 shows a schematic of a novel electrochemical deposition/etching procedure to produce high surface area nanobamboo and nanodisk structures. First, the multilayered Au/CoAu nanowires with various aspect ratios will be prepared via template-guided electrodeposition. Various layer sizes can be achieved by controlling the electrodeposition time for each layer. After the nanowires are released and 40 μL nanowire suspension was placed on a carbon electrode, electrochemical etching is carried out in a 2 M KCl solution. Solid nanobamboo structures will be achieved after being partially etched, and Au nanodisk arrays will be achieved after complete etching.

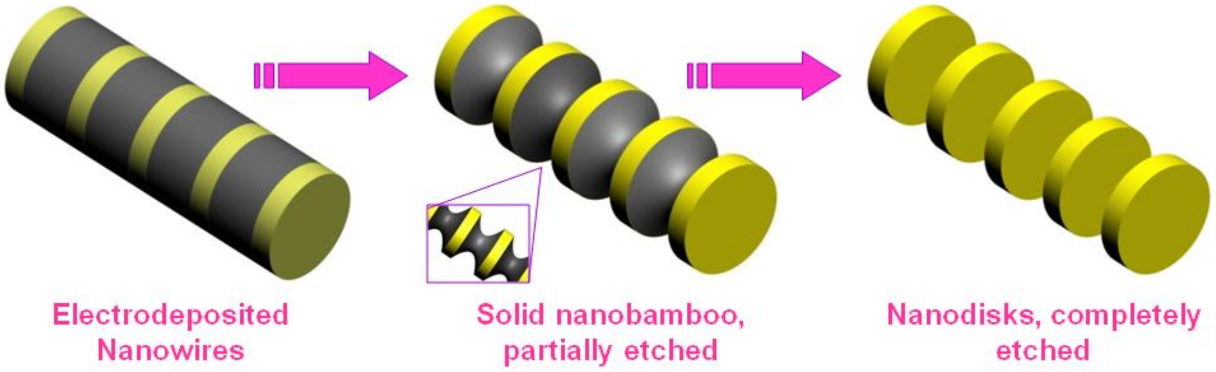

Figure 4-32 Schematic illustration of the procedure for fabrication of porous nanobamboo and nanodisks through selective electrochemical etching of Au/CoAu nanowires

4.6.1 Nanowires with Various Layer Sizes

Based on the anodic polarization curves of elemental Au and the Co-rich CoAu alloy in **Figure 4-28**, the potential range of -0.60 ~ 0.04 V vs. SCE was used for selective etching of the Co-rich CoAu alloy layer in the multilayered Au/CoAu nanowires. In order to account for small changes in the reversible potential from sample to sample, the electrochemical etching process was controlled by setting the same overpotential of 0.04 V above the open circuit potential.

After the etching potential range was determined, electrochemical etching of Au/CoAu multilayered nanowires with various Co layer sizes, while keeping the Au layer size constant, were investigated. Two series of Au/CoAu nanowires, Au 25 nm / CoAu 150 nm and Au 25 nm / CoAu 50 nm, were electrodeposited in a 0.1 μm AAO membrane by using galvanostatic square-wave pulse plating. The average length of each nanowire is 25 μm. The electrodeposition details are found in **Section 4.1**. After electrodeposition, the alumina template was dissolved in 2 M KOH, and then the nanowires were cleaned by sequential ultrasonication, centrifugation and rinsing with deionized distilled water. The nanowires were then transferred and stored in ethanol. Before electrochemical etching, a drop of the nanowires suspended in ethanol was put on the working electrode surface and the solvent was allowed to evaporate. Consequently, mono-dispersive nanowires were fixed on the electrode surface.

First, the electrochemical etching of Au 25 nm / CoAu 150 nm nanowires was examined and the current response as a function of time was shown in **Figure 4-33**. In **Figure 4-33**, the current decreased dramatically from 0.103 mA to 0.038 mA at the beginning 10 s right after an etching potential was applied. Then the current remained stable at 0.038 mA for the next 80 s. As the etching process continued, the current increased once again, approaching a maximum value of 0.045 mA. After this peak value, the current drops once again until the final end of the etching process.

In the process of electrochemical etching of Co-rich CoAu alloy layers from Au 25 nm / CoAu 150 nm nanowires, SEM images were taken at four different etching times, (a) 120 s, (b) 420 s, (c) 900 s and (d) 960 s as shown in **Figure 4-34**. As expected, during the potentiostatic electrochemical etching of nanowires, the anodic current depends on the mass-transport conditions and the effective surface area of the working electrode. Therefore, the anodic current

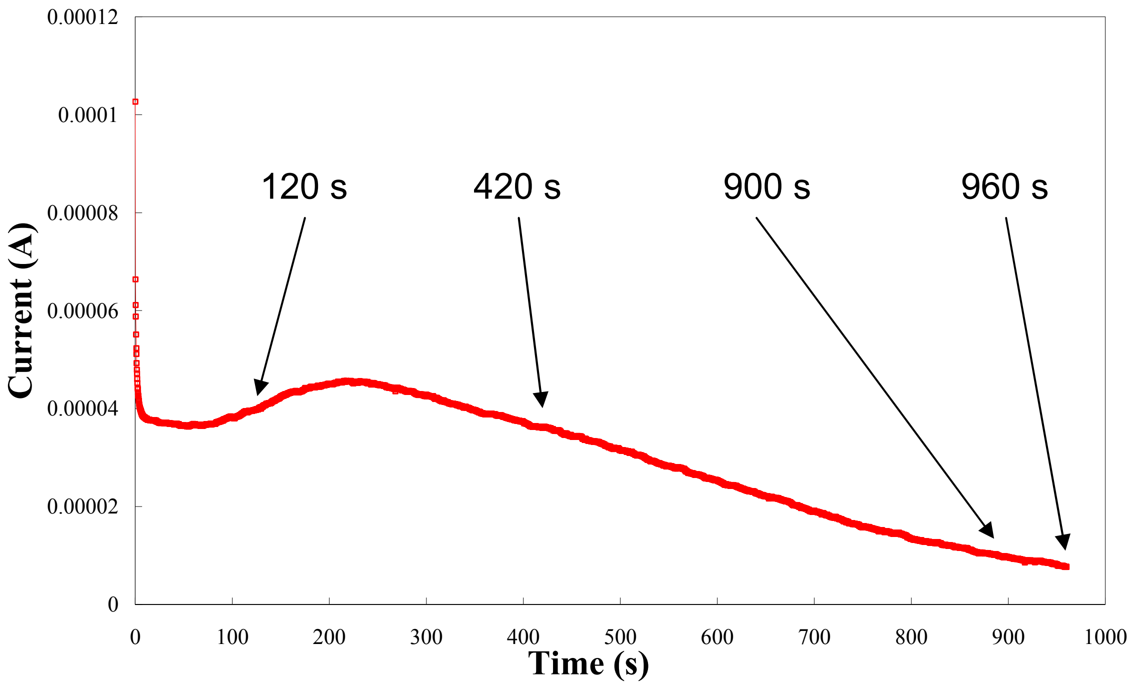

Figure 4-33 Current response as the function of time during the process of the selective electrochemical etching of Au 25 nm / CoAu 150 nm nanowires on carbon electrode

response with time in **Figure 4-33** is initially due to the charging of the electrical double layer, followed by a decrease of current from the transient of the diffusion controlled species. As the electrochemical etching continues, Co-rich CoAu alloy layers are dissolved gradually and the surface becomes rough (**Figure 4-34 (a)**), resulting in an enhanced surface area and subsequent increase in current. Later, when more and more Co-rich CoAu alloy layers are dissolved, the diameter of the CoAu alloy layer becomes smaller than that of the Au layer (**Figure 4-34 (b)**). Due to the loss of mass, the surface area becomes smaller and the current starts to decrease. After being etched for 900 s, the diameter difference between the CoAu alloy layer and Au layer is more obvious, and nano-bamboo structures are created (**Figure 4-34 (c)**). Finally, when the Co-rich CoAu alloy layers are completely etched away, there is no further material left for etching and then the anodic current approaches zero. For example in **Figure 4-34 (d)**, after being etched for 960 s, the CoAu alloy layers are completely etched and only Au nanodisk structures are left.

Unfortunately, not all the nanowires are electrochemically etched, due to the problem of conductivity. Not all the wires made electric contact with the substrate.

Similarly, the selective electrochemical etching of the nanowires with thinner CoAu alloy layers were examined. The Au 25 nm / CoAu 50 nm nanowire etching process exhibited similar anodic current behavior, but with smaller current responses and a small shift of time, as shown in **Figure 4-35**. In detail, the current decreased dramatically from 0.040 mA to 0.020 mA at the beginning 10 s right after the etching potential was applied. Then the current remained stable at 0.020 mA for the next 30 s. As the etching process continued, the current increased once again, approaching a maximum value of 0.026 mA. After this peak value, the current drops once again until the final end of the etching process.

Similarly as in the previous example, SEM images were taken at four different etching times, (a) 120 s, (b) 420 s, (c) 900 s and (d) 960 s, shown in **Figure 4-36**. In the SEM images, the bright areas on each nanowire represent the Au layer, and the dark areas represent the Co-rich CoAu alloy layer. The electrochemical etching with short times (e.g. 120 and 420 s) does not change the nanowire surface morphology significantly. When the etching time is longer, for example 900 s, the diameter of the Co-rich CoAu alloy layer, containing a small amount of Au, decreases dramatically, while the diameter of the Au layer remains similar to the size prior to etching (300 nm). As a result of electrochemical etching, shown in **Figure 4-36 (c)**, the nanowire surface morphology was modified and the nanowire surface area was significantly enhanced, which is advantageous for potential applications in surface reactions, immobilizing molecules and nanoelectronics. An EDS spectrum in **Figure 4-37** confirmed the existence of a Co-rich CoAu alloy layer in the nano-bamboo structures. Finally, when all the Co-rich CoAu alloy layers in each nanowire were dissolved completely after 960 s, only Au nanodisk structures were left, as shown in **Figure 4-36 (d)**.

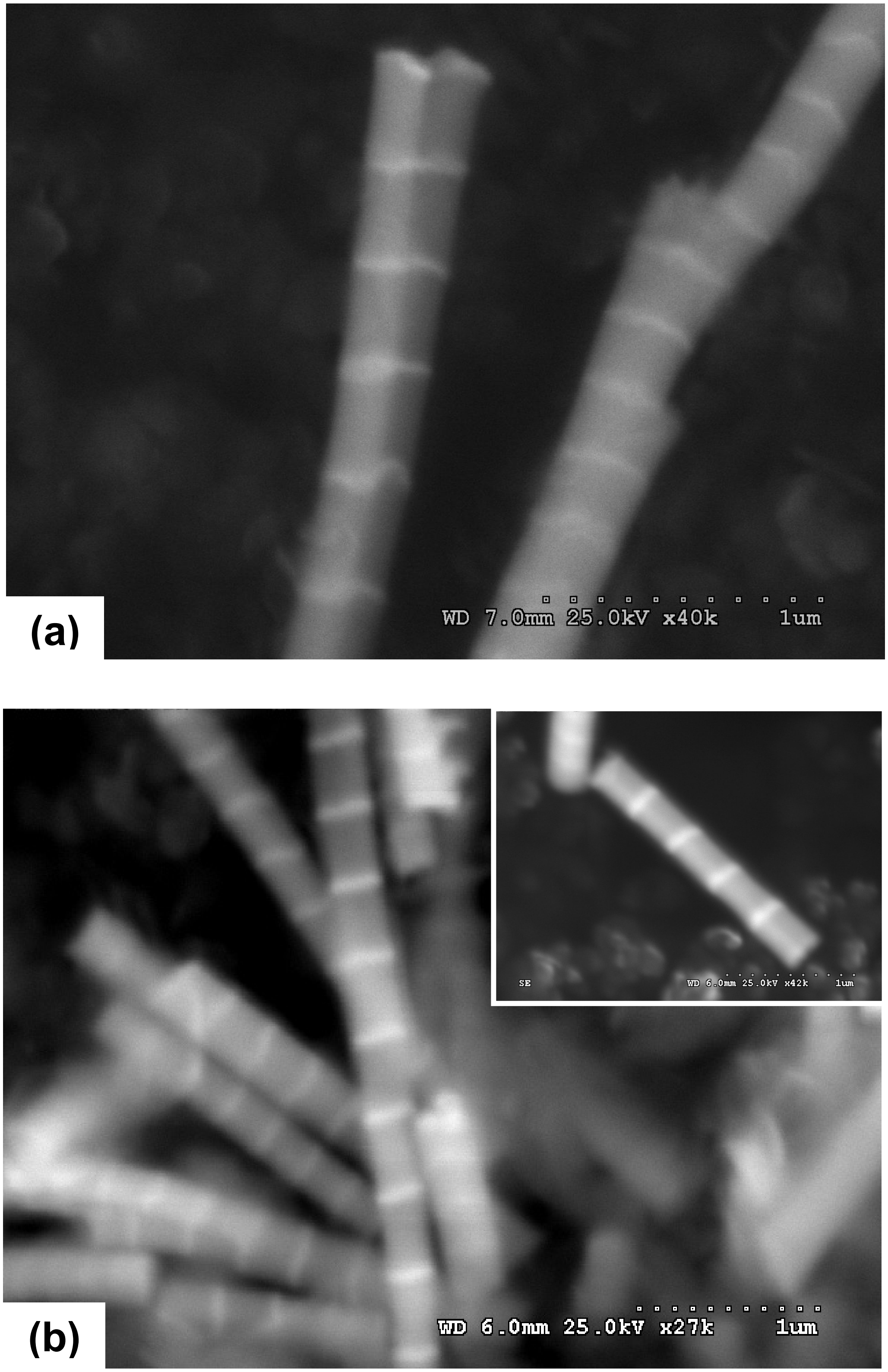

Figure 4-34 SEM images taken at four different times: (a) 120 s, (b) 420 s, (c) 900 s, and (d) 960 s in the process of electrochemical etching of Au 25 nm / CoAu 150 nm nanowires

Figure 4-34 continued

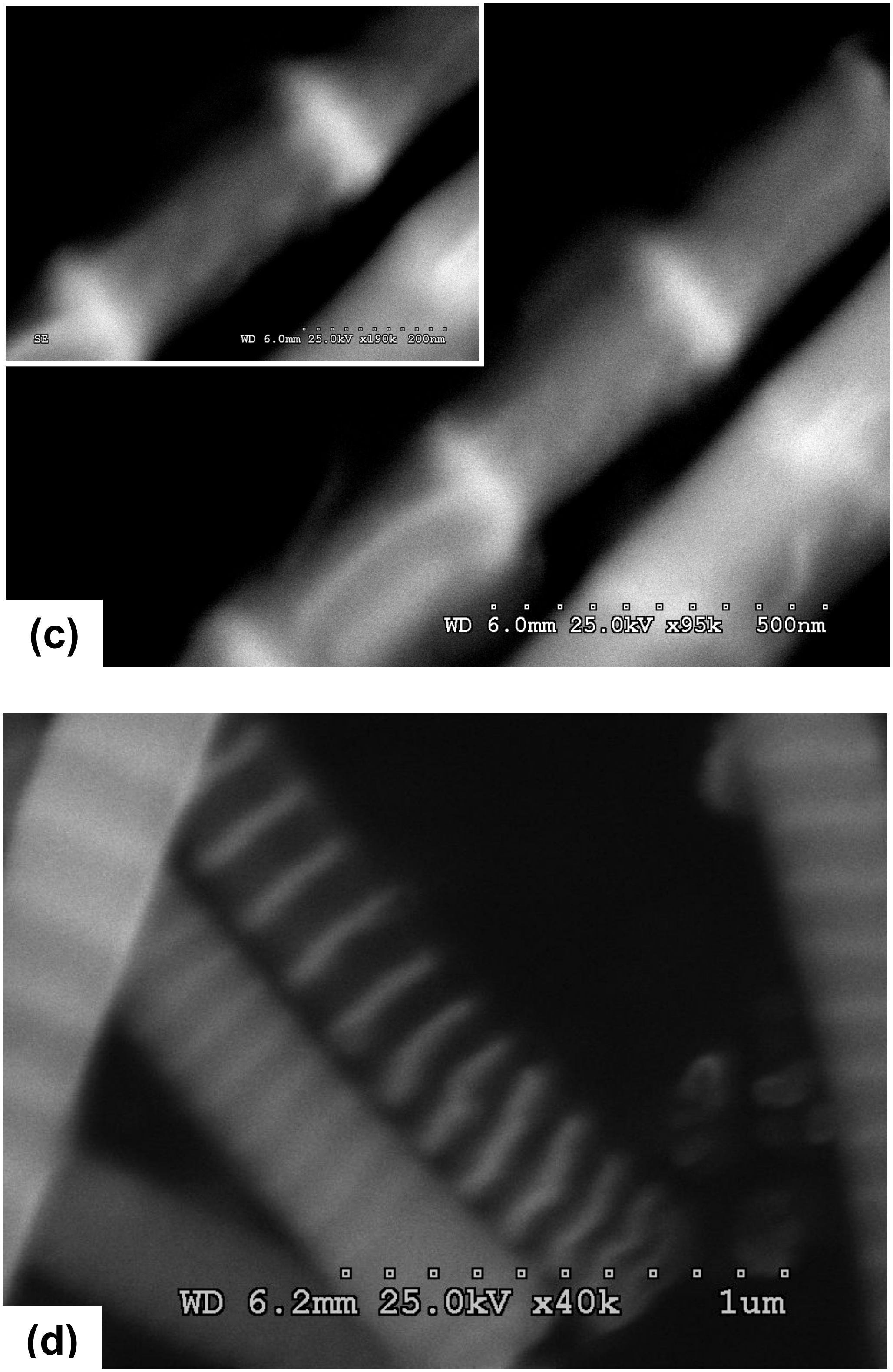

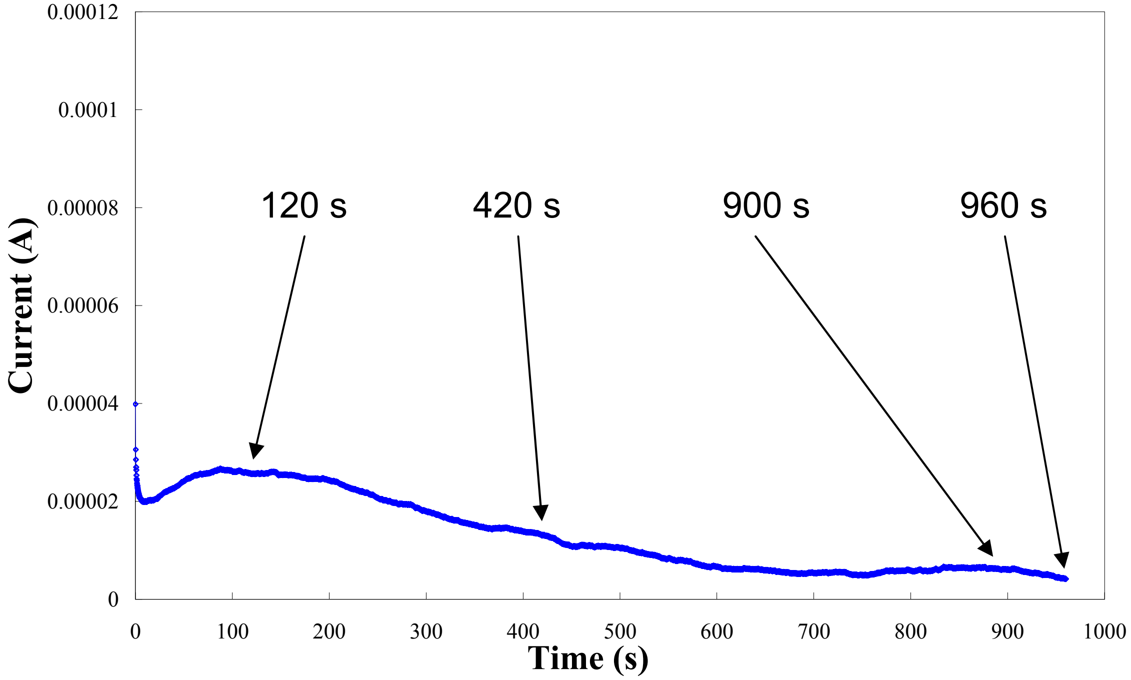

Figure 4-35 Current response as the function of time during the process of the selective electrochemical etching of Au 25 nm / CoAu 50 nm nanowires on carbon electrode

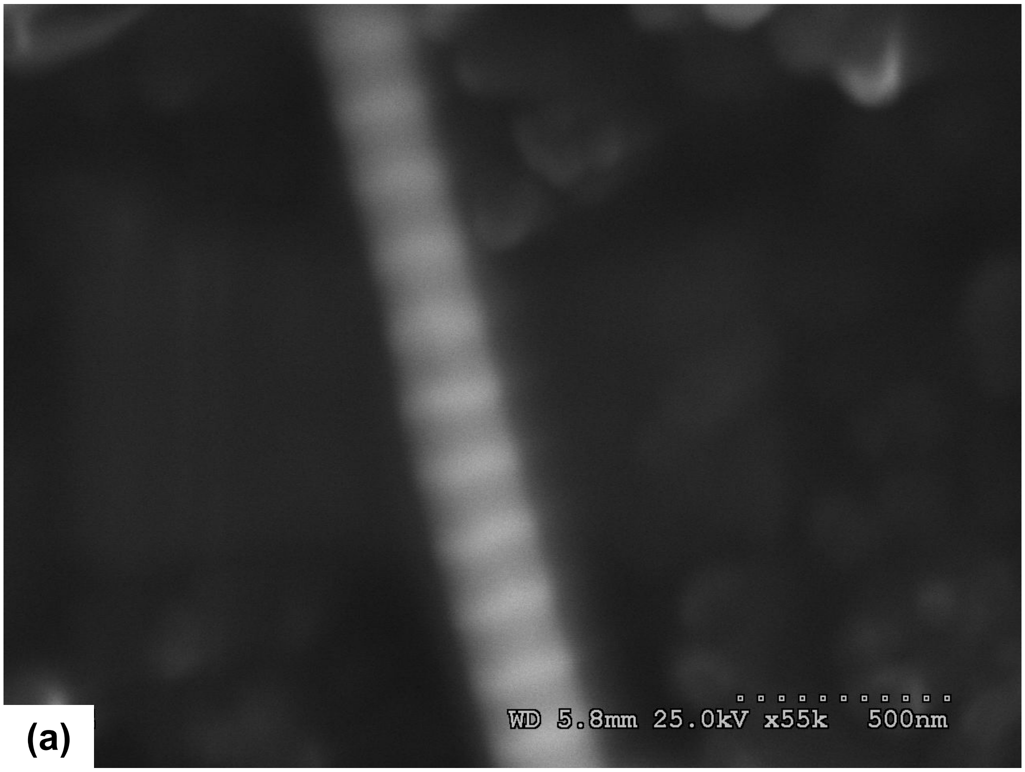

Figure 4-36 SEM images taken at four different times: (a) 120 s, (b) 420 s, (c) 900 s, and (d) 960 s in the process of electrochemical etching of Au 25 nm / CoAu 50 nm nanowires

Figure 4-36 continued

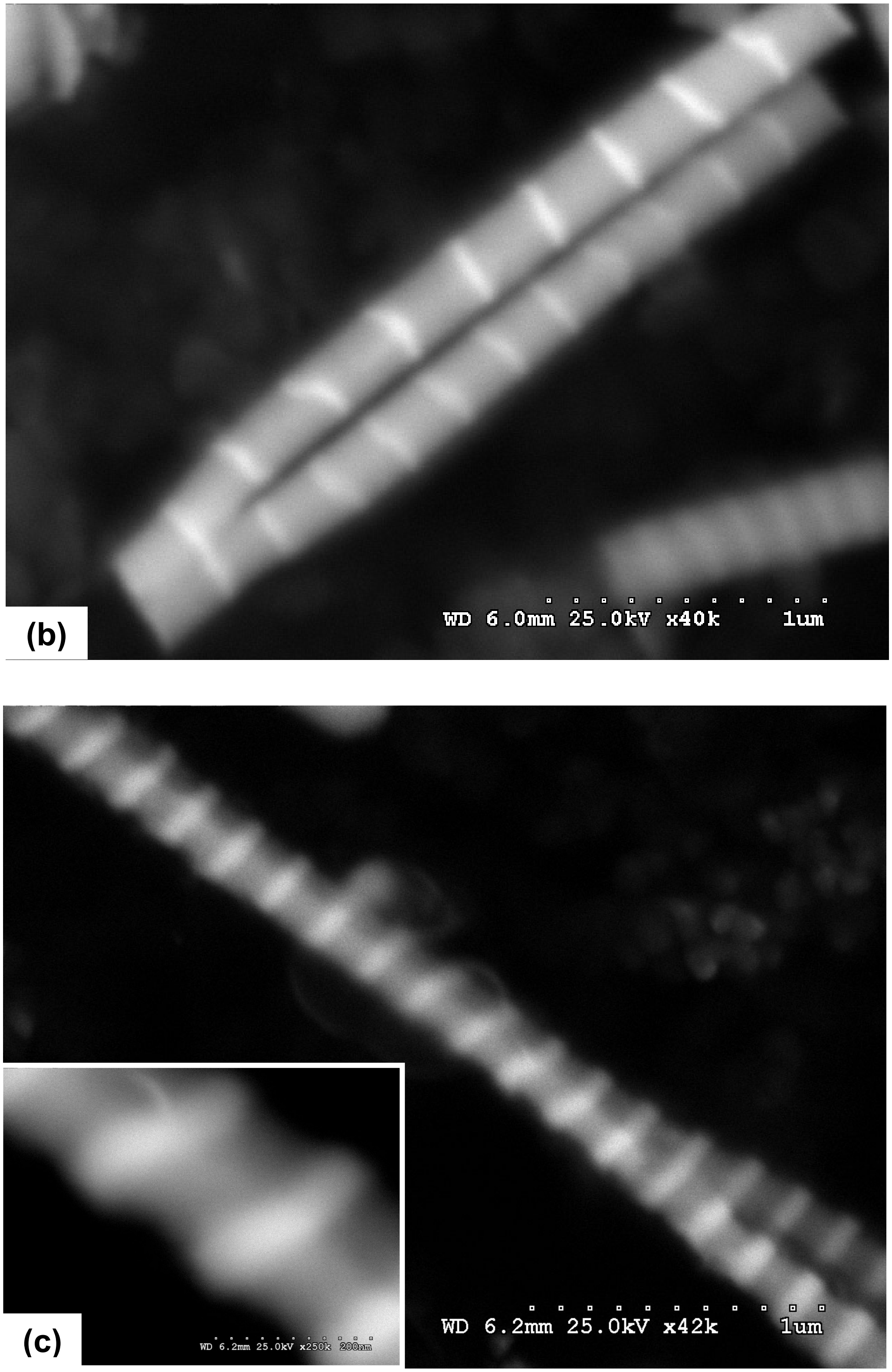

Figure 4-36 continued

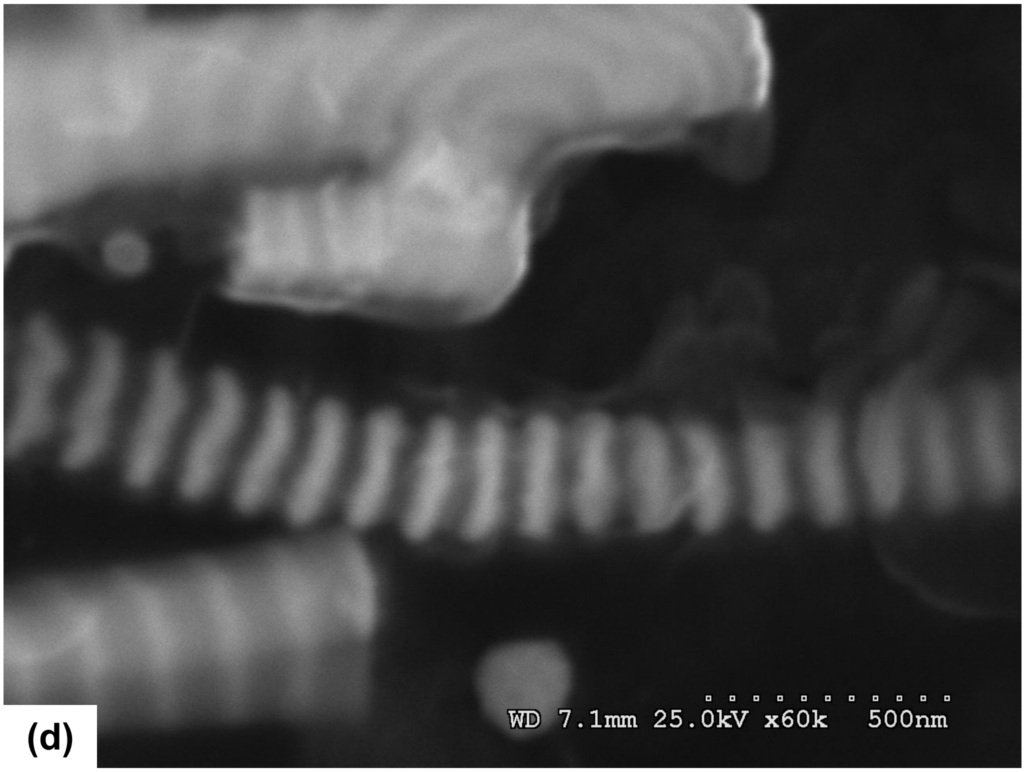

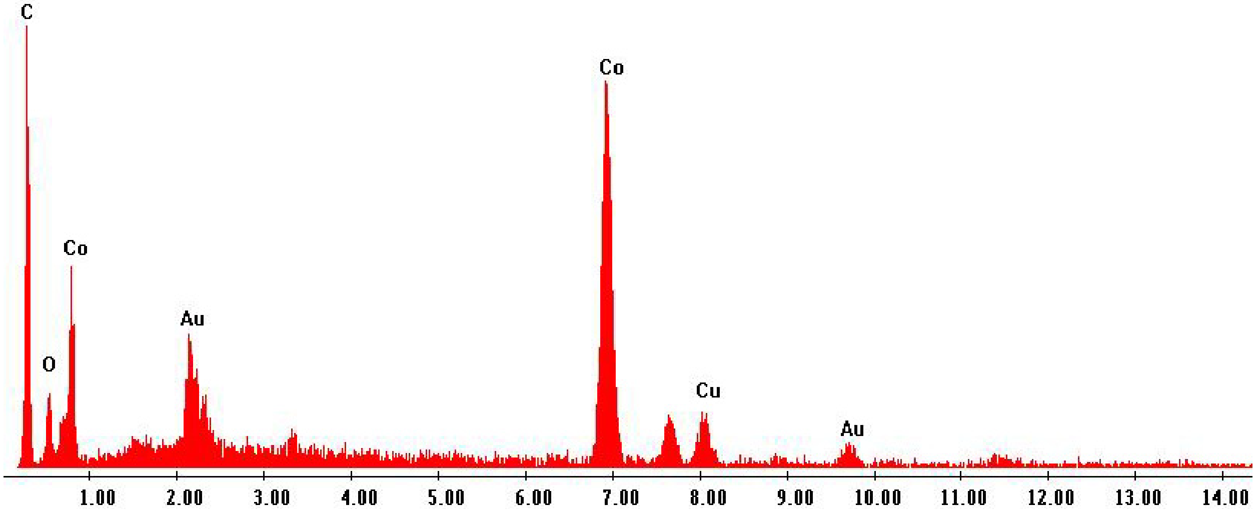

Figure 4-37 EDS spectrum of the CoAu alloy layer in the nanowires

Next, **Figure 4-33** and **4-35** are replotted together in **Figure 4-38** and the electrochemical etching of nanowires with various layer sizes was compared. **Figure 4-38** shows the current responses versus square root of time of the selective electrochemical etching of Au 25 nm / CoAu 150 nm and Au 25 nm / CoAu 50 nm nanowires on carbon substrate for 960 s. The square root of time is used to identify regions that may be diffusion controlled. As shown in **Figure 4-38**, both nanowire samples exhibited similar current responses. When comparing the current responses of the two different groups of nanowires, etching of the nanowires with thinner CoAu alloy layer size (50 nm) exhibits a smaller current response. The current difference was due to the different surface area exposed to the electrolyte. In **Figure 4-38**, both current response curves displayed a linear relationship as a function of square root of time after the peak in current, which confirms the diffusion control in certain regions during the electrochemical etching of nanowires.

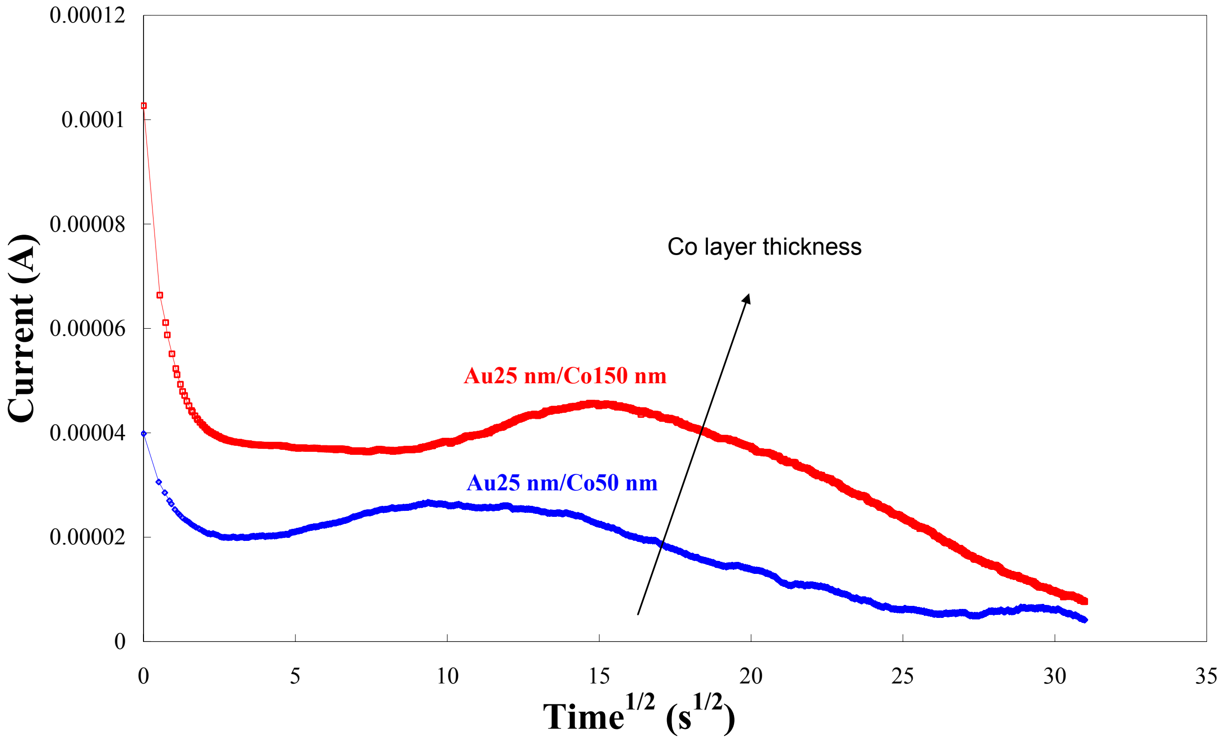

Figure 4-38 Current responses as the function of square root of time during the process of the selective electrochemical etching of Au/CoAu nanowires on carbon electrode

By integrating the areas under each current response as a function of time, anodic charges were achieved for each nanowire anodic dissolution process. The results are summarized in **Table 4-4**. The Co-rich CoAu alloy layer size is 150 nm, and the total charge of anodic dissolution is 3.17×10^{-2} C. When the Co-rich CoAu alloy layer size is 50 nm, the total charge of anodic dissolution is 1.26×10^{-2} C. As shown in the last column in **Table 4-4**, the ratio of anodic charge is 2.52, which is close to 3, i.e. the ratio of CoAu layer size.

Table 4-4 Ratio of CoAu layer sizes and ratio of charges

CoAu layer size (nm)	***Ratio of CoAu layer size***	***Anodic charge (C)***	***Ratio of charge***
150	3	3.17×10^{-2}	**2.52**
50	**1**	$\mathbf{1.26\times10^{-2}}$	**1**

Additional samples with a larger CoAu layer size were electrodeposited, however, due to internal stress, the deposit severely cracked and so etching was not continue. The AAO membrane always broke in the process of plating. Therefore, another series of Au/CoAu multilayered nanowires with shorter total length were fabricated and then been tested for the electrochemical etching.

Nanowires with four various AuCo layer size were electrodeposited in AAO membranes with pore size of 0.1 μm. Each of them has the same total length of 12 μm and the same Au layer thickness of 25 nm, but different CoAu layer sizes, including 20, 50, 100, 150 nm. Following the similar steps as previous described, nanowires were first released from the AAO membrane. Second, due to the use of larger size carbon substrates, 60 μL nanowire suspension was carefully transferred to the surface of the substrate, instead of 40 μL used before. After the samples were fully dried, electrochemical etching experiments were tested in the 2 M KCl solution.

Current responses as a function of time in the process of electrochemical etching of four Au/CoAu nanowires were plotted in **Figure 4-39**. Each of them exhibited a typical peak shape similar to **Figure 4-38**. The thicker the CoAu layer size, the higher value of the peak is achieved. The larger CoAu alloy layer size means more mass for electrochemical etching, consequently larger surface area is created during the etching process and a larger current arises, keeping the same total length and diameter. Since the Au 25 nm / CoAu 20 nm nanowires have less CoAu alloy to be etched, (**Figure 4-39**), the current response looks like a flat curve with a broader peak compared to those of the other three nanowires containing more CoAu alloy segments.

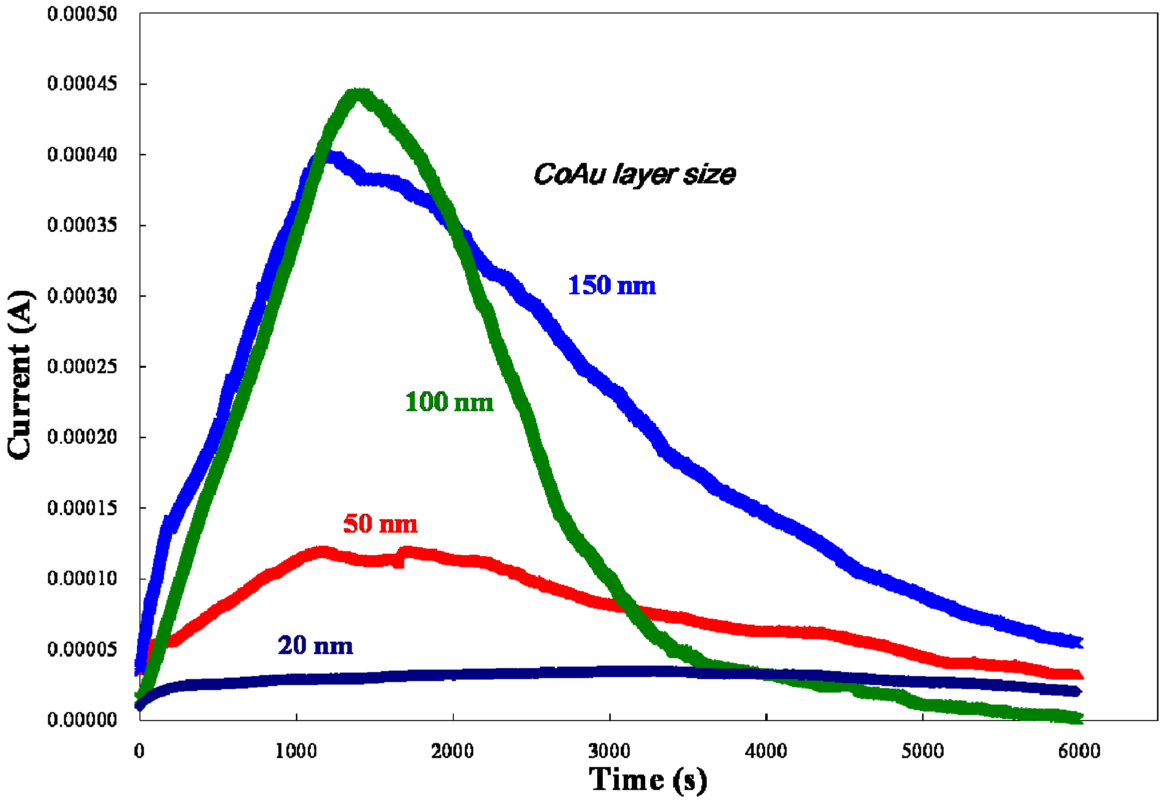

Figure 4-39 Current responses as the function of time during the process of the selective electrochemical etching of Au/CoAu nanowires on carbon electrodes with four different CoAu layer sizes including 20, 50, 100, and 150 nm

In this research the aim is to control the electrochemical etching degree in a precise way so that intermediate structures can be identified and obtained by partial etching. Both

nanobamboo and hollow nanobamboo structures are examined. A convenient and effective way to characterize the etching degree and to correlate the etching time to the exact shape of nanostructure needs to be developed without the need to take samples out of electrochemical cell for SEM or TEM examination. Considering previous current response curves and the SEM images of nanobamboo structures taken at different etching times, it was confirmed that current response as a function of time can be one effective tool to characterize the real time etching degree and predict the shape of nanostructure.

A more reproducible way to monitor the shape change is to inspect the charge over time. For example, the anodic charge as a function of time during the process of electrochemical etching of the four Au/CoAu nanowires are plotted in **Figure 4-40**. Compared with the current responses in **Figure 4-39**, at the initial stage of etching, the anodic charges accumulates gradually. As more and more CoAu alloy layers are etched away and the surface becomes rougher, surface area is enhanced and current (or etching rate) increases dramatically. Consequently, the slope of anodic charge response curves becomes steeper. At this moment, partially etched nanobamboo structures are created. When a current response curve reaches its peak value, the corresponding anodic charge response curve exhibits an inflexion. After that, due to the loss of mass, the surface area becomes smaller and the current starts to decrease. As a result, the charge response curve is getting close to a plateau. Since the anodic charge can be automatically recorded and shown on the monitor of a potentiostat for real time monitoring, the exact degree of electrochemical etching and the detailed shape of the nanostructure can also be predicted. Especially, even though there is minor deviation of current response curve of CoAu layer size 100 nm in **Figure 4-39**, the corresponding anodic charge response in **Figure 4-40** is not affected.

The comparison of anodic charge change and the CoAu alloy layer size change was calculated and shown in **Table 4-5**. In this series of experiments, the samples were prepared very carefully and 60 μL of nanowire suspension transferred to the carbon substrates were controlled precisely; the ratio of anodic charges and the corresponding ratios of CoAu layer sizes were almost equal to each other. Those numbers further confirmed the feasibility of controlling the etching degree and predicting the shape of nanostructures by monitoring the anodic charge response. For example, at half of the total charge, partially etched nanobamboo structures are expected. Then, when the charge response curve approaches the plateau, completely etched nanodisk structures are created.

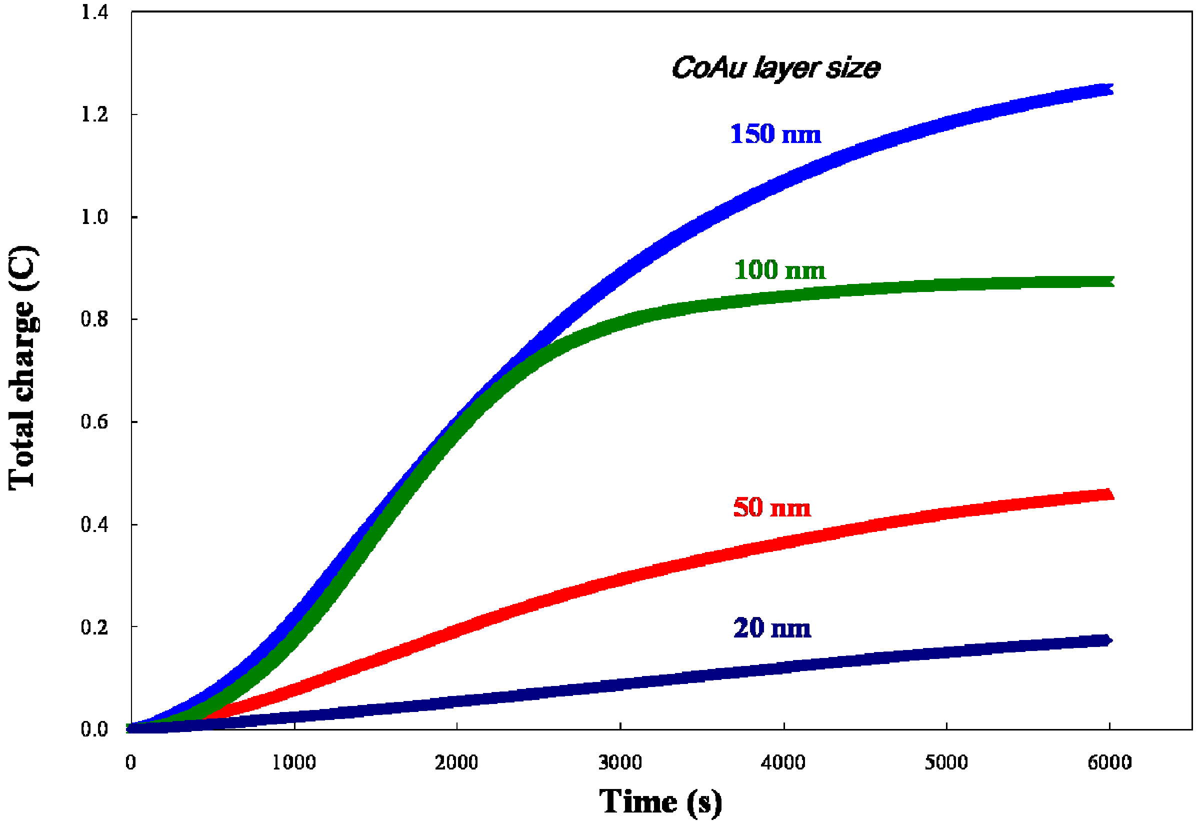

Figure 4-40 Anodic charges as the function of time during the process of the selective electrochemical etching of Au/CoAu nanowires on carbon electrodes with four different CoAu layer sizes including 20, 50, 100, and 150 nm

Table 4-5 Comparison of CoAu layer sizes and anodic charges during the process of the selective electrochemical etching of Au/CoAu nanowires on carbon electrodes with four different CoAu layer sizes: 20, 50, 100, and 150 nm

CoAu Layer Size (nm)	*Ratio of CoAu layer*	*Anodic charge (C)*	*Ratio of Q*
150	7.5	1.2509	7.2
100	5.0	0.8737	5.0
50	2.5	0.4597	2.6
20	1.0	0.1746	1.0

4.6.2 Cyclic Voltammetry (CV) Analysis

Cyclic voltammetry (CV) is the potential-scan equivalent of double potential step chronoamperometry. It is used here as a way to further charactirize the changes of the nanowire or nanotube during etching.

Creating porosity in nanowires to increase the surface area has been examined by Searson *et al.*[16, 17] They electrodeposited an alloy of AgAu and then selectively dissolved the Ag leaving a Au porous structure by wet-chemical etching. After that they used liquid nitrogen adsorption to measure the surface change, which is a time consuming process. Compared to nitrogen adsorption, cyclic voltammetry usually takes only half a minute. The samples don't have to experience an extreme low temperature and therefore no change was caused to the surface morphology. Finally and financially speaking, no extra instruments are needed for an electrochemical lab.

Ferricyanide ($\mathrm{Fe(CN)}_6^{3-}$) reduction to ferrocyanide ($\mathrm{Fe(CN)}_6^{4-}$) and the reverse reaction, oxidation of ($\mathrm{Fe(CN)}_6^{4-}$) to $\mathrm{Fe(CN)}_6^{3-}$, are two fairly popular electrochemical reactions which are often used as a model redox reference system in electrochemical studies. Even though cyanide

(CN^-) is well-known for its toxic effects, it is complexed at a high pH environment, and thus not toxic. Since both ferricyanide and ferrocyanide are soluble, the reduction of ferricyanide does not leave any reduced solid materials on the electrode surface and consequently causes no change to the surface area. Therefore, in this research, cyclic voltammetry in a ferricyanide/ferrocyanide solution on carbon electrodes covered with various nanowires will be investigated as an effective method to qualitatively characterize the surface change in the electrochemical etching process of Au/CoAu nanowires.

The ferricyanide reduction solution contained 0.001 M potassium ferricyanide and 0.003 M potassium ferrocyanide in 0.5 M NaOH which were made with distilled deionized water. In order to easily distinguish the reduction of ferricyanide and the oxidization of ferrocyanide in the cyclic voltammograms, the concentration of ferrocyanide was made three times larger than that of ferricyanide. Since ferrocyanide hydrolyzes slowly when exposed to light, the solution has to be stored in the dark and not used for more than a few days (less than a week).

The cyclic voltammetry was first tested with a carbon electrode on which 40 µL Au 25 nm / CoAu 100 nm unetched nanowire suspension were added. In the above ferricyanide/ferrocyanide solution, three different potential sweep rates (50, 100 and 150 mV/s) were examined and the potential range was between 0.45 ~ -1.0 V vs. SCE. The corresponding cyclic voltammograms were shown in **Figure 4-41**. Those three current responses as a function of electrode potentials are well behaved for a typical ferricyanide/ferrocyanide redox couple. For each sweep rate, in the forward scan, the main reaction at the working electrode was the reduction of the ferricyanide ion:

$$\mathrm{Fe(CN)}_6^{3-} + e^- \rightarrow \mathrm{Fe(CN)}_6^{4-}$$

When the potential becomes more negative than the equilibrium potential of the main reaction, the side reaction of water reduction occurs at the working electrode of Au/CoAu nanowires on the carbon substrate.

$$2H_2O + 2e^- \rightarrow H_2 + 2OH^-$$

Then the applied potential was reversed and the potential was scanned in a positive direction. Close to the working electrode surface, there is a large concentration of the ferrocyanide ion reduced from the previous forward scan. When the potential approached and passed the equilibrium potential of ferricyanide/ferrocyanide redox couple, the concentrated ferrocyanide ion was oxidized again and ferricyanide ion was formed in the vicinity of electrode.

$$Fe(CN)_6^{4-} \rightarrow Fe(CN)_6^{3-} + e^-$$

Additionally, the original concentration of ferrocyanide is triple of the concentration of ferricyanide, so that the concentration gradient of ferrocyanide between the bulk solution and the electrode surface was much higher the concentration gradient of ferricyanide in the previous forward scan. As a result, the current response peak (or the reaction rate) of ferrocyanide oxidization is much higher than the current response peak of previous ferricyanide reduction. Also, since in each of the three cyclic voltammograms the scan rate was very high, the system was under non-steady state. If it is under diffusion control, the current response peak in the mass transport region will be proportional to the square root of the scan rate, which is described by Randles-Sevick equation,

$$i_p = k_{rs} n^{3/2} D^{1/2} C^b \lambda^{1/2}$$

where i_p is the peak current, k_{rs} is the Randles-Sevick constant (2.69×10^5 at 25 °C), n is the electrons transferred, D is the diffusion coefficient, C^b is the bulk concentration, and λ is the sweep rate.

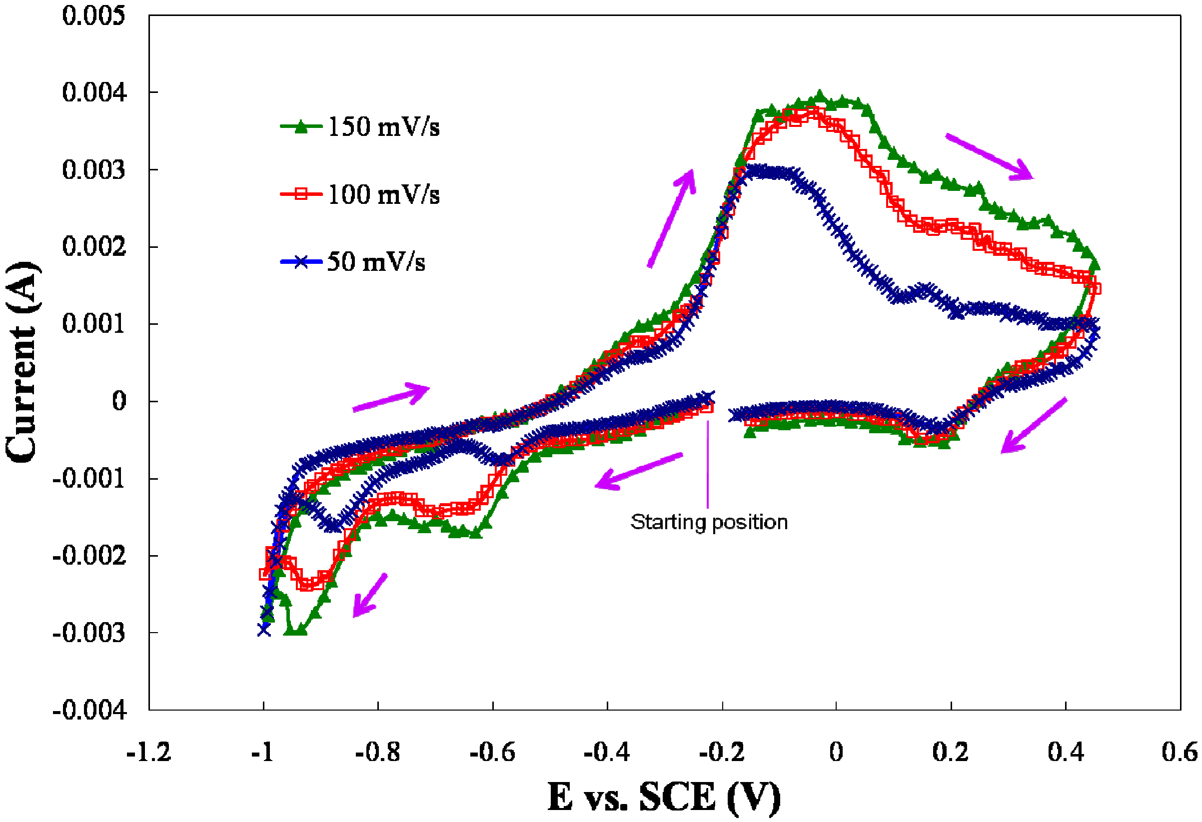

Figure 4-41 Cyclic voltammograms measured at three different sweep rates: 50, 100 and 150 mV/s in the ferricyanide/ferrocyanide solution on a carbon electrode with unetched nanowires Au 25 nm / CoAu 100 nm

Based on **Figure 4-41**, the peak current of ferricyanide reduction at -0.6 V vs. SCE of each cyclic voltammetry as a function of the square root of the scan rate was plotted in **Figure 4-42**. The peak current vs. the square root of sweep rate was obviously a linear relationship, which confirms a diffusion control of the ferricyanide reduction reaction.

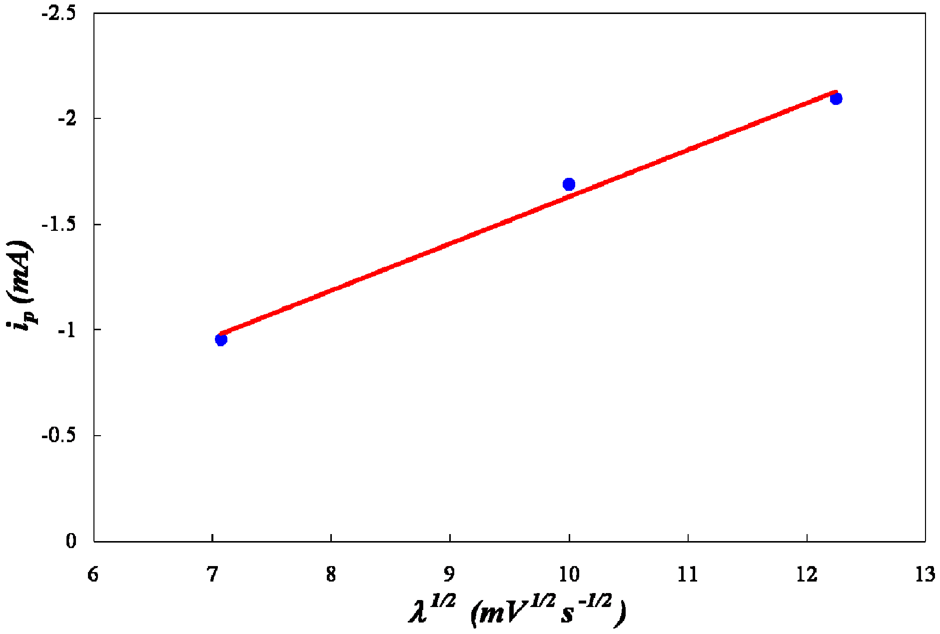

Figure 4-42 Peak current as a function of to the square root of the scan rate

4.6.3 CV with Different CoAu Layer Sizes

Next, a series of etched nanowires having different layer sizes were examined by cyclic voltammetry. These Au/CoAu multilayered nanowire samples have four different CoAu layer sizes (20, 50, 100, 150 nm), but with same Au layer size of 25 nm and same total length of 12 μm. These nanowire samples were previously electrochemically etched in a 2 M KCl solution under the same overpotential for the same amount of time of 6000 s. The etching process was reflected in **Figure 4-39**.

When applying cyclic voltammetry to those etched nanowires to characterize the surface change, a scan rate of 100 mV/s was employed and the potential sweep range was narrowed down to -0.3 ~ -0.95 V vs. SCE, instead of using the previous sweep range of 0.45 ~ -1.0 V vs. SCE shown in **Figure 4-44**. The reason for this change is twofold: (*i*) at the end of forward scan, by reversing the direction of potential scan before -0.95 V vs. SCE, further severe side reactions could be avoided, consequently, ferrocyanide species formed by reduction on the first (forward)

scan could be detected during the reverse scan as long as the scan rate is faster than the rate of diffusion of the ferrocyanide ion away from the electrode surface; (*ii*) as found in **Figure 4-28**, if the applied potential is approaching 0 V vs. SCE or even more positive, the Co-rich CoAu layer will reach its maximum dissolution rate and the Au layer will start being etched. These unwanted etching will definitely change the original surface of nanowire structures, resulting in interference to the cyclic voltammetry characterization of surface change.

An electrode with only a carbon substrate was first examined by cyclic voltammetry within the above potential sweep range (-0.3 ~ -0.95 V vs. SCE) and with a sweep rate of 100 mV/s. The cyclic voltammograms are plotted in **Figure 4-43**. The potential scan was repeated twice and the current responses were reproducible. However, there is no obvious current peak for ferricyanide reduction.

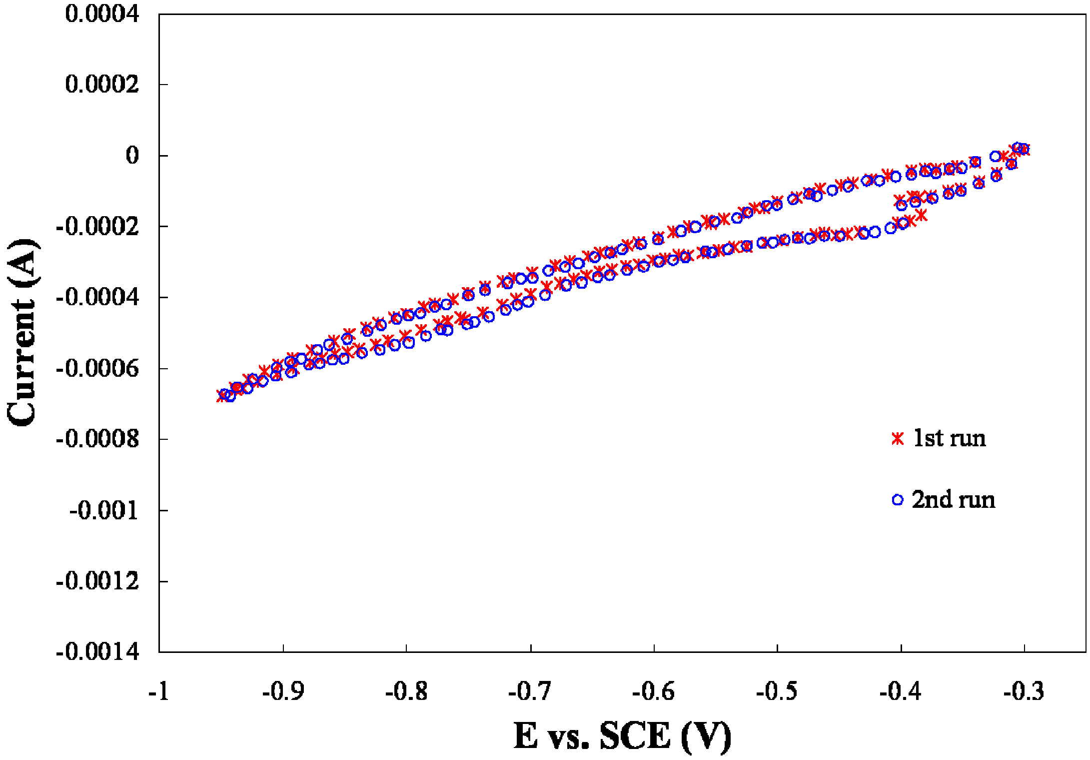

Figure 4-43 Cyclic voltammograms of pure carbon substrate measured at sweep rate of 100 mV/s in the ferricyanide/ferrocyanide solution

The cyclic voltammograms of the four electrochemically etched Au/CoAu nanowires with the same Au layer size of 25 nm but different CoAu layer sizes (20, 50, 100, and 150 nm) are plotted in **Figure 4-44**.

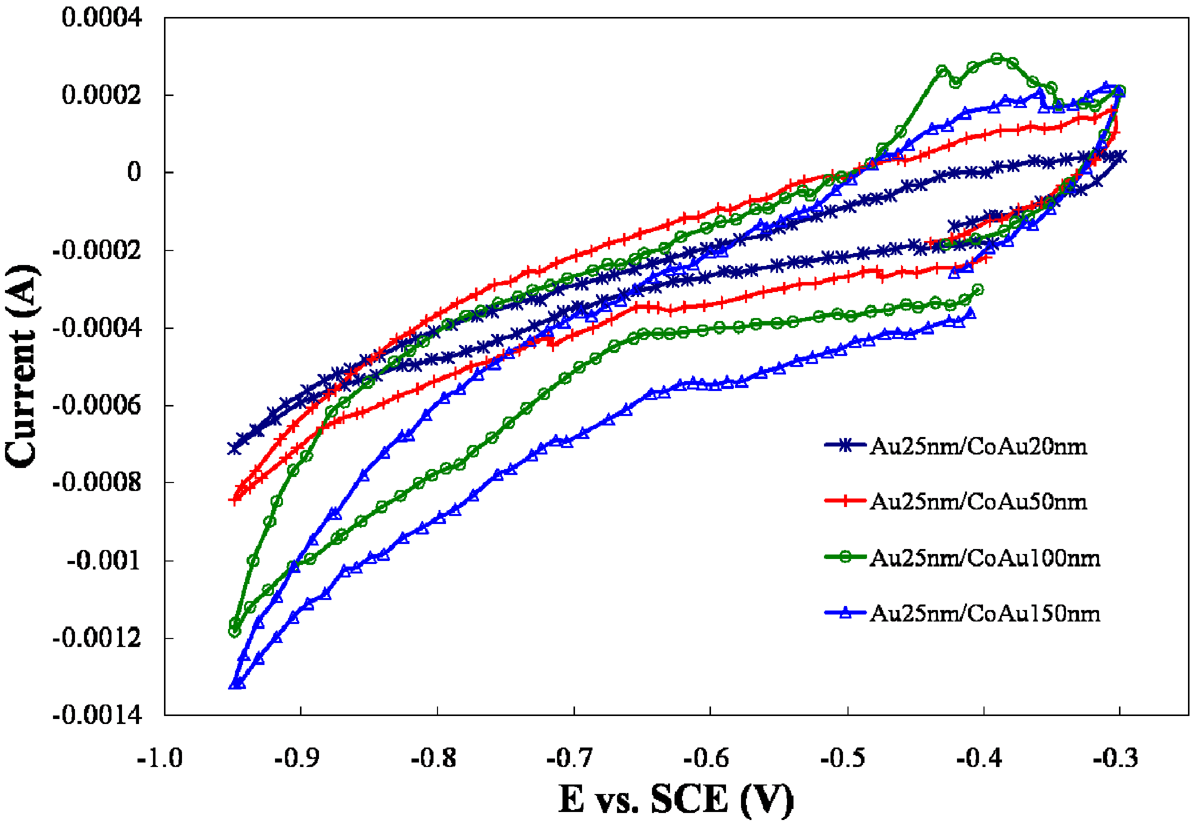

Figure 4-44 Cyclic voltammograms of four electrochemically etched Au/CoAu nanowires with same Au layer size of 25 µm but different CoAu layer sizes (20, 50, 100, and 150 nm); measured at sweep rate of 100 mV/s in the ferricyanide/ferrocyanide solution

These four current-potential curves exhibited similar shape. During the forward scan (toward more negative potentials), the reduction of ferricyanide occurred at a similar position (-0.6 V vs. SCE) and the current increased dramatically. And due to a more porous surface, and hence a larger surface area caused by electrochemical etching, the current increased. Among these four nanowire samples, the Au 25 nm / CoAu 150 nm nanowire had the highest current response under the same working potential. At the end of the reverse scan (toward more positive

potentials), the electrode potentials were limited to a more negative value; the reoxidization of ferrocyanide did not occur and no typical current peaks were observed. Therefore, based on the cyclic voltammograms in **Figure 4-44**, it is possible to qualitatively characterize the surface change of electrochemically etched nanowires by means of cyclic voltammetry (CV).

Based on the above voltammograms, the current responses as a function of CoAu layer size at different potentials during the cyclic voltammetry process were plotted in **Figure 4-45**.

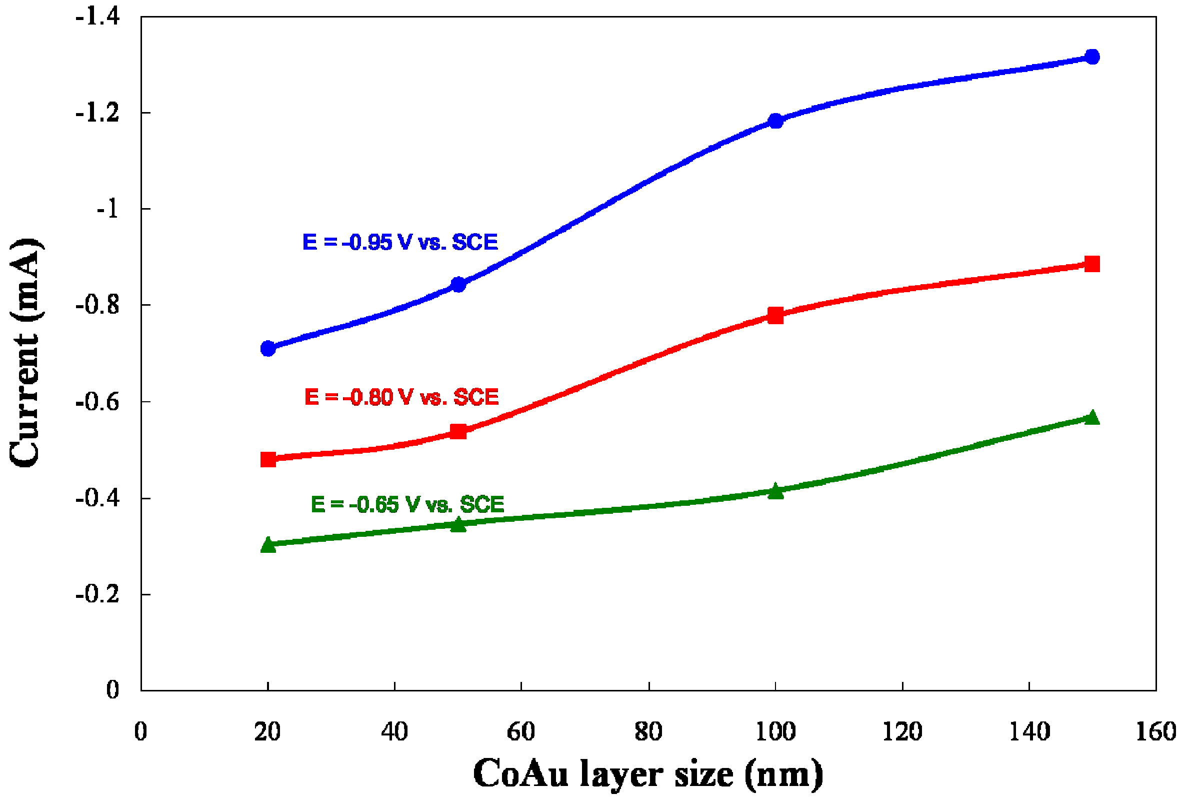

Figure 4-45 Current responses as a function of CoAu layer size at different potentials during the cyclic voltammetry process with four different Au/CoAu nanowires

Three different potentials (-0.65, -0.80, and -0.95 V vs. SCE) were chosen. The working potential of -0.65 V vs. SCE is where the ferricyanide reduction occurs and the potential of -0.95 V vs. SCE is where the side reaction (water reduction) occurs. As shown in **Figure 4-45**, since in the electrolyte, water is much more abundant than the ferricyanide ions, the reaction rates (or

current responses) at higher potential (-0.95 V vs. SCE) are much higher than that at lower potential (-0.65 V vs. SCE). Especially at each working potential, the current response increases when increasing the CoAu layer size from 20 to 150 nm and consequently enhancing the surface area, which further confirmed the qualitative analysis of the surface change of Au/CoAu nanowires during the electrochemical etching process by employing cyclic voltammetry.

In order to find a way to analyze the surface change quantitatively, the double layer charging effects when fast sweep rate are used has to be studied. When applying a potential to the electrochemical cell, the total current response consists of two parts: faradaic current (i_F) and capacitive current (i_C).

$$i = i_F + i_C$$

Faradaic current (i_F) is the current used for electrochemical reactions (anodic reactions and cathodic reactions) and is governed by Faraday's law (i.e., the amount of chemical reaction caused by the follow the current is proportional to the amount of electricity passed). Capacitive current (i_C) refers the current used to charge the electrode-solution interface which is called the electrical double layer and behaves like an electrical capacitor. The capacitive current is governed by the equation

$$i_C = C_{dl} \frac{dE}{dt} = C_{dl} \lambda$$

where C_{dl} is the capacitance of the electrical double layer capacitor, and λ is the potential sweep rate.

For a given double layer capacitor, its capacitance is relative to the surface area. Therefore the capacitances of those four electrochemically etched Au/CoAu multilayered

nanowires discussed in the previous cyclic voltammetry (**Figure 4-44**) were calculated and then plotted in **Figure 4-46** as a function of CoAu alloy layer size.

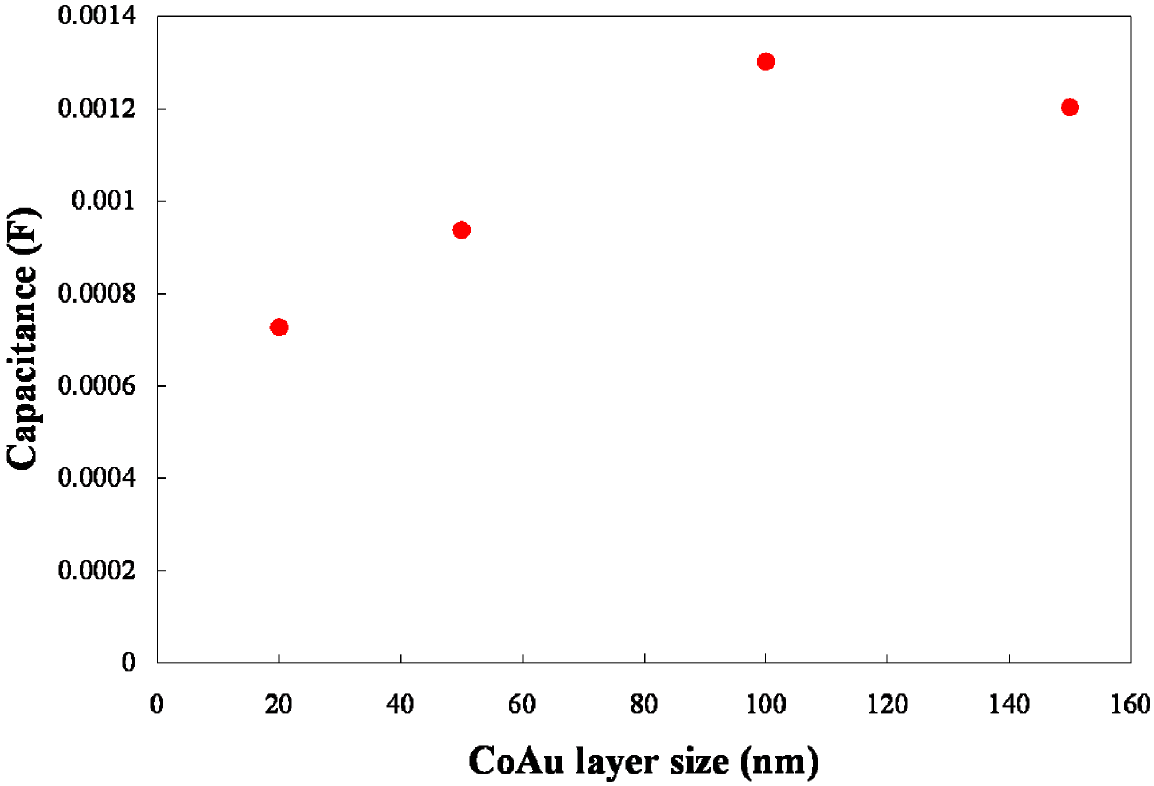

Figure 4-46 Capacitance changes as a function of the CoAu layer size

According to **Figure 4-46**, the capacitances of the nanowires with CoAu layer sizes of 20, 50, 100, 150 nm were 0.7, 0.9, 1.3, and 1.2 mF, respectively. In general, compared to a nanowire with smaller CoAu alloy layer size, the one with larger CoAu alloy layer size, after electrochemical etching, will have a more porous surface and larger surface area. Consequently, the capacitance of electrical double layer will be proportional to the CoAu alloy layer size, which is similar to the trend reflected in **Figure 4-45**. But in order to use capacitance as a quantitative analysis technique, there is still a long way to go. Too many factors affect the capacitance, such as the total mass of nanowires, the nanowire distribution on the carbon substrate, the

conductivity between nanowires and the substrate, and etc. Better control of releasing the nanowire from membranes and more precise control of preparing etching sample will be helpful.

4.6.4 CV with Different Etching Times

Next, cyclic voltammetry will be used to characterize the nanowire surface change at different time across the whole electrochemical etching process. The nanowire being tested here is multilayered Au 25 nm / CoAu 50 nm nanowires with an overall length of 12 μm, which had ever been used with other three nanowires with different CoAu layer sizes to compare the relationship between CoAu layer size and the current response, as shown in previous **Figure 4-39**. Here the current response curve of the electrochemical etching of Au 25 nm / CoAu 50 nm nanowires was replotted in **Figure 4-47**.

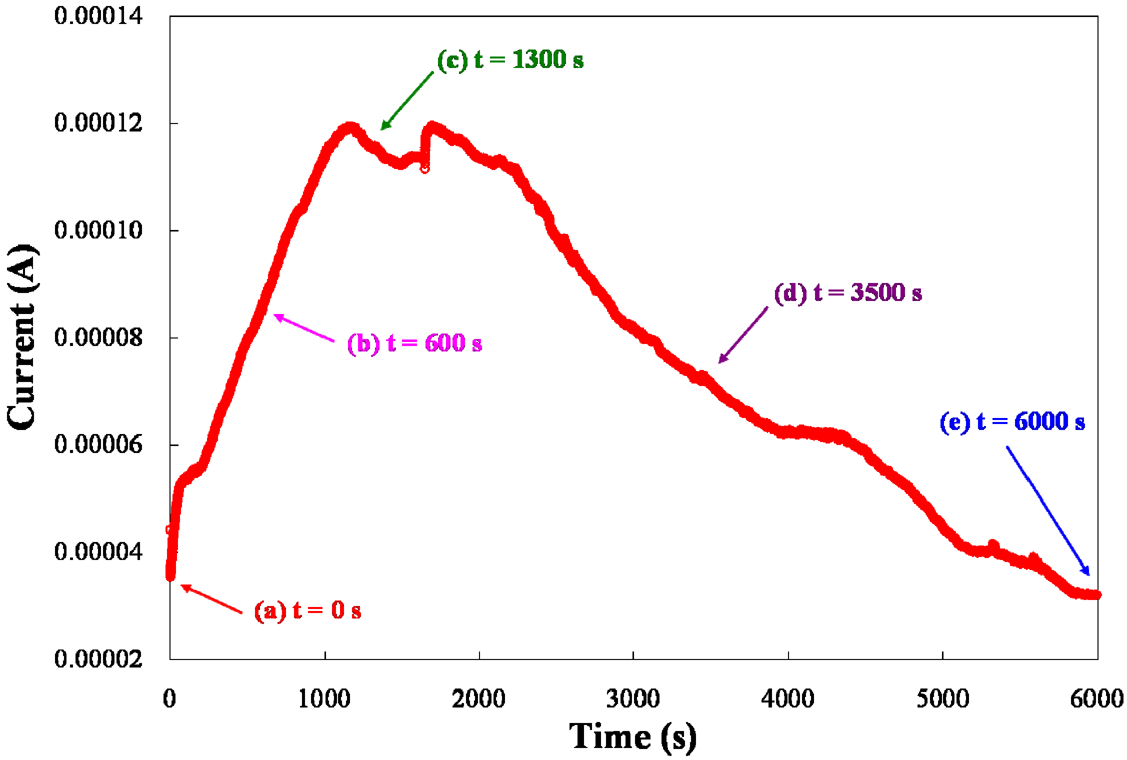

Figure 4-47 Current responses as the function of time during the process of the selective electrochemical etching of Au 25 nm / CoAu 50 nm nanowires on carbon electrodes

This typical nanowire electrochemical etching process takes up to 6000 s to complete. On this current response curve, five different etching times are chosen for further cyclic voltammetry examinations, including the initial point (t = 0 s), the middle point where current keep increasing (t = 600 s), the point where current reaches the peak (t = 1300 s), the middle point where current keep decreasing (t = 3500 s), and the end point where the etching complete (t = 6000 s).

Since the cyclic voltammetry in the ferricyanide/ferrocyanide solution will not cause any change to the electrode surface, another sample which was the same as the one used in **Figure 4-47** was prepared, and then used for electrochemical etching with various time and then cyclic voltammetry. At the starting time of (a) 0 s there is no etching, therefore no current response were recorded. Four current responses of consequent electrochemical etching are plotted in **Figure 4-48**, the accumulated time for each etching were 600 s, 1300 s, 3500 s and 6000 s, which are corresponding to the time points (b), (c), (d), (e) in **Figure 4-47**.

Time (b) and (c) are, respectively, located prior to or close to the moment when the etching current reaches its maximum value. During this time as more and more Co-rich CoAu alloy is being dissolved, a rough surface is created, leading to an enhanced surface area and subsequent continuous increasing of current as plotted in **Figure 4-48** (b) and (c). Later when more CoAu alloy is etched away and the total dissolvable mass decreases substantially, the surface area drops and consequent current response decreases dramatically, as shown in plot (d). Finally there is not enough CoAu alloy left for further etching, the current response as a function of time exhibits a very flat curve and the value approaches zero.

After each etching, the nanowire electrode was taken out of the electrochemical etching cell and rinsed with DI water completely. Then it was moved into the ferricyanide/ferrocyanide solution for cyclic voltammetry characterization. The cyclic voltammetry parameters were the

same as before: potential scan range was -0.3 ~ -0.95 V vs. SCE and the scan rate was 100 mV/s. As a result, five cyclic voltammograms were shown in **Figure 4-49**. As for curve (a) t = 0 s, since it was not electrochemically etched, the surface area was at a minimum and the consequent current responses for both ferricyanide reduction and ferrocyanide reoxidization was very small. As the etching process progressed, the current response of each cyclic voltammetry increased. At time (d) 3500 s, the current reached a maximum value. At the last point (e) 6000 s, the current decreased a lot again.

Similarly, for each cyclic voltammogram, at three different working potentials of -0.65, -0.80, and -0.95 V vs. SCE, the current responses as a function of etching time were plotted in **Figure 4-50.** It is obvious to see that, no matter which potential is chosen, across the whole 6000 s electrochemical etching process, the total surface area has been increasing during the first half time and then decreasing at the second half time. In other words, the electrochemical etching of the CoAu alloy layer does change surface morphology and enhance the average surface area of nanowires. Because of some electrical conduction problems between the released nanowires and the carbon electrode surface, not all the nanowires were completely etched. That's why the surface area at time 6000 s was still much higher than that of the initial state before etching.

Additionally, the electrical double layer capacitance were calculated and then plotted as a function of etching time in **Figure 4-51** in order to find some quantitative evidence across the whole electrochemical etching process of Au 25 nm / CoAu 50 nm nanowires. At those five different etching times: 0, 600, 1300, 3500, and 6000 s, the capacitances were 1.1, 0.6, 1.3, 2.2 and 2.5 mF, respectively. The increasing of capacitances as a function of etching time further confirmed the effectiveness of selective etching of CoAu alloy and consequent surface area enhancement as discussed previously.

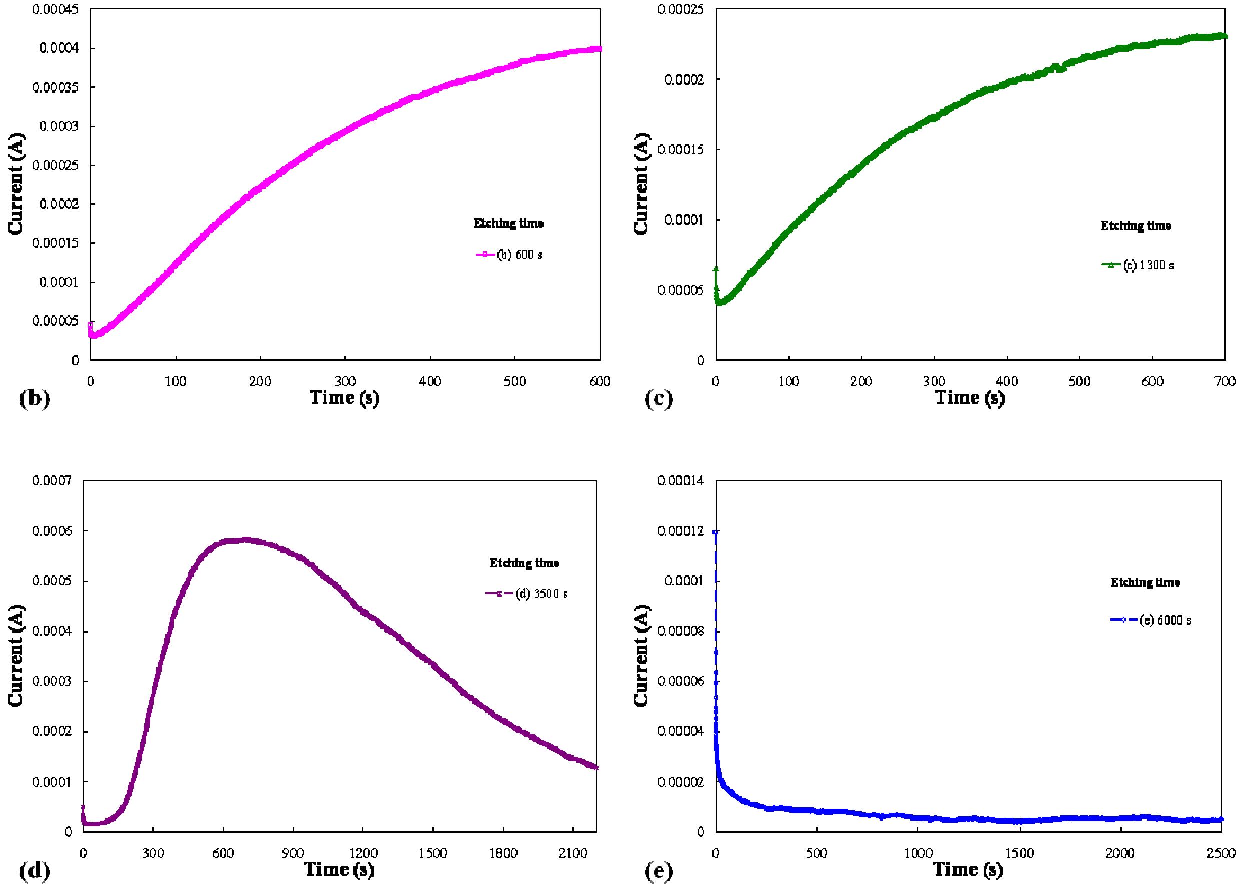

Figure 4-48 Current responses as the function of time for the electrochemical etching of Au 25 nm / CoAu 50 nm nanowires with different accumulated etching time: (a) 0 s, not shown, (b) 600 s, (c) 1300 s, (d) 3500 s and (e) 6000 s

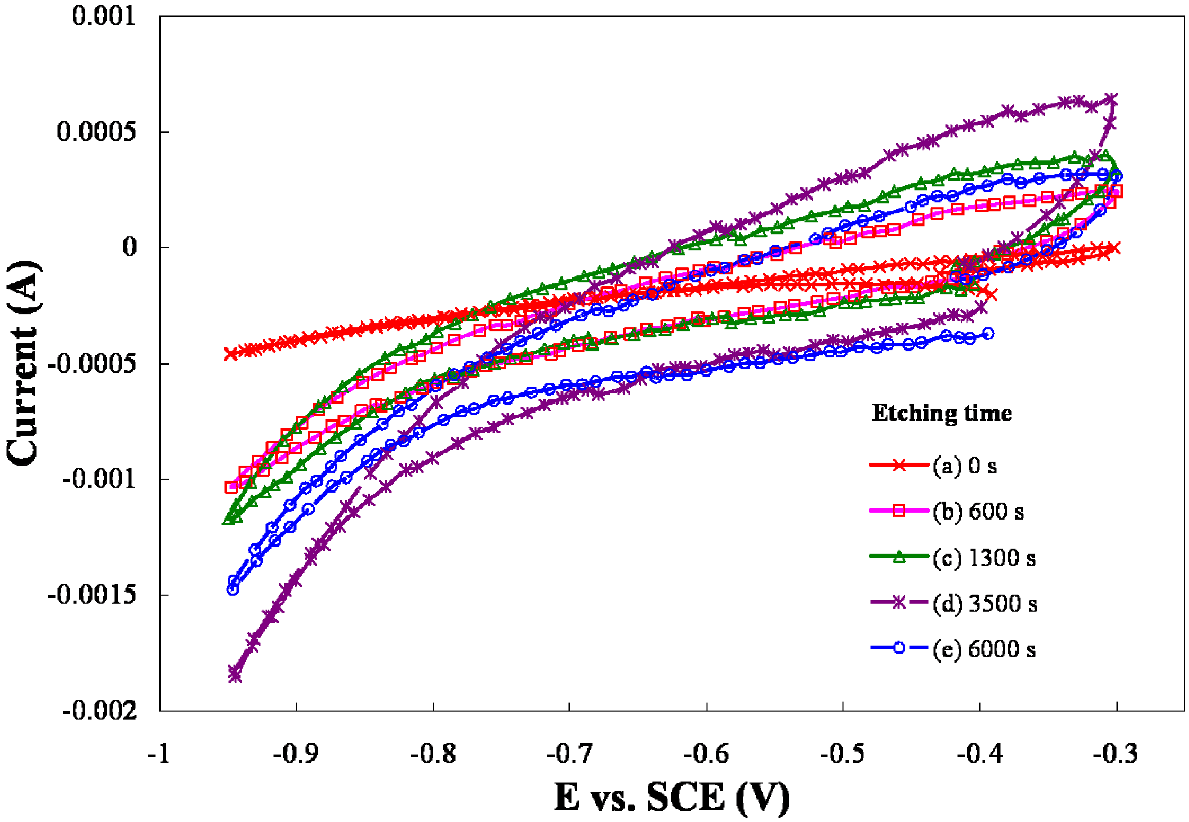

Figure 4-49 Cyclic voltammograms of Au 25 nm / CoAu 50 nm nanowires which were electrochemically etched with different etching time: (a) 0 s, (b) 600 s, (c) 1300 s, (d) 3500 s and (e) 6000 s

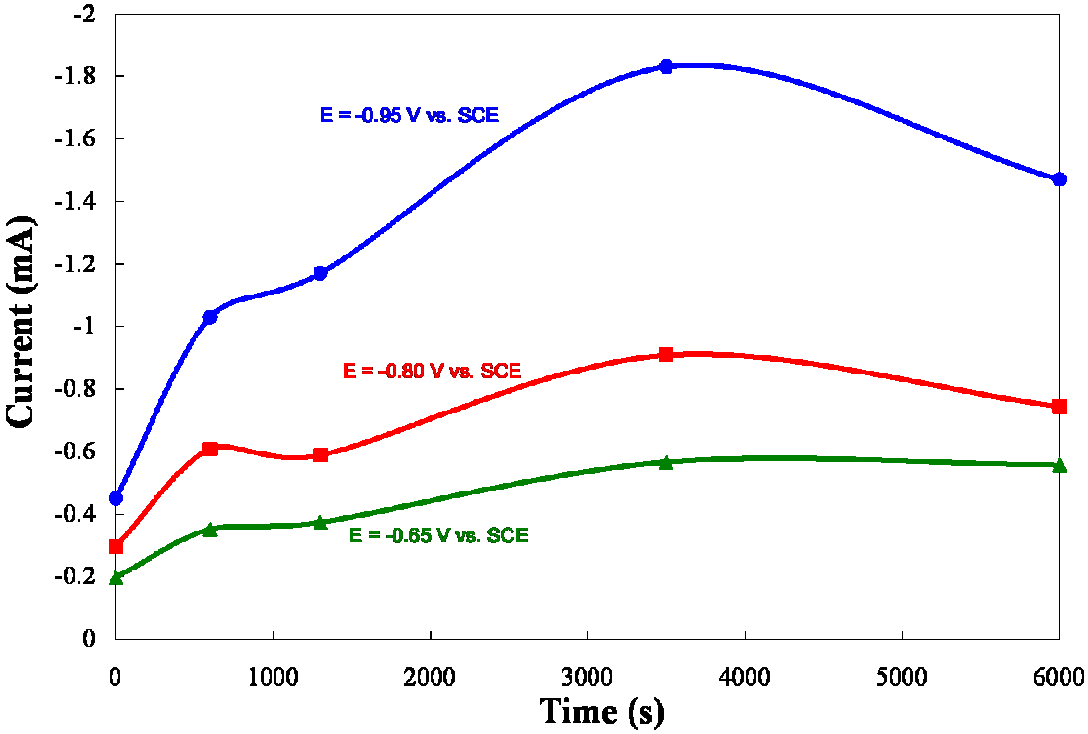

Figure 4-50 Current responses as a function of etching time at different potentials during the cyclic voltammetry process

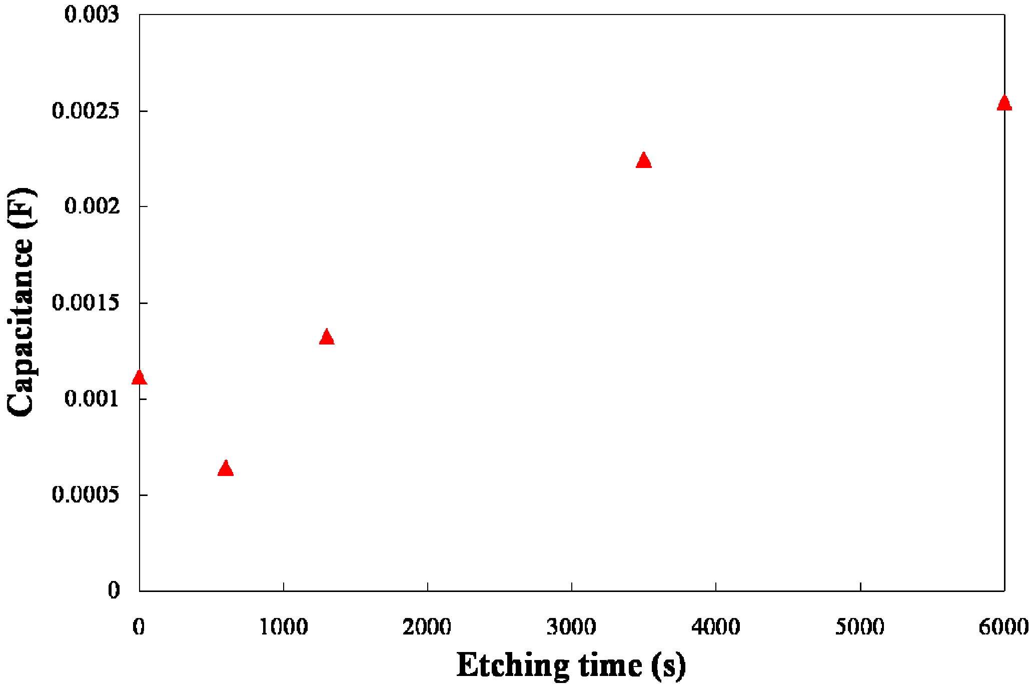

Figure 4-51 Capacitance changes as a function of the etching time

4.6.5 Nanowires with Various Pore Sizes

The electrochemical etching of Au/CoAu multilayered nanowires was also investigated with different membrane pore size. Nanowires with layer sizes Au 25 nm / CoAu 50 nm were electrodeposited in an AAO membrane with the pore size of 0.2 μm. After being prepared with the same procedure as described above, the mono-dispersive nanowires were electrochemically etched, and SEM was used to examine the selective etching results. The electrochemical etching conditions were the same as discussed in **Section 4.4.3.1**.

Figure 4-52 shows a plain-view SEM images of Au 25 nm / CoAu 50 nm multilayered nanowires, selectively etched to different extents. In **Figure 4-52 (a)**, uncorroded nanowire arrays were shown and the multilayered structure was not very clear. The length difference between each nanowire was due to the ultrasonication and centrifugation in the process of sample preparation. **Figure 4-52 (b)** shows partially etched nanowires in nano-bamboo like structures. Images in different magnification scales were displayed. The multilayered structure became very obvious in low or high magnification observation. After completely etching of Co-rich CoAu alloy layers, uniform and parallel Au nanodisk series were formed, as shown in **Figure 4-52 (C)**.

Figure 4-52 (a) also reflected a problem in the process of sample preparation. When preparing nanowire samples after electrodeposition, even though the AAO membrane was dissolved in 2 M KOH and then cleaned by sequential ultrasonication, centrifugation, and rinsing with deionized distilled water for several times, not all nanowires were released from the sputtered Au substrate. Some nanowires arrays still existed, which would cause nonuniform distribution of nanowires on the substrate and consequently leading to electrical conduction

problem. In the future, ionic milling or plasma etching could be employed to remove that Au substrate before dissolving the AAO membrane.

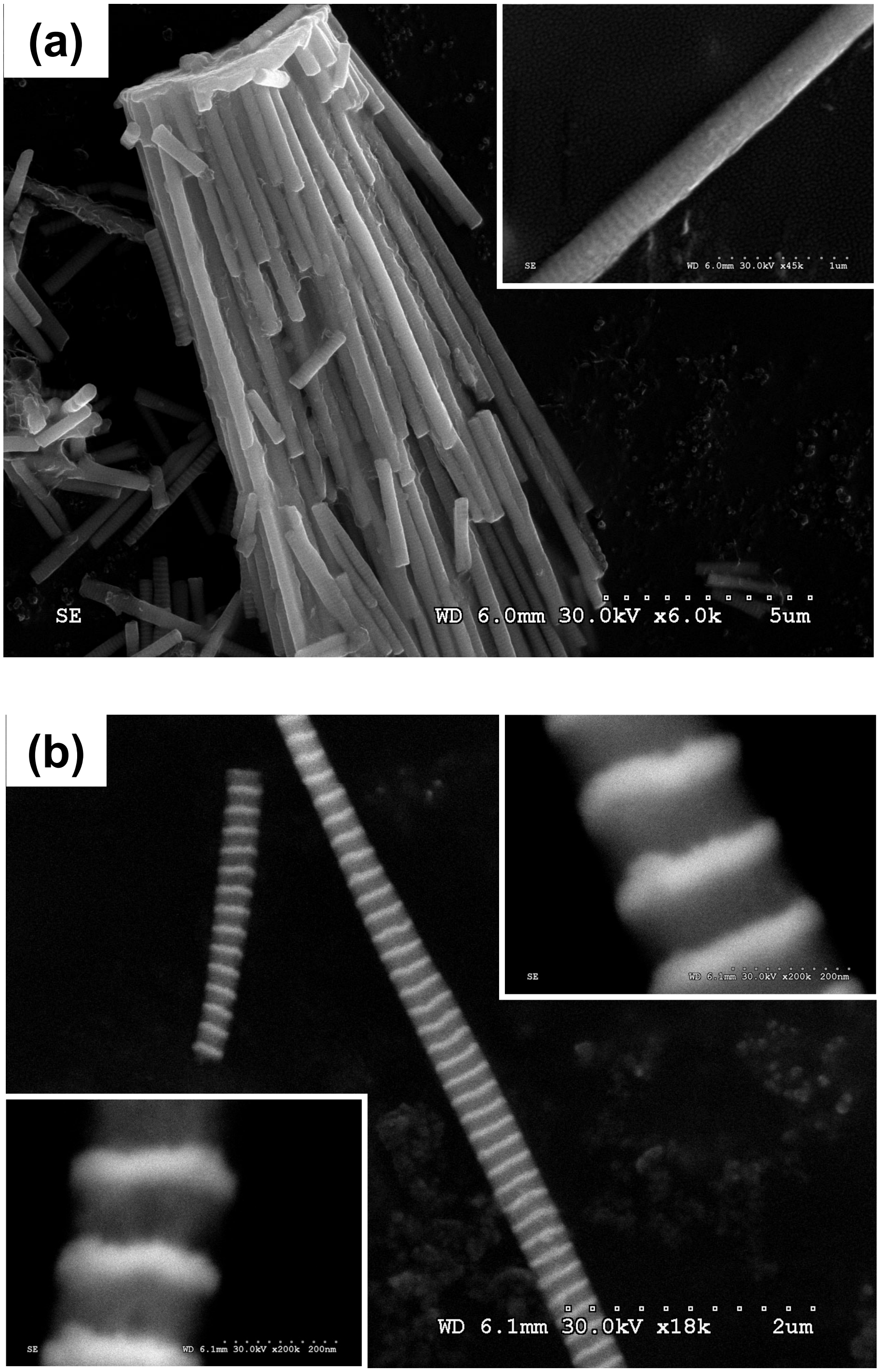

Figure 4-52 SEM images of controllable selective etching results of Au 25 nm / CoAu 50 nm nanowires electrodeposited in 0.2 μm AAO membrane: (a) nanowires not etched, (b) nanowires partially etched (nano-bamboo structures), and (c) nanowires completely etched (nanodisk series)

Figure 4-52 continued

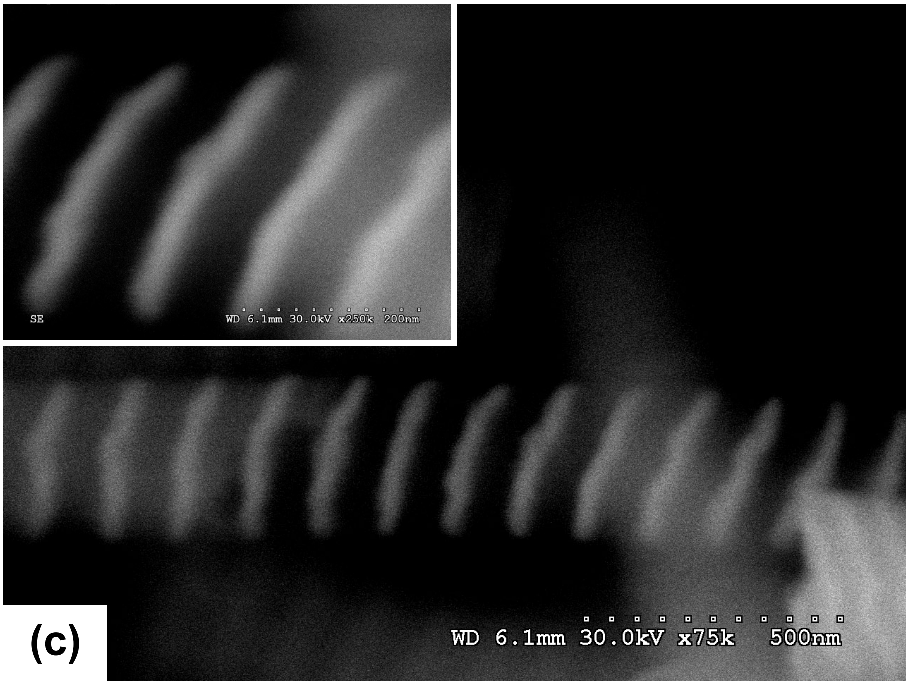

4.6.6 Annealing Effects on Nanowire Etching

The annealing effect is expected to improve the quality of the multilayer interface by promoting phase segregation. The annealing post-treatment can also help improve the procedure for fabricating the bamboo-like etched nanowires for the same reason. Therefore, next, this method was expanded to investigate the fabrication of bamboo-like nanostructures with the assistance of annealing treatment. X-ray diffraction (XRD) is a necessary technique for the microstructure examination of annealed samples in order to indicate phase segregation.

The electrodeposition and post-deposition annealing of Au/CoAu multilayered nanowires were carried out in anodic aluminum oxide (AAO) membranes, which have a high density of pores and remain stable at 500 °C in air.[94] The wires will be plated from the electrolyte presented in **Chapter 3** with different layer size of Au 25 nm / CoAu 50 nm by the use of galvanostatic square-wave pulse plating. After electrodeposition, those nanowires were released

and then annealed in a mixture of 5 % H_2 and 95 % Ar at 300 °C for 30 min. The experimental details were described in **Section 4.3.3**.

The microstructure of the Au/CoAu multilayered nanowires was first examined by X-ray diffraction (XRD) to compare the microstructure change before and after annealing. The pattern of the Au/CoAu nanowires was shown in **Figure 4-53**. The prominent peaks for Au are (111), (200), (220), and (311) and the prominent peaks for Co are (002) and (200). After the annealing treatment, the Au peaks of (200) and (220) could not be found any more in the second XRD spectra, while Co peaks did not change significantly. The disappearance of Au peaks after the annealing treatment means that Au and Co phases are not completely separated any more. This also explained why annealing made Au/CoAu CIP GMR values decreased so much. Additionally the peaks became much narrower and the relative intensity of them decreased a lot due to the annealing.

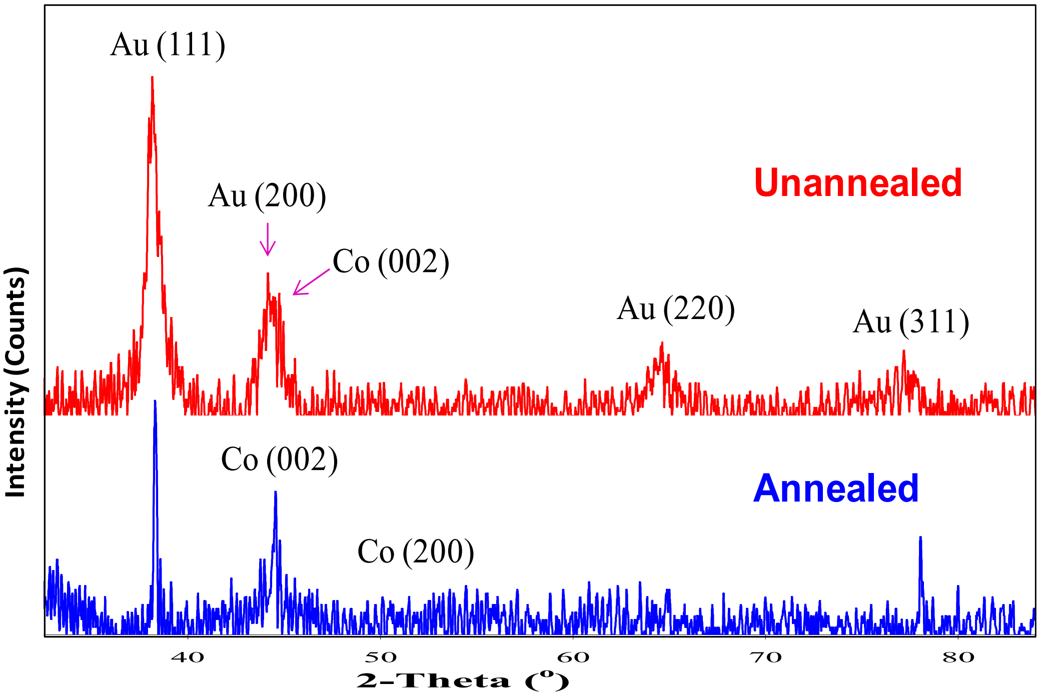

Figure 4-53 XRD spectra of Au/CoAu multilayered nanowires in AAO membrane before and after annealing treatment

Scanning electron microscope (SEM) images were also taken to assist the investigation of annealing effects on Au/CoAu nanowires. **Figure 4-54** shows a close look at those nanowires before annealing treatment. According to the electrodeposition parameters, the average length of each original nanowire should be 30 μm. However, due to the ultrasonication in the sample releasing process, most of them were broken into shorter ones and the left length was about 5 μm. Those nanowire exhibited uniform cylindrical structure with a flat surface and similar diameter. Multilayered structures were also obvious.

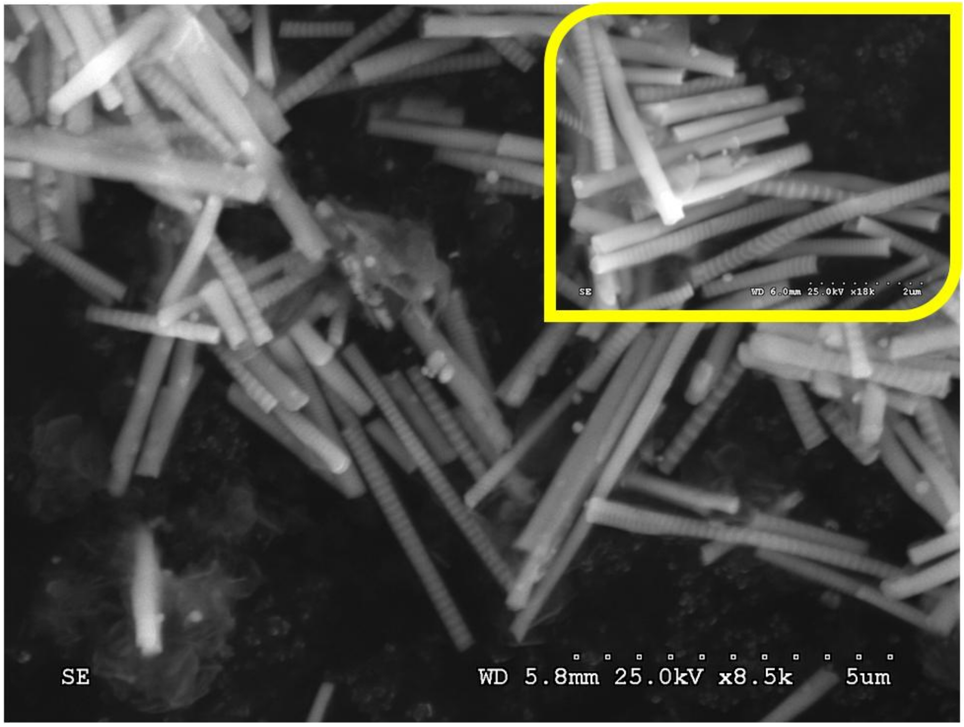

Figure 4-54 Unannealed multilayered Au 25 nm / CoAu 50 nm nanowires electrodeposited from 0.1 μm AAO membrane

Figure 4-55 shows the SEM characterization results of annealed Au/CoAu multilayered nanowires. Those wires were electrodeposited under the same conditions and then released from the AAO membrane by using the same procedure as before. But, it was very clear that the average length (~ 1 μm) of annealed nanowires were much shorter than that of previous

unannealed ones. Possible reasons to explain the break of long nanowires into shorter ones could be: (1) annealing at high temperatures will increase the internal stress of the deposit and the pores will be distorted, destroying the long, parallel nanowires; (2) the thermal expansion coefficients (CTE) of CoAu alloy and of AAO membrane mismatch dramatically, which cause the breakage of long wires. The coefficient of thermal expansion (linear) is defined as the change in length per unit length of material for a one degree Centigrade change in temperature. The CTE of Au, Co, and Al_2O_3 are 14, 12, and 6.5 ($\times 10^{-6}$/°C), respectively.[95] When the nanowire samples are annealed, the thermal expansion of Au and CoAu alloy layer will be restricted by the outer Al_2O_3 wall due to the difference of CTE numbers, and leading to the breakage of long nanowires. However, from the inset of **Figure 4-53**, the Au/CoAu layers are still discrete. Therefore, in order to get uniform Au/CoAu nanowires with certain length, annealing process should be very cautious.

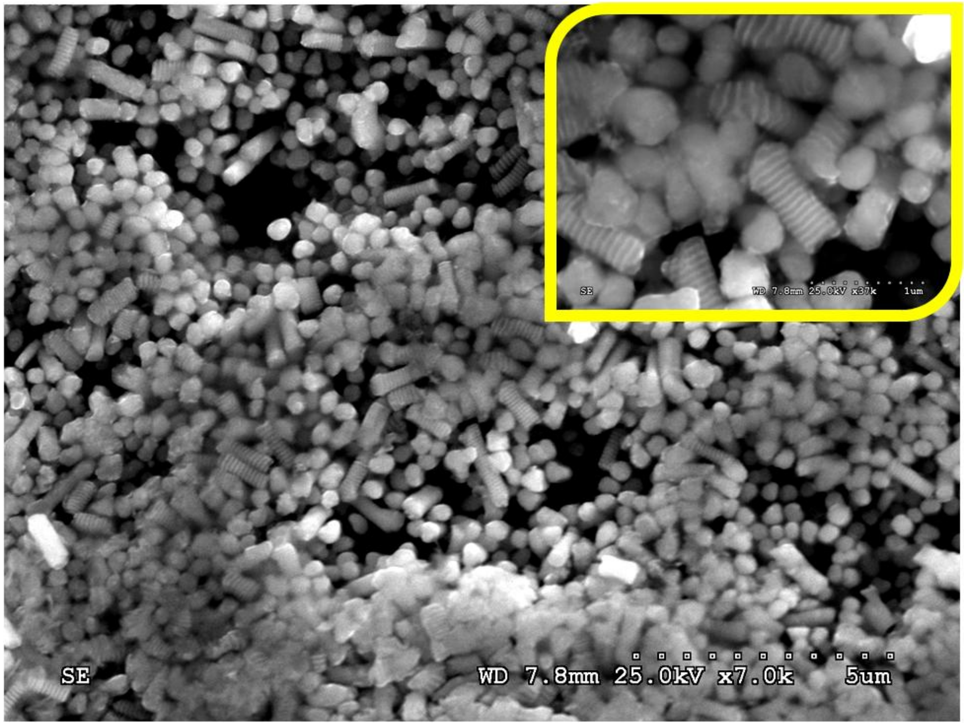

Figure 4-55 Annealed multilayered Au 25 nm / CoAu 50 nm nanowires electrodeposited from 0.1 μm AAO membrane

Annealing effects on the electrochemical etching of nanobamboo structure have also been tested. Annealed Au/CoAu nanowires were electrochemically etched in the same way described in previous section and the results are examined by SEM, as shown in **Figure 4-56**. After being electrochemically etched for 1920 s, the CoAu alloy layers were partially dissolved and nanobamboo structures were left. Because of the disturbance from the external magnetic field, there is always a continuous minor shifting of SEM imaging system. That's why compared to the original clear nanobamboo structures, the SEM pictures in **Figure 4-56** were a little bit fuzzy and did not reflect the structures well enough.

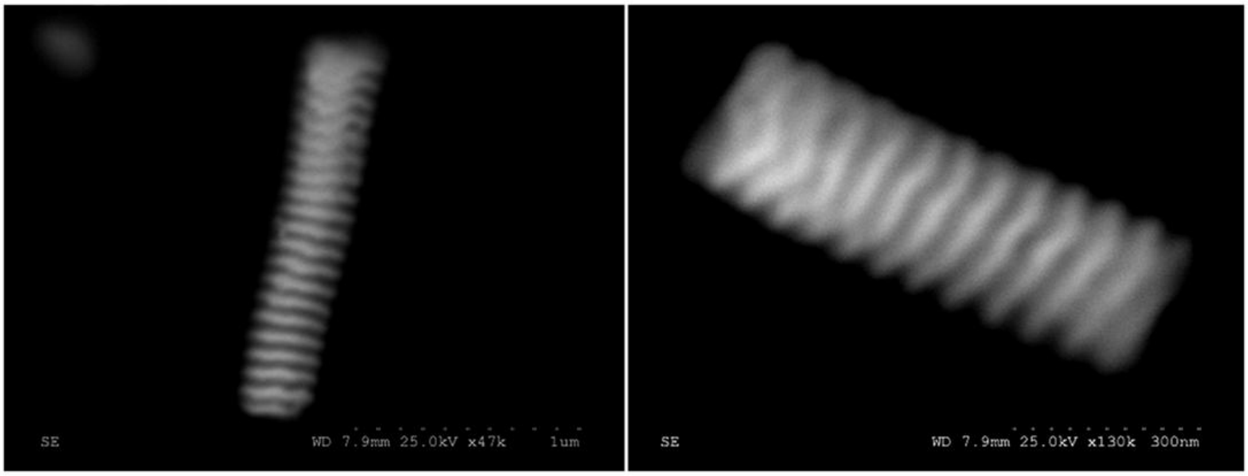

Figure 4-56 Electrochemical etching results of annealed multilayered Au 25 nm / CoAu 50 nm nanowires electrodeposited from 0.1 μm AAO membrane

The details of the etching are shown in **Figure 4-57**: (a) Current responses and (b) charge responses as the function of time during the electrochemical etching of annealed and unannealed Au 25 nm / CoAu 50 nm nanowires on carbon electrodes. By comparing the current responses and the anodic charge responses between annealed and unannealed nanowires, their etching behavior were obviously different. For example, it took the unannealed nanowires 960 s to finish the complete etching, which was confirmed by the complete peak shaped current response and the plateau in the anodic charge response. However, as for the electrochemical etching of

annealed nanowires under same overpotential, after double period of time (1920 s) the nanowires were still in the range of partial etching. The current response just passed the peak and started decreasing, and the anodic charge response has not reached the inflexion point.

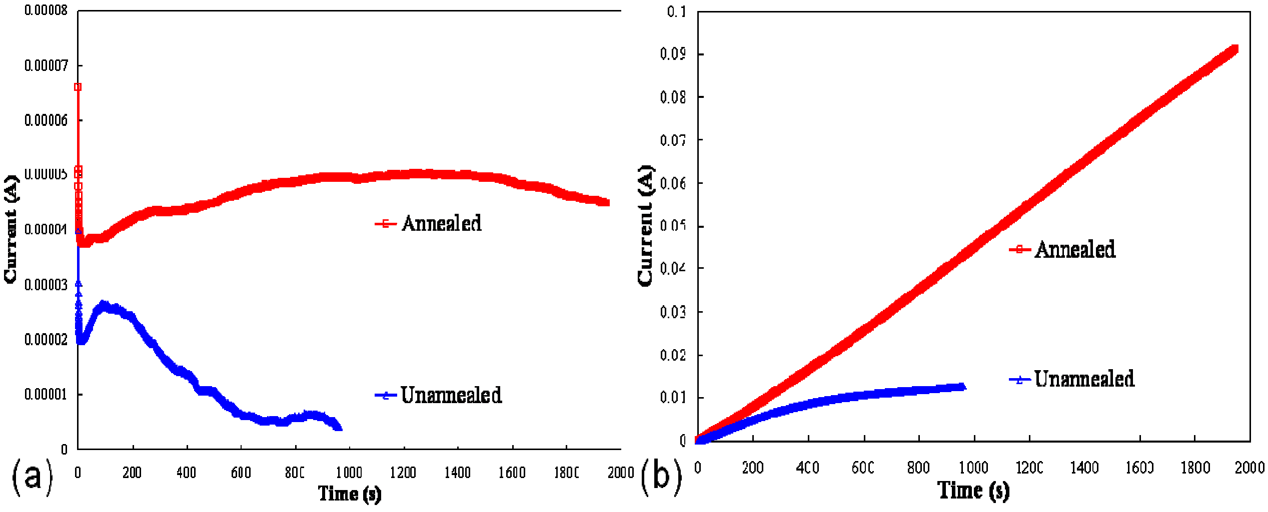

Figure 4-57 (a) Current responses and (b) charge responses as the function of time during the electrochemical etching of annealed and unannealed Au 25 nm / CoAu 50 nm nanowires on carbon electrodes

The possible explanation is twofold: (*i*) Due to the annealing treatment, there are certain degree intermixing between Au and Co interfaces, which was verified by previous XRD analysis. The annealed Au/AuCo nanowires exhibited more porous structure after selective electrochemical etching started, and consequently resulted in a larger diffusion resistance for further etching. (*ii*) The annealing treatment made the nanowires much shorter than before, as shown in previous SEM images. After being released from the membrane and dispensed on the carbon substrate, the shorter nanowires were prone to be overlapped with one another, which caused more serious nonuniform current distribution and a larger diffusion resistance. Therefore, the etching process for annealed nanowires took much longer time than that of unannealed samples.

4.6.7 Conclusion to Nanowire Etching

Thus far, a two-step process for the fabrication of Au/CoAu nanoscale bamboo-like structures and disk-shape nanoparticles has been developed, which could be used as catalysts for reactions that use gold. First, multilayered Au/CoAu nanowires were electrochemically deposited into nanoporous membranes in a non-cyanide electrolyte with a two step galvanostatic, square-wave pulsed plating. Second, the solid nanowires were then removed from the template and one component was electrochemically etched from the nanowires. By precisely controlling the electrochemical etching potential and time, nanobamboo structures can be achieved and therefore the surface area of the nanowires can be enhanced. Even if complete etching occurs, nanoparticles and nanodisks can be fabricated by this unique method. Cyclic voltammetry technique was employed to characterize (*i*) the surface differences among multilayered nanowires with various segment ratios, and (*ii*) the changes of surface area of a Au/CoAu nanowire sample across the whole process of electrochemical etching.

This nanoparticle fabrication process is controllable, high-yielding, simple to carry out, and uses non-toxic, benign solution. It can be extended to other metallic systems, or to synthesize other types of nanoparticles. To the best of the author's knowledge, this is the first time to demonstrate a nanowire etching process precisely controlled by electrochemical etching.

4.7 Electrochemical Etching of Nanotubes

In our previous study, discussed in **Section 4.6**, bamboo-like nanostructures from etching nanowires have been successfully fabricated. The next step in this work is to develop a similar process for the fabrication of nanorings by combining electrochemical deposition of nanotubes and electrochemical etching. Nanorings have attracted increasing attention due to their unique properties in recent years. For example, small thin-film ring-shaped magnetic structures have

potential use in magnetic random access memories.[96] The optical properties of gold nanorings significantly deviate from the properties of compact spheres and can be tuned by varying the diameter and wall thickness of the ring.[97] Rings have an extra degree of freedom (the ring width) compared to topologically simply connected elements, such as disks. This allows for adjusting both the static and dynamics magnetic properties (which are expected to be distinctly different from the conventionally studied geometries).[98] Most attention was focused on the fabrication of magnetic nanorings.[98-102] Only a few reports were concerned about Au nanoring fabrication. For example, Zhang *et al.*[103] presented a simple and effective method for preparing epitaxial and two-dimensionally arranged gold rings on mica substrates by depositing a polymeric membrane bearing a dense array of uniform pores onto a mica substrate, filling the pores with a solution of a gold precursor, evaporation of the solvent and calcinations. Aizpurua *et al.*[104] produced Au rings and disks on soda-glass substrate using colloidal lithography. All rings and disks had the same outer radius of about 60 nm while the heights were about 40 nm and 20 nm, respectively. Therefore, our work would be the first example of Au nanoring fabricated through nanoporous template electrodeposition and following electrochemical etching.

Figure 4-58 shows the novel electrochemical deposition/etching procedure to produce nanorings proposed here. First, the multilayered Au/CoAu nanotubes with various diameters will be prepared via template-guided electrodeposition. Various layer sizes could be achieved by controlling the electrodeposition time. After the nanotubes are released and placed on a carbon electrode, electrochemical etching will be carried out in a KCl solution. Nanorings with different dimension will be achieved, and various etching method will be tested.

Compared with other methods, such as electron beam techniques and nanosphere lithography, the nanoporous template methods have two advantages: first, the alumina template methods are scalable and parallel, providing a method to fabricate large, ordered nanoring arrays.

Second, the nanoring height is independent of the ring diameter allowing high aspect ratio rings to be fabricated. Ring diameter, height, and spacing are controllable by varying the process conditions. In addition, the electrochemical method does not require expensive instrumentation, high temperature or low vacuum pressures.

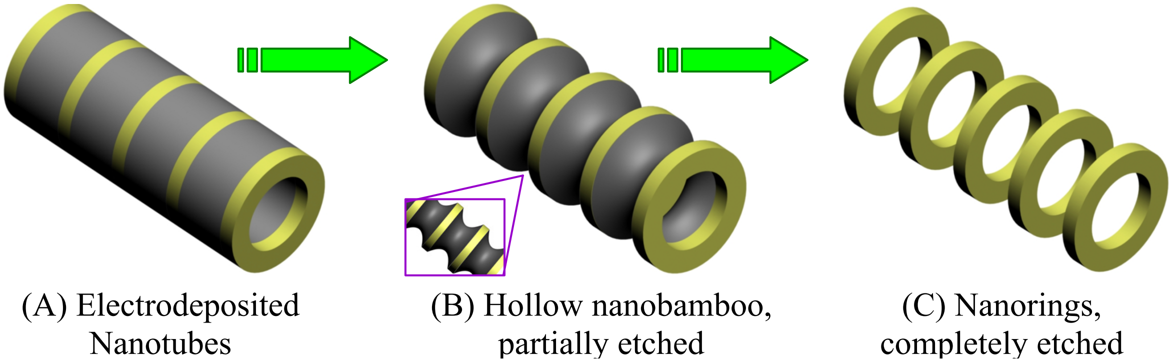
(A) Electrodeposited Nanotubes

(B) Hollow nanobamboo, partially etched

(C) Nanorings, completely etched

Figure 4-58 Schematic illustration of the procedure for fabrication nanorings through selective electrochemical etching of Au/CoAu nanotubes

4.7.1 Nanotubes with Various Layer Sizes

Au/CoAu multilayered nanotubes were electrodeposited from the non-cyanide electrolyte (**Table 3-1**) and the electrodeposition parameters were shown in **Section 4.2**. We found that the pore size plays an important role in the electrodeposition of nanowires vs. nanotubes. Membranes with pore size smaller than or equal to 0.2 µm will give nanowires, while membranes with pore size greater than or equal to 0.4 µm will give nanotubes. Therefore membranes with larger pore size are preferred for the electrodeposition of Au/CoAu multilayered nanotubes. AAO or PC membrane with pore size equal to or larger than 0.4 µm will be used.

Electrochemical etching conditions were similar to **Section 4.4**. The etching solution was 2 M KCl, and the etching potential will be in the range of -0.60 ~ 0.04 V vs. SCE. Various Co-rich CoAu layer sizes (50 ~ 250 nm) and tube diameters (1.0. 2.0 µm) were examined in order to

study different etching modes and to obtain Au rings with various dimensions. Since a large pore size of the polycarbonate membrane favors the formation of high quality nanotubes, nanotubes deposited in PC membrane with 2.0 μm pore size were first been tested.

Figure 4-59 showed the current responses as the function of square root of time during the selective electrochemical etching of (red curve) Au 25 nm / CoAu 50 nm, (blue curve) Au 25 nm / CoAu 150 nm, and (pink curve) Au 25 nm / CoAu 250 nm nanotubes deposited from 2.0 μm PC membranes. Those three etching curves exhibited a similar current response behavior as what was observed in the etching of nanowires. The anodic current response depends on the mass-transport conditions and effective surface areas in the process of potentiostatic electrochemical etching of nanotubes. As a result, due to the charging of the electrical double layer and followed by the transient of diffusion controlled species, the current decreased dramatically at the beginning several seconds right after the etching potential was applied. When electrochemical etching continues, Co-rich CoAu alloy layers were dissolved gradually and simultaneously from both inside and outside of large diameter nanotubes. As both inside and outside surfaces become rough, total surface area was enhanced and current response increased consequently. At this moment, partially electrochemically etched hollow nanobamboo structures were formed. Later after the current reached the peak value, due to the loss of mass, the surface area becomes smaller and the current starts to decrease. When finally the Co-rich CoAu alloy layers are completely dissolved and no further material was left for etching, the anodic current approaches zero.

When comparing the current responses of the three nanotubes with different CoAu layer sizes, the Au 25 nm / CoAu 250 nm nanotube has the largest CoAu layer size. Consequently, it exhibited the largest surface area created during the etching process and then took the longest

time for completely etching. For example, it took 1766 s and 442 s for the complete etching of Au 25 nm / CoAu 150 nm and Au 25 nm / CoAu 50 nm nanotubes, respectively. In **Figure 4-59**, due to the employment of square root of time as x-axis, the diffusion controlled regions could be identified. Those three current response curves displayed a liner relationship as a function of square root of time after the current peaks, which confirmed the diffusion control in certain regions during the electrochemical etching of nanotubes.

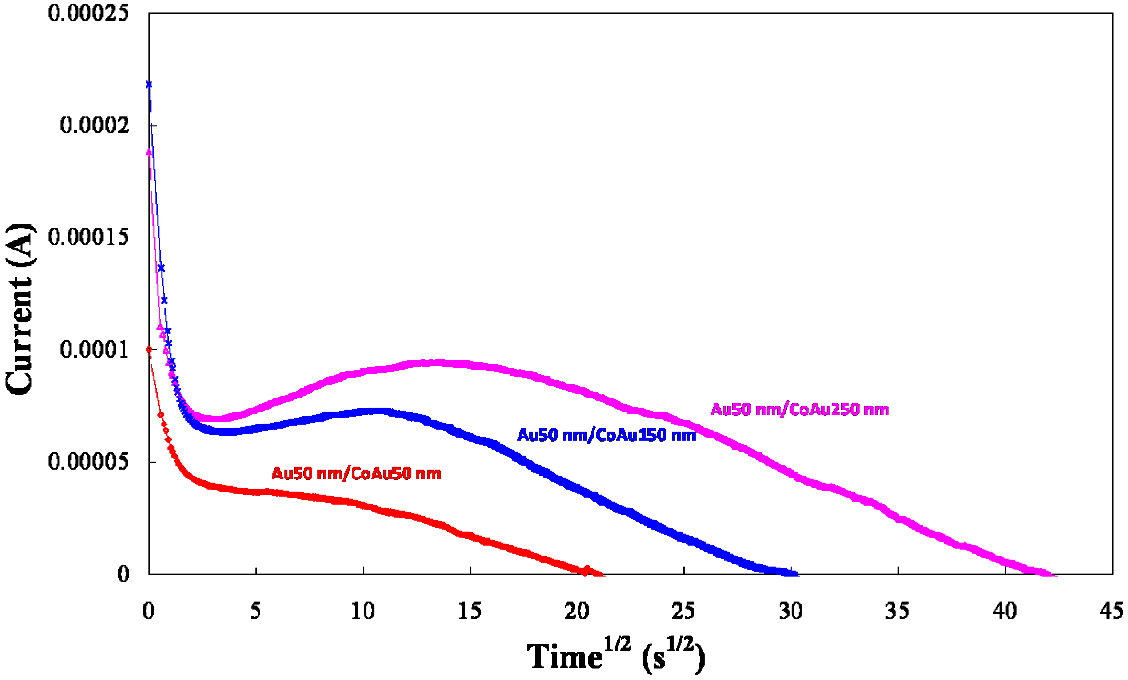

Figure 4-59 Current response as the function of square root of time during the process of the selective electrochemical etching of (red curve) Au 25 nm / CoAu 50 nm, (blue curve) Au 25 nm / CoAu 150 nm, and (pink curve) Au 25 nm / CoAu 250 nm nanotubes deposited from 2.0 µm polycarbonate (PC) membrane

By integrating the areas under each current response as a function of time, anodic charges were calculated and plotted in **Figure 4-60** for each nanotube anodic etching process. These three charge responses exhibited a typical shape similar to the charge response measured in the previous study of nanowire etching. Among those three nanotubes, the one with the thickest CoAu layer size of 250 nm exposed the largest active surface of Co-rich CoAu alloy to the

electrolyte, which consequently resulted to the highest etching rate (anodic current) and the steepest curve of the charge response. Also, it had much more CoAu alloy than other two tubes; therefore, it takes four times longer time than the nanotube with CoAu Layer size of 50 nm to completely dissolve CoAu layer. However for all of three nanotube etching processes, the anodic charge response curve will reach a plateau, which means the complete etching of CoAu layer is approached.

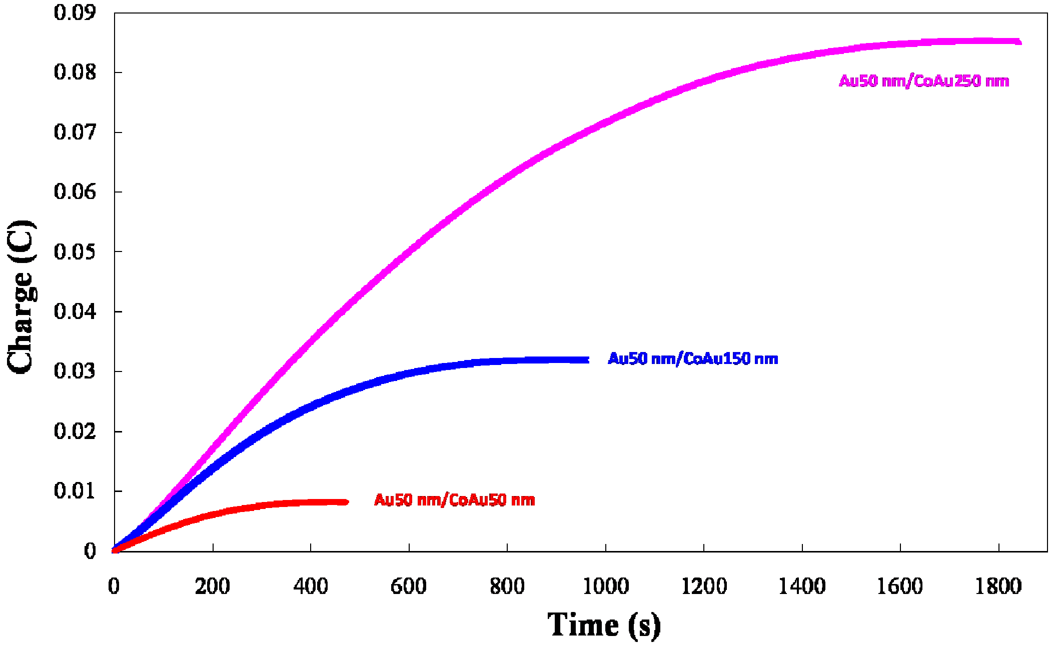

Figure 4-60 Anodic charges as the function of time during the process of the selective electrochemical etching of Au/CoAu nanotubes on carbon electrodes with three different CoAu layer sizes: 50, 100, and 250 nm

The ratio of CoAu layer size and ratio of anodic charges are compared in **Table 4-6**. Basically, the ratios of anodic charge are close to the ratios of CoAu layer sizes correspondingly, which means electrochemical etching can be used as an useful tool to characterize the surface area difference of the nanotube layer.

Corresponding to the current responses in **Figure 4-59**, SEM images of Au 25 nm / CoAu 150 nm nanotubes with diameter of 2.0 µm were taken (a) before applied anodic potential and (b)

after electrochemical etching for 900 s, as shown in **Figure 4-61**. Compared with previous solid nanobamboo and nanodisk structures from electrochemical etching of Au/CoAu nanowires (d=0.1 μm), the quality of those hollow nanobamboo and nanoring structure resulted from etching of nanotubes (d=2.0 μm) was not as good as we expected. In **Figure 4-61 (b)**, Co-rich CoAu alloy layers were not fully etched away; the ring structures were still connected partially. The possible reason could be connected to the nanotube depositions and etching sample preparation process.

Table 4-6 Ratios of CoAu layer sizes and ratios of anodic charges of Au/CoAu nanotube electrochemical etching

CoAu layer (nm)	*Ratio of CoAu layer*	*Anodic charge (C)*	*Ratio of total charge*
250	5	8.52×10^{-2}	10.3
150	3	3.20×10^{-2}	3.8
50	1	8.23×10^{-3}	1

According to the manufactures report, the average thickness of polycarbonate (PC) membranes used for nanotube electrodepositing was only between 6 ~ 10 μm, which is much shorter than that of the anodic aluminum oxide (AAO) membrane (60 μm) used for nanowires deposition. In addition, the average diameter (2 μm) of above nanotubes was at least one order larger than that of the nanowires, i.e. 0.1 μm. Those differences were confirmed by SEM images in our research, as shown in **Figure 4-62**. Even though chloroform dissolution and ultrasonication were employed during the post-deposition etching sample preparation, this small aspect ratio of nanotubes makes it harder to fully release nanotubes from the sputtered Au seed layer, leading to the stack of nanotubes on carbon substrate and more electrical conduction problems.

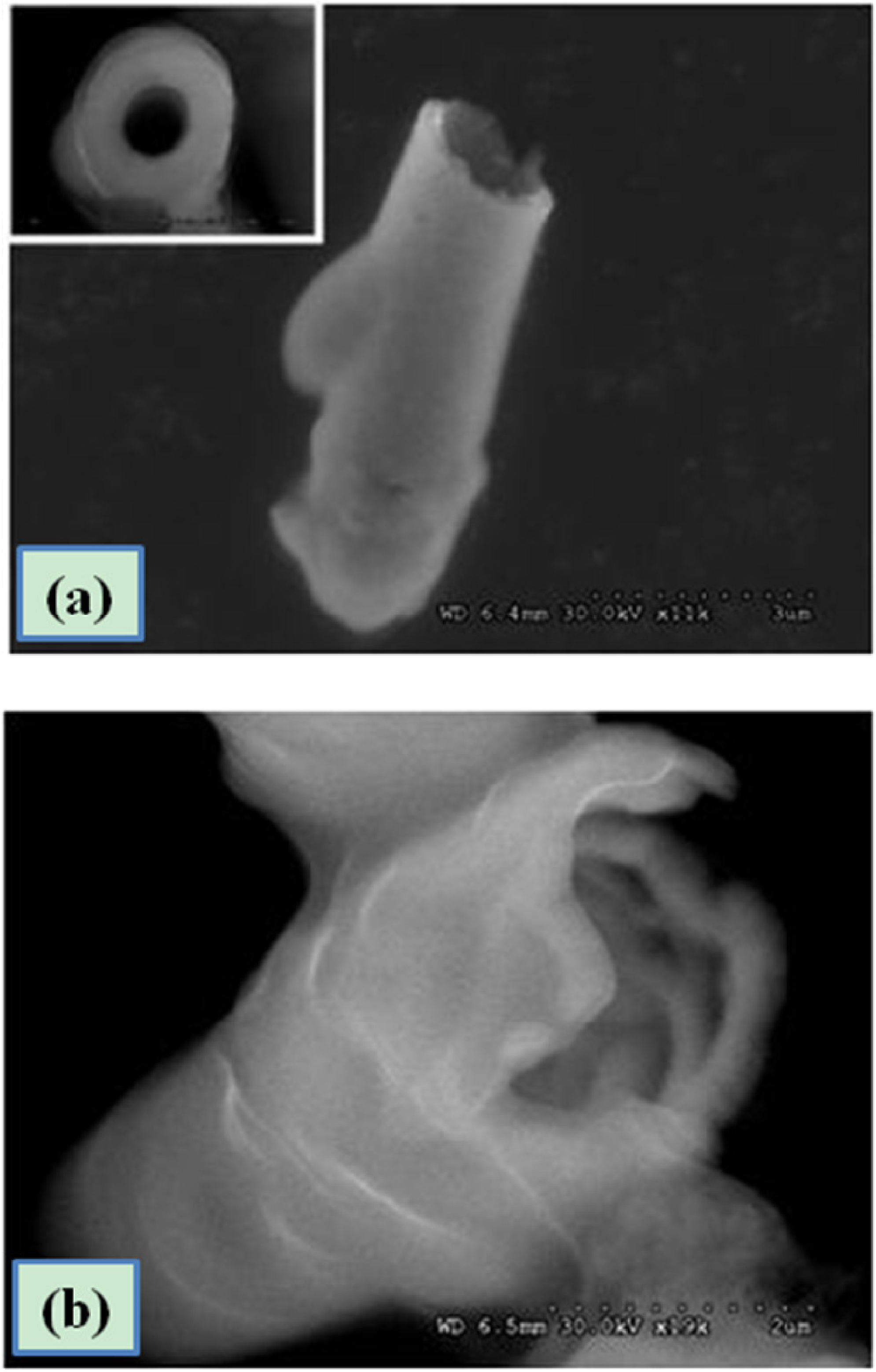

Figure 4-61 SEM images of Au 25 nm / CoAu 150 nm nanotubes with diameter of 2.0 μm taken (a) before and (b) after electrochemical etching for 900 s

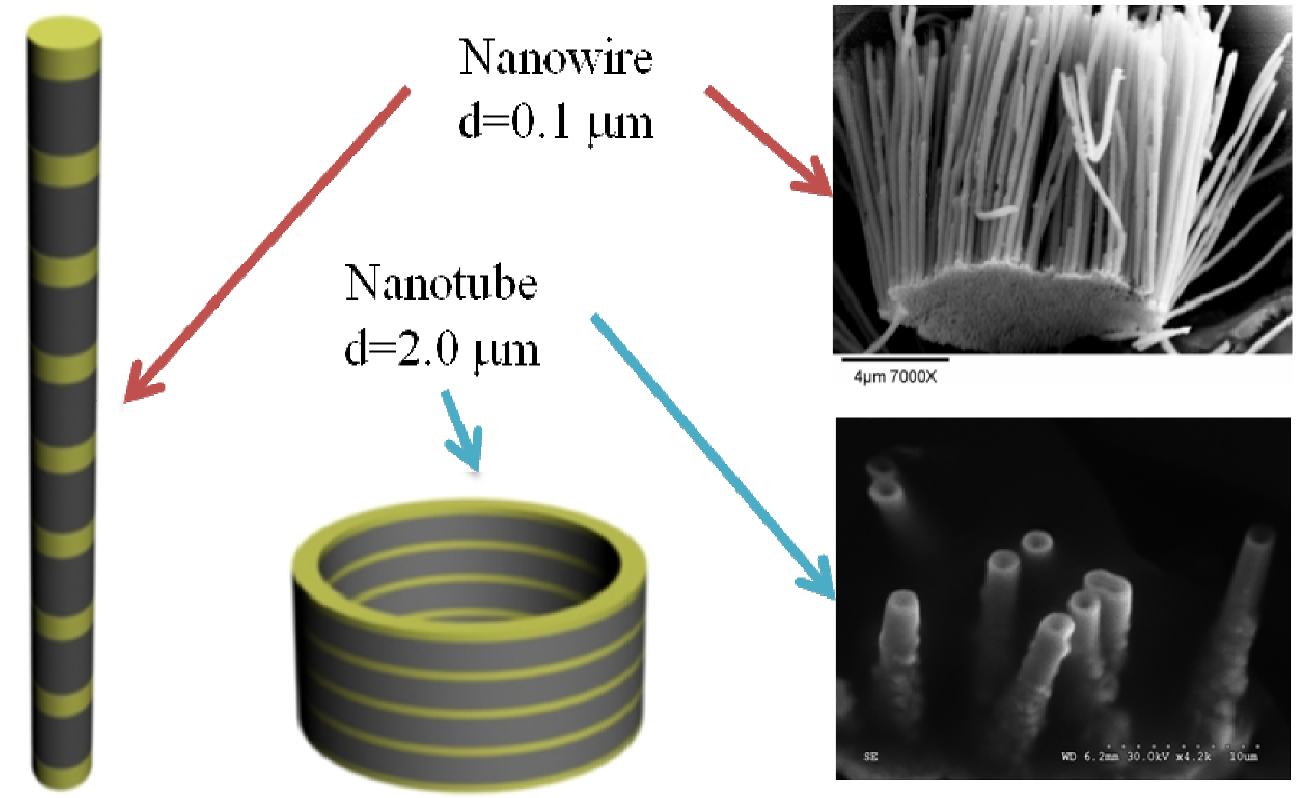

Figure 4-62 Different aspect ratios of nanotube and nanowire

Next, nanotubes with larger aspect ratios were examined by using PC membranes with pore size of 1.0 µm. As shown in **Figure 4-63** and **4-64**, the etching quality was improved dramatically for both partial and complete electrochemical etching. Au nanoring arrays were created after completely removing the CoAu alloy layers.

4.7.2 Conclusion to Nanotube Etching

By combining electrochemical deposition of nanotubes and electrochemical etching of them, a process for the fabrication of nanoparticles, including hollow nanobamboo and nanorings, was developed. Various SEM images of those nanostructures were shown and different electrochemical characterization techniques were applied. The etching charge was also comparable to the layer size.

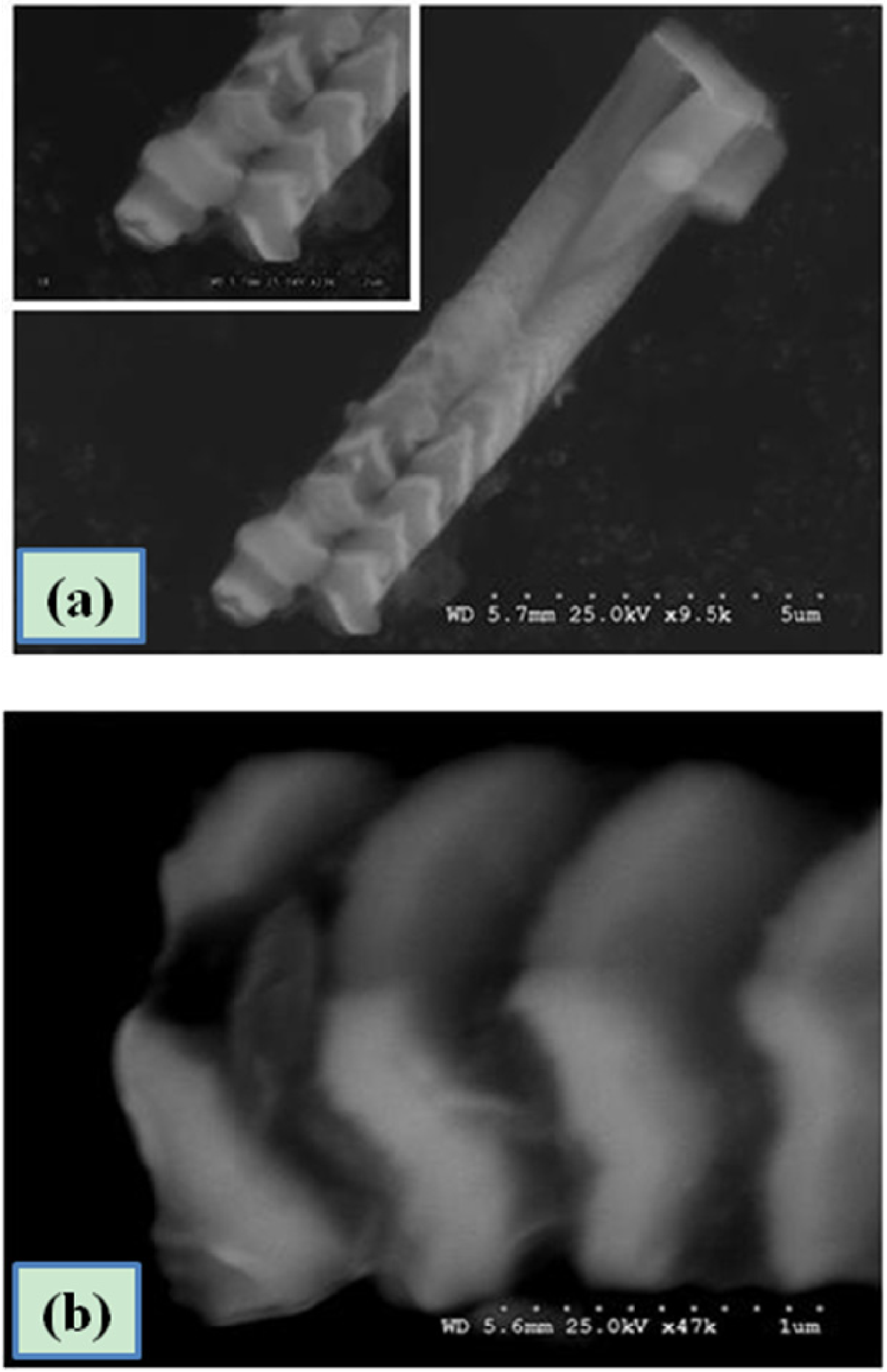

Figure 4-63 SEM images of Au 25 nm / CoAu 150 nm nanotubes with diameter of 1.0 μm after (a) partial and (b) complete electrochemical etching of Co-rich CoAu layer

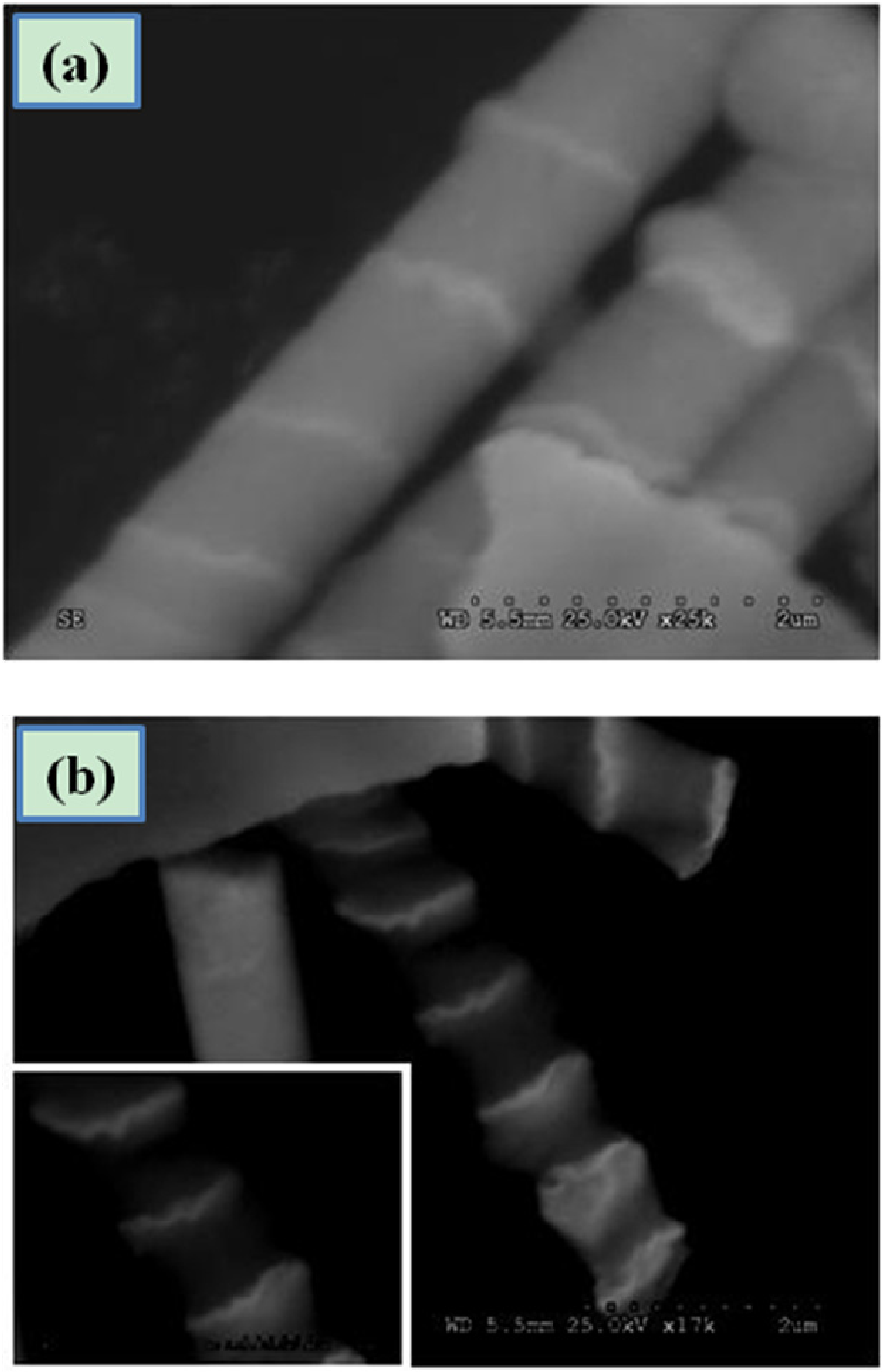

Figure 4-64 SEM images of Au 25 nm / CoAu 250 nm nanotubes with diameter of 1.0 μm after (a) partial and (b) complete electrochemical etching of Co-rich CoAu layer

CHAPTER 5   CONCLUSIONS

In this study, conditions to electrodeposit Au/CoAu multilayered nanowires and nanotubes in various porous templates from non-cyanide electrolytes have been developed. The template pore size plays an important role in determining whether nanowires or nanotubes are formed. Membranes with pore sizes reported by the manufacturer that are smaller than or equal to 0.2 μm yield nanowires, while membranes with pore sizes greater than or equal to 0.4 μm result in nanotubes, under the applied current conditions of -0.2 and -6 mA/cm^2 for electrodeposition of Au and CoAu layers, respectively.

The magnetoresistance and magnetic properties of Au/CoAu multilayered thin films and nanowires were examined. Au/CoAu multilayered thin films with different layer sizes exhibited both normal GMR and inverse GMR depending on both Au and CoAu layer thicknesses. Maximum current-in-plane GMR values of negative 13 % and negative 7 % at a magnetic field of 9 Tesla were observed for Au 3 nm / CoAu 5 nm and Au 4 nm / CoAu 4 nm thin films, respectively. This was the first demonstration of GMR in an electrodeposited Au/Co system. However, no significant current-perpendicular-to-plane GMR values were observed for Au/CoAu multilayered nanowires. In order to improve the GMR properties, annealing treatment was employed. Unfortunately, the results showed that annealing did not favor GMR enhancement.

After electrodeposition, the solid nanowires were then removed from the template and one component was electrochemically etched from the nanowires. KCl solutions were chosen as the etching electrolyte due to its outstanding depassivation ability and low cost. The preferred concentration of KCl was 2 M for higher efficiency and better selectivity. The potential range of -0.60 ~ 0.04 V vs. SCE was determined from anodic polarization curves of Au and Co-rich

CoAu alloy thin films in the 2 M KCl solution, which established the anodization conditions of the nanowires. All the etching efficiencies were 100 % or close to 100 %, which implies that under the above etching conditions, only Co was etched. The difference in the slopes of the etching current responses as a function of the square root of time suggested a higher diffusion resistance in the de-alloying process.

By precisely controlling the electrochemical etching potential and time, a porous surface of the nanowires was achieved and consequently the surface area was enhanced. Nano-bamboo structures were created after partial etching and ordered Au nanodisk structures were created after complete etching. Compared to the conventional chemical etching, by using anodization, etching of the layers can be controlled much better to form these intermediate bamboo structures with no evolution of harmful gases and byproducts. The anodization process was monitored by two techniques. The current was recorded during etching and the total charge was proportional to the layer size. In addition, cyclic voltammetry (CV) was used as a way to observe the partial etching of the nanowires. Specific nanostructures could be recognized by monitoring either the current responses, or the anodic charge responses, or the cyclic voltammograms. To the best of the author's knowledge, this has not been done before.

In addition, the annealing post-treatment was tested to improve the quality of the multilayer interface by promoting phase segregation. However, XRD spectra showed certain intermixing of Au/Co interface due to the annealing, which also explained the decrease of CIP GMR of Au/CoAu multilayered thin films after annealing. SEM images of Au/CoAu nanowires before and after annealing treatment disclosed the fact that annealing will break the long nanowires into shorter ones because of the internal stress of the deposit and the mismatch of thermal expansion coefficients between metallic deposits and AAO membrane.

Furthermore, hollow nano-bamboo structure and ordered nanorings with various aspect ratios were developed through the electrochemical etching of Au/CoAu nanotubes in a similar way. This has never been fabricated before by using electrochemistry. Similar current responses and anodic charge responses were observed and used to monitor the etching degree.

REFERENCES

1. K. M. H. Lenssen, D.J. Adelerhof, H.J. Gassen, A.E.T. Kuiper, G.H.J. Somers, and J. van Zon, *Robust giant magnetoresistance sensors.* Sensors and Actuators A-Physical, 2000. **85**(1-3): p. 1-8.

2. S. Valizadeh, L. Hultman, J.M. George, and P. Leisner, *Template synthesis of Au/Co multilayered nanowires by electrochemical deposition.* Advanced Functional Materials, 2002. **12**(11-12): p. 766-772.

3. S. Valizadeh, E.B. Svedberg, and P. Leisner, *Electrodeposition of compositionally modulated Au/Co alloy layers.* Journal of Applied Electrochemistry, 2002. **32**(1): p. 97-104.

4. M. Guan, *MS Thesis.* Louisiana State University, 2004.

5. L. Piraux, S. Dubois, and A. Fert, *Perpendicular giant magnetoresistance in magnetic multilayered nanowires.* Journal of Magnetism and Magnetic Materials, 1996. **159**(3): p. L287-L292.

6. W.P. Pratt, S.F. Lee, J.M. Slaughter, R. Loloee, P.A. Schroeder, and J. Bass, *Perpendicular Giant Magnetoresistances of Ag/Co Multilayers.* Physical Review Letters, 1991. **66**(23): p. 3060-3063.

7. S. Dubois, C. Marchal, J.M. Beuken, L. Piraux, J.L. Duvail, A. Fert, J.M. George, and J.L. Maurice, *Perpendicular giant magnetoresistance of NiFe/Cu multilayered nanowires.* Applied Physics Letters, 1997. **70**(3): p. 396-398.

8. E. Velu, C. Dupas, D. Renard, J.P. Renard, and J. Seiden, *Enhanced Magnetoresistance of Ultrathin (Au/Co)n Multilayers With Perpendicular Anisotropy.* Physical Review B, 1988. **37**(1): p. 668-671.

9. A. Hutten, D. Sudfeld, K. Wojczykowski, P. Jutzi, and G. Reiss, *Giant magnetoresistance and magnetic aspects in granular structures.* Journal of Magnetism and Magnetic Materials, 2003. **262**(1): p. 23-31.

10. L. Piraux, J.M. George, J.F. Despres, C. Leroy, E. Ferain, R. Legras, K. Ounadjela, and A. Fert, *Giant Magnetoresistance In Magnetic Multilayered Nanowires.* Applied Physics Letters, 1994. **65**(19): p. 2484-2486.

11. S. Dubois, J.M. Beuken, L. Piraux, J.L. Duvail, A. Fert, J.M. George, and J.L. Maurice, *Perpendicular giant magnetoresistance of NiFe/Cu and Co/Cu multilayered nanowires.* Journal of Magnetism and Magnetic Materials, 1997. **165**(1-3): p. 30-33.

12. A. Blondel, J. Meier, B. Doudin, and J. Ansermet, *Giant Magnetoresistance of Nanowires of Multilayers.* Applied Physics Letters, 1994. **65**(23): p. 3019-3021.

13. A. Yamada, T. Houga, and Y. Ueda, *Magnetism and magnetoresistance of Co/Cu multilayer films produced by pulse control electrodeposition method.* Journal of Magnetism and Magnetic Materials, 2002. **239**(1-3): p. 272-275.

14. A. Blondel, B. Doudin, and J. Ansermet, *Comparative study of the magnetoresistance of electrodeposited Co/Cu multilayered nanowires made by single and dual bath techniques.* Journal of Magnetism and Magnetic Materials, 1997. **165**(1-3): p. 34-37.

15. N.V. Myung, B.Y. Yoo, M. Schwartz, and K. Nobe, Electrochemical Society Proceedings, 2000. **29**: p. 154.

16. C.X. Ji and P.C. Searson, *Fabrication of nanoporous gold nanowires.* Applied Physics Letters, 2002. **81**(23): p. 4437-4439.

17. C.X. Ji and P.C. Searson, *Synthesis and characterization of nanoporous gold nanowires.* Journal of Physical Chemistry B, 2003. **107**(19): p. 4494-4499.

18. L.D. Qin, S. Park, L. Huang, and C.A. Mirkin, *On-wire lithography.* Science, 2005. **309**(5731): p. 113-115.

19. Pickerin.Hw and C. Wagner, *Electrolytic Dissolution of Binary Alloys Containing A Noble Metal.* Journal of The Electrochemical Society, 1967. **114**(7): p. 698-&.

20. J. Erlebacher, M.J. Aziz, A. Karma, N. Dimitrov, and K. Sieradzki, *Evolution of nanoporosity in dealloying.* Nature, 2001. **410**(6827): p. 450-453.

21. H. Schwanbeck and U. Schmidt, *Preparation and characterisation of magnetic nanostructures using filtration membranes.* Electrochimica Acta, 2000. **45**(27): p. 4389-4398.

22. G. Millazzo and S. Caroli, *Tables of Standard Electrode Petentials*. 1978, New York: Wiley.

23. M. Guan and E.J. Podlaha, *Electrodeposition of AuCo alloys and multilayers.* Journal of Applied Electrochemistry, 2007. **37**(5): p. 549-555.

24. M. Guan and E.J. Podlaha, *Electrodeposition and Electrochemical Etching of Au/CoAu Multilayered Nanowires.* ECS Transactions, 2007. **3**(25): p. 347-356.

25. S. Valizadeh, J.M. George, P. Leisner, and L. Hultman, *Electrochemical synthesis of Ag/Co multilayered nanowires in porous polycarbonate membranes.* Thin Solid Films, 2002. **402**(1-2): p. 262-271.

26. S. Valizadeh, G. Holmbom, and P. Leisner, *Electrodeposition of cobalt-silver multilayers.* Surface & Coatings Technology, 1998. **105**(3): p. 213-217.

27. L. Cagnon, A. Gundel, T. Devolder, A. Morrone, C. Chappert, J.E. Schmidt, and P. Allongue, *Anion effect in Co/Au(111) electrodeposition: structure and magnetic behavior.* Applied Surface Science, 2000. **164**: p. 22-28.

28. I. Cagnon, T. Devolder, R. Cortes, A. Morrone, J.E. Schmidt, C. Chappert, and P. Allongue, *Enhanced interface perpendicular magnetic anisotrophy in electrodeposited Co/Au(111) layers.* Physical Review B, 2001. **63**(10).

29. A. Gundel, L. Cagnon, C. Gomes, A. Morrone, J. Schmidt, and P. Allongue, *In-situ magnetic measurements of electrodeposited ultrathin Co, Ni and Fe/Au(111) layers.* Physical Chemistry Chemical Physics, 2001. **3**(16): p. 3330-3335.

30. M.N. Baibich, J.M. Broto, A. Fert, F.N. Vandau, F. Petroff, P. Eitenne, G. Creuzet, A. Friederich, and J. Chazelas, *Giant Magnetoresistance of (001)Fe/(001) Cr Magnetic Superlattices.* Physical Review Letters, 1988. **61**(21): p. 2472-2475.

31. C.A. Ross, *Electrodeposited Multilayer Thin-Films.* Annual Review of Materials Science, 1994. **24**: p. 159-188.

32. W. Schwarzacher and D.S. Lashmore, *Giant magnetoresistance in electrodeposited films.* IEEE Transactions on Magnetics, 1996. **32**(4): p. 3133-3153.

33. S. Tumanski, *Thin film magnetoresistivity sensors.* 2001: p. 1-4.

34. J.E. Lenz, *A Review of Magnetic Sensors.* Proceedings of The IEEE, 1990. **78**(6): p. 973-989.

35. E.Y.Tsymbal and D.G.Pettifor, *Perspectives of Giant Magnetoresistance.* Solid State Physics, 2001. **56**: p. 113-237.

36. H. Ehrenreich and F. Spaepen, Solid State Physics, 2001. **56**: p. 6.

37. G.P. Heydon, S.R. Hoon, A.N. Farley, S.L. Tomlinson, M.S. Valera, K. Attenborough, and W. Schwarzacher, *Magnetic properties of electrodeposited nanowires.* Journal of Physics D-Applied Physics, 1997. **30**(7): p. 1083-1093.

38. B. Dieny, V.S. Speriosu, S.S.P. Parkin, B.A. Gurney, D.R. Wilhoit, and D. Mauri, *Giant Magnetoresistance In Soft Ferromagnetic Multilayers.* Physical Review B, 1991. **43**(1): p. 1297-1300.

39. M.R. Khan, C.S.L. Chun, G.P. Felcher, M. Grimsditch, A. Kueny, C.M. Falco, and I.K. Schuller, Physical Review B, 1983. **27**: p. 7186.

40. E. Velu, C. Dupas, W. Nabhan, F. Trigui, J.P. Renard, and D. Renard, *Strong Magnetoresistance Reduction at The Coercive-Field Crossover of 2 Uncoupled Magnetic-Films.* Journal of Applied Physics, 1992. **71**(1): p. 503-505.

41. T. Takahata, S. Araki, and T. Shinjo, *Magnetism and Magnetoresistance of Au/Co Multilayers.* Journal of Magnetism and Magnetic Materials, 1989. **82**(2-3): p. 287-293.

42. W. Vavra, C.H. Lee, F.J. Lamelas, H. He, R. Clarke, and C. Uher, *Magnetoresistance and Hall-Effect In Epitaxial Co-Au Superlattices.* Physical Review B, 1990. **42**(7): p. 4889-4892.

43. V. Grolier, D. Renard, B. Bartenlian, P. Beauvillain, C. Chappert, C. Dupas, J. Ferre, M. Galtier, E. Kolb, M. Mulloy, J.P. Renard, and P. Veillet, *Unambiguous Evidence of Oscillatory Magnetic Coupling Between Co Layers in Ultrahigh-Vacuum Grown Co/Au(111)/Co Trilayers.* Physical Review Letters, 1993. **71**(18): p. 3023-3026.

44. S. Araki, T. Takahata, and T. Shinjo, *Journal of the Magnetism Society of Japan.* 1989. **13**: p. 339-342.

45. S. Honda, T. Fujimoto, and M. Nawate, *Giant magnetoresistance of perpendicular magnetic Co/Au multilayers.* Journal of Applied Physics, 1996. **80**(9): p. 5175-5182.

46. K. Liu, K. Nagodawithana, P.C. Searson, and C.L. Chien, *Perpendicular Giant Magnetoresistance of Multilayered Co/Cu Nanowires.* Physical Review B, 1995. **51**(11): p. 7381-7384.

47. J. Barnas, A. Fuss, R.E. Camley, P. Grunberg, and W. Zinn, *Novel Magnetoresistance Effect In Layered Magnetic-Structures - Theory and Experiment.* Physical Review B, 1990. **42**(13): p. 8110-8120.

48. C.F. Majkrzak, J.W. Cable, J. Kwo, M. Hong, D.B. McWhan, Y. Yafet, J.V. Waszczak, and C. Vettier, *Observation of A Magnetic Antiphase Domain-Structure With Long-*

Range Order In A Synthetic Gd-Y Superlattice. Physical Review Letters, 1986. **56**(25): p. 2700-2703.

49. S.S.P. Parkin, N. More, and K.P. Roche, *Oscillations in Exchange Coupling and Magnetoresistance in Metallic Superlattice Structures - Co/Ru, Co/Cr, And Fe/Cr.* Physical Review Letters, 1990. **64**(19): p. 2304-2307.

50. S.S.P. Parkin, *Systematic Variation of The Strength and Oscillation Period of Indirect Magnetic Exchange Coupling Through The 3d, 4d, and 5d Transition-Metals.* Physical Review Letters, 1991. **67**(25): p. 3598-3601.

51. V. Bartenlian, P. Beauvillain, C. Chappert, C. Dupas, J. Ferre, M. Galtier, E. Kolb, M. Mulloy, J.P. Renard, and P. Veillet, Physical Review Letters, 1993. **71**(18): p. 3023.

52. P. Bruno and C. Chappert, *Oscillatory Coupling Between Ferromagnetic Layers Separated By A Nonmagnetic Metal Spacer.* Physical Review Letters, 1991. **67**(12): p. 1602-1605.

53. S.S.P. Parkin, R.F.C. Farrow, R.F. Marks, A. Cebollada, G.R. Harp, and R.J. Savoy, Physical Review Letters, 1994. **72**(23): p. 3718.

54. Y. Roussigne, F. Ganot, C. Dugautier, P. Moch, and D. Renard, *Brillouin-Scattering in Co/Cu/Co and Co/Au/Co Trilayers - Anisotropy Fields And Interlayer Magnetic Exchange.* Physical Review B, 1995. **52**(1): p. 350-360.

55. E. Kolb, M.J. Walker, E. Velu, M.A. Howson, P. Veillet, D. Greig, J.P. Renard, and C. Dupas, *Giant magnetoresistance of dissymmetrical Co/Au multilayers.* Journal of Magnetism and Magnetic Materials, 1996. **156**(1-3): p. 377-378.

56. C.X. Ji, PhD dissertation, Johns Hopkins University, 2002.

57. Q.T. Wang, G.Z. Wang, X.H. Han, X.P. Wang, and J.G. Hou, *Controllable template synthesis of Ni/Cu nanocable and Ni nanotube arrays: A one-step coelectrodeposition and electrochemical etching method.* Journal of Physical Chemistry B, 2005. **109**(49): p. 23326-23329.

58. J.H. Lim, N.H. Kim, and E.G. Chang, *Electrochemical patterning of copper using microcontact printing.* Journal of The Electrochemical Society, 2004. **151**(7): p. C455-C458.

59. S.M. Yi, S.H. Jin, J.D. Lee, and C.N. Chu, *Fabrication of a high-aspect-ratio stainless steel shadow mask and its application to pentacene thin-film transistors.* Journal of Micromechanics and Microengineering, 2005. **15**(2): p. 263-269.

60. B. Ren, G. Picardi, and B. Pettinger, *Preparation of gold tips suitable for tip-enhanced Raman spectroscopy and light emission by electrochemical etching.* Review of Scientific Instruments, 2004. **75**(4): p. 837-841.

61. C. Albonetti, I. Bergenti, M. Cavallini, V. Dediu, M. Massi, J.F. Moulin, and F. Biscarini, *Electrochemical preparation of cobalt tips for scanning tunneling microscopy.* Review of Scientific Instruments, 2002. **73**(12): p. 4254-4256.

62. C. Albonetti, M. Cavallini, M. Massi, J.F. Moulin, and F. Biscarini, *Electrochemical fabrication of cobalt and nickel tips for scanning tunneling microscopy.* Journal of Vacuum Science & Technology B, 2005. **23**(6): p. 2564-2566.

63. M. Cavallini and F. Biscarini, *Electrochemically etched nickel tips for spin polarized scanning tunneling microscopy.* Review of Scientific Instruments, 2000. **71**(12): p. 4457-4460.

64. A.J. Nam, A. Teren, T.A. Lusby, and A.J. Melmed, *Benign Making of Sharp Tips for Stm and Fim - Pt, Ir, Au, Pd, and Rh.* Journal of Vacuum Science & Technology B, 1995. **13**(4): p. 1556-1559.

65. M. Iwami, Y. Uehara, and S. Ushioda, *Preparation of silver tips for scanning tunneling microscopy imaging.* Review of Scientific Instruments, 1998. **69**(11): p. 4010-4011.

66. A.D. Muller, F. Muller, M. Hietschold, F. Demming, J. Jersch, and K. Dickmann, *Characterization of electrochemically etched tungsten tips for scanning tunneling microscopy.* Review of Scientific Instruments, 1999. **70**(10): p. 3970-3972.

67. A.L. Morales, *Electrodeposited metal matrix nanocomposites as thin films and high aspect ratio microstructures for MEMS*. 2006, Louisiana State University: Baton Rouge, LA.

68. W.R. Moser, *Advanced Catalysts and Nanostructured Materials*. 1996, San Diego, California: Academic Press, Inc.

69. D. Davis, *Electrodeposition of multilayered nanostructures for giant magnetoresistance and thermoelectric applications*. 2007, Louisiana State University: Baton Rouge, LA.

70. M. Schlesinger and M. Paunovic, *Modern Electroplating, 4th Edition*. 2000, Wiley: New York. p. 676.

71. J.J. Kelly, N. Yang, T. Headley, and J. Hachman, Journal of The Electrochemical Society, 2003. **150**(6): p. C445-C450.

72. http://nobelprize.org/nobel_prizes/physics/laureates/2007/.

73. D.R. Baselt, G.U. Lee, M. Natesan, S.W. Metzger, P.E. Sheehan, and R.J. Colton, *A biosensor based on magnetoresistance technology.* Biosensors & Bioelectronics, 1998. **13**(7-8): p. 731-739.

74. R.L. Edelstein, C.R. Tamanaha, P.E. Sheehan, M.M. Miller, D.R. Baselt, L.J. Whitman, and R.J. Colton, *The BARC biosensor applied to the detection of biological warfare agents.* Biosensors & Bioelectronics, 2000. **14**(10-11): p. 805-813.

75. J. Schotter, P.B. Kamp, A. Becker, A. Puhler, D. Brinkmann, W. Schepper, H. Bruckl, and G. Reiss, *A biochip based on magnetoresistive sensors.* IEEE Transactions on Magnetics, 2002. **38**(5): p. 3365-3367.

76. H. Bruckl, M. Brzeska, D. Brinkmann, J. Schotter, G. Reiss, W. Schepper, P.B. Kamp, and A. Becker, *Magnetoresistive logic and biochip.* Journal of Magnetism and Magnetic Materials, 2004. **282**: p. 219-224.

77. J.M. George, L.G. Pereira, A. Barthelemy, F. Petroff, L. Steren, J.L. Duvail, A. Fert, R. Loloee, P. Holody, and P.A. Schroeder, *Inverse Spin-Valve-Type Magnetoresistance In Spin Engineered Multilayered Structures.* Physical Review Letters, 1994. **72**(3): p. 408-411.

78. A. Dinia and M. Guth, *Interfacial origin of inverse magnetoresistance in uncoupled Fe/Si/Fe/Ru sandwiches.* Applied Physics Letters, 1998. **73**(24): p. 3592-3594.

79. K. Rahmouni, A. Dinia, D. Stoeffler, K. Ounadjela, H.A.M. Van den Berg, and H. Rakoto, *Inverse magnetoresistance in Co/Ru/Co and doped Co/Ru/Co0.92Ru0.08 sandwiches.* Physical Review B, 1999. **59**(14): p. 9475-9481.

80. Z.C. Zhao, H. Wang, S.Q. Xiao, D. Huang, Y.Z. Gu, Y.X. Xia, Q.Y. Jin, C.L. Zha, and X.S. Wu, *Inverse magnetoresistance caused by nano-nitride-layer doping at the inner interfaces in the sandwich of Co/Cu/Co.* Journal Of Applied Physics, 2006. **99**(8).

81. A. Blondel, J. Meier, B. Doudin, J. Ansermet, K. Attenborough, P. Evans, R. Hart, G. Nabiyouni, and W. Schwarzacher, *Wire-shaped Magnetic Multilayers for Current Perpendicular to Plane Magnetoresistance Measurements.* Journal of Magnetism and Magnetic Materials, 1995. **148**(1-2): p. 317-318.

82. R.C. O'Handley, *Modern Magnetic Materials: Principles and Applications*. 2000, John Wiley & Sons, Inc.: New York. p. 640.

83. F.J.A. den Broeder, D. Kuiper, A.P. van de Mosselaer, and W. Hoving, *Perpendicular Magnetic Anisotropy of Co-Au Multilayers Induced by Interface Sharpening.* Physical Review Letters, 1988. **60**(26): p. 2769.

84. T.L. Hylton, K.R. Coffey, M.A. Parker, and J.K. Howard, *Giant Magnetoresistance At Low Fields In Discontinuous Nife-Ag Multilayer Thin-Films.* Science, 1993. **261**(5124): p. 1021-1024.

85. H. Vrenken, B.J. Kooi, and J.T.M. De Hosson, *Microstructure and properties of giant magnetoresistive granular Au80Co20 alloys.* Journal of Applied Physics, 2001. **89**(6): p. 3381-3387.

86. P.R. Evans, G. Yi, and W. Schwarzacher, *Current perpendicular to plane giant magnetoresistance of multilayered nanowires electrodeposited in anodic aluminum oxide membranes.* Applied Physics Letters, 2000. **76**(4): p. 481-483.

87. D.A. Jones, *Principles and prevention of corrosion*. 2nd ed. 1996, Upper Saddle River, NJ: Prentice Hall. 572.

88. R.G. Kelly, J.R. Scully, D.W. Shoesmith, and R.G. Buchheit, *Electrochemical Techniques in Corrosion Science and Engineering*, in *Corrosion Technology*, P.A. Schweitzer, Editor. 2003, Marcel Dekker, Inc.: New York. p. 21.

89. M. Pourbaix, *Atlas of Electrochemical Equilibria*. 1966, Pergamon Press: New York. p. 326.

90. D. Pletcher and F.C. Walsh, *Industrial Electrochemistry*. 2nd ed. 1990, New York, NY: Chapman and Hall Ltd.

91. G. Prentice, *Electrochemical engineering principles*. Prentice-Hall international series in the physical and chemical engineering sciences. 1991, Englewood Cliffs, NJ: Prentice Hall.

92. C.R. Martin and P. Kohli, *The emerging field of nanotube biotechnology.* Nature Reviews Drug Discovery, 2003. **2**(1): p. 29-37.

93. L. Nie, H. Chen, M. Tan, and N. He, J. Southeast Univ., 2002. **20**(4): p. 463-466.

94. D. Carlier and J.P. Ansermet, *Electrochemical synthesis and magnetic properties of CoFe2O4 nanowire arrays.* Journal of The Electrochemical Society, 2006. **153**(5): p. C277-C281.

95. *Thermal Expansion Values of Materials.* http://www.mse.iastate.edu/fileadmin/www.mse.iastate.edu/mate423/f03/Lecture%2013.%20Thermal%20Expansion%20Coefficient.ppt.

96. J.G. Zhu, Y.F. Zheng, and G.A. Prinz, *Ultrahigh density vertical magnetoresistive random access memory (invited).* Journal of Applied Physics, 2000. **87**(9): p. 6668-6673.

97. J. Aizpurua, P. Hanarp, D.S. Sutherland, M. Kall, G.W. Bryant, and F.J.G. de Abajo, *Optical properties of gold nanorings.* Physical Review Letters, 2003. **90**(5).

98. I. Neudecker, M. Klaui, K. Perzlmaier, D. Backes, L.J. Heyderman, C.A.F. Vaz, J.A.C. Bland, U. Rudiger, and C.H. Back, *Spatially resolved dynamic eigenmode spectrum of Co rings.* Physical Review Letters, 2006. **96**(5): p. Art. No. 057207.

99. F.J. Castano, C.A. Ross, A. Eilez, W. Jung, and C. Frandsen, *Magnetic configurations in 160-520-nm-diameter ferromagnetic rings.* Physical Review B, 2004. **69**(14): p. Art. No. 144421.

100. D.D. Jia and A. Goonewardene, *Two-dimensional nanotriangle and nanoring arrays on silicon wafer.* Applied Physics Letters, 2006. **88**(5): p. Art. No. 053105.

101. K.L. Hobbs, P.R. Larson, G.D. Lian, J.C. Keay, and M.B. Johnson, *Fabrication of nanoring arrays by sputter redeposition using porous alumina templates.* Nano Letters, 2004. **4**(1): p. 167-171.

102. C.A. Ross, F.J. Castano, D. Morecroft, W. Jung, H.I. Smith, T.A. Moore, T.J. Hayward, J.A.C. Bland, T.J. Bromwich, and A.K. Petford-Long, *Mesoscopic thin-film magnetic rings (invited).* Journal of Applied Physics, 2006. **99**(8): p. Art. No. 08S501.

103. X.W. Zhang, N.F. Chen, F. Yan, and W.A. Goedel, *Heteroepitaxial gold (111) rings on mica substrates.* Applied Physics Letters, 2005. **86**(20): p. Art. No. 203102.

104. J. Aizpurua, P. Hanarp, D.S. Sutherland, M. Kall, G.W. Bryant, and F.J.G. de Abajo, *Optical properties of gold nanorings.* Physical Review Letters, 2003. **90**(5): p. Art. No. 057401.

APPENDIX: SUPPLEMENTARY DATA

In this investigation of the current-perpendicular-to-plane giant magnetoresistance (CPP GMR), multilayered Au/CoAu nanowires with various layer thicknesses were electrodeposited. The CoAu layer was deposited at -6 mA/cm^2, and the Au layer was deposited at –0.2 mA/cm^2 in the non-cyanide Au/Co electrolyte. The layer thickness was controlled by varying the deposition time. **Figure A-1** shows magnetoresistance behaviors of two series of Au/CoAu nanowires at room temperature. As denoted on the left side of **Figure A-1**, the first series of nanowires contains two samples: Au 8 nm / CoAu 7.5 nm with 4221 bilayers and Au 8 nm / CoAu 12 nm with 3263 bilayers. As denoted on the right side of **Figure A-1**, the second series of nanowires contains three samples: Au 5 nm / CoAu 7.5 nm with 5185 bilayers, Au 5 nm / CoAu 15 nm with 3230 bilayers, and Au 5 nm / CoAu 25 nm with 2114 bilayers. All of those five nanowire samples were electrodeposited in AAO membranes with pore size of 20 nm. Even though each sample had its own bilayer number, all of them had same total thickness of 60 µm. In **Figure A-1**, the magnetoresistance behaviors were noisy and irregular and the resistances are time dependant. The thinner CoAu layer (7.5 nm) sample showed a bigger change in resistance at zero magnetic field.

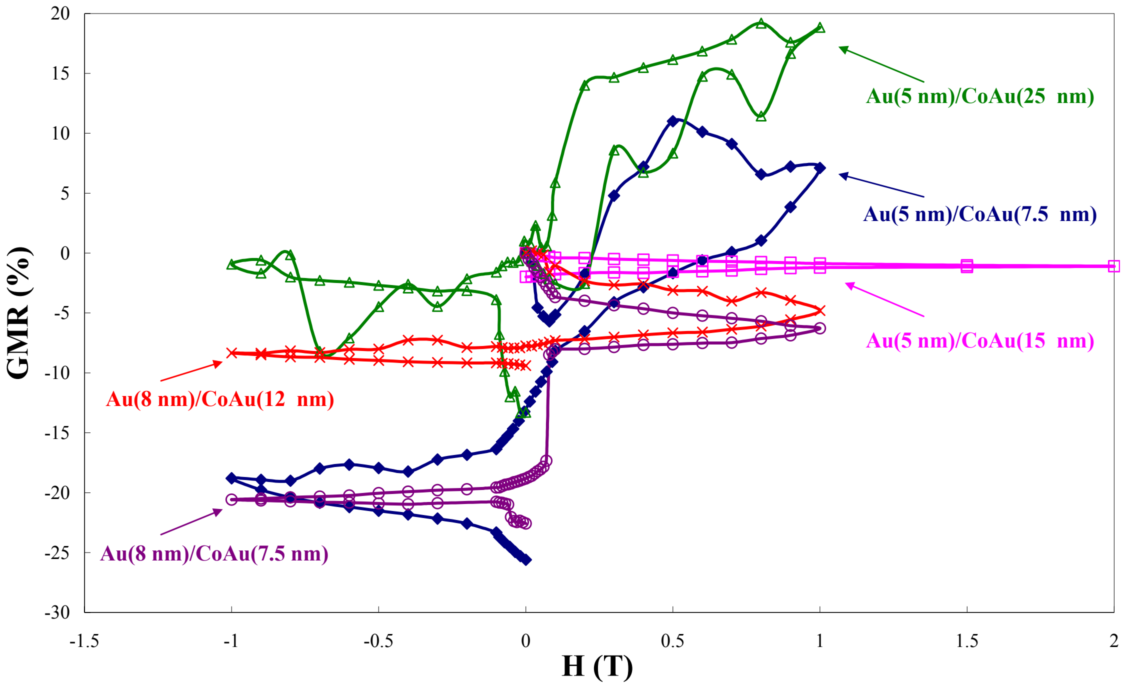

Figure A-1 CPP GMR behaviors of Au/CoAu multilayered nanowires in alumina template, including (Au 8 nm / CoAu 8 nm) × 4221, (Au 8 nm / CoAu 12 nm) × 3263, (Au 5 nm / CoAu 7.5 nm) × 5185, (Au 5 nm / CoAu 15 nm) × 3230, and (Au 5 nm / CoAu 25 nm) × 2114

VITA

Mr. Maoshi Guan is a doctoral candidate in The Interdepartmental Program in Engineering Science at Louisiana State University. He was born in Shandong Province, People's Republic of China, in 1977. He was enrolled in University of Petroleum (East China) in 1995 and obtained the degree of Bachelor of Science in chemical engineering in 1999. In 2002, he came to Louisiana State University to pursue the degree of Master of Science in Chemical Engineering, which was conferred in May 2005. The degree of Doctor of Philosophy will be conferred in May 2008.